# PERFORMANCE OF REINFORCED CONCRETE PANELS DURING BLAST LOADING

by

Timothy T. Garfield

A thesis submitted to the faculty of
The University of Utah
in partial fulfillment of the requirements for the degree of

Master of Science

Department of Civil and Environmental Engineering

The University of Utah

December 2011

**The University of Utah Graduate School**

# STATEMENT OF THESIS APPROVAL

The thesis of **Timothy T. Garfield**

has been approved by the following supervisory committee members:

| | | |
|---|---|---|
| **Chris P. Pantelides** | , Chair | **August 19, 2011** Date Approved |
| **Lawrence D. Reaveley** | , Member | **August 15, 2011** Date Approved |
| **Pedro Romero** | , Member | **August 15, 2011** Date Approved |

and by **Paul J. Tikalsky** , Chair of the Department of **Civil and Environmental Engineering**

and by Charles A. Wight, Dean of The Graduate School.

# ABSTRACT

The structural integrity of reinforced concrete structures subjected to blast loading is important for critical facilities. This thesis presents experimental data generated that evaluate the performance of reinforced concrete wall panels with a wide range of construction details under blast loading. The test specimens were 4 ft. square wall panels constructed using Normal Weight Concrete (NWC) or Fiber Reinforced Concrete (FRC). FRC consists of macrosynthetic fibers dispersed in NWC. Five types of panels were tested: NWC panels with steel bar reinforcement (Type A); FRC panels without additional reinforcement (Type B); FRC panels with steel bar reinforcement (Type C); NWC panels with glass fiber reinforced polymer (GFRP) bar reinforcement (Type D); and NWC panels reinforced with steel bar reinforcement and external bidirectional GFRP overlays on both faces (Type E). Three additional Type D panels were used as control specimens (CON). Each panel type was constructed with three thicknesses: 6 in., 10 in., and 14 in. The panels were instrumented with strain gauges, and accelerometers; in addition, pressure sensors and high speed video were used during the blast events.

Panel types C and E consistently were visually damaged the least by the explosion; the damage that was visually inspected was the crack width, loss of concrete by fragmentation, and deflection of the panel. Based on these criteria panel types C and E were the best panels at resisting the blast loading. The 6 in. and 10 in. thick type B panels consistently broke into two pieces causing complete structural failure of the panel; panel

type B was the worst performing panel because of the complete structural failure. The spacing of the reinforcement proves to be very important. The closer the spacing the better the panel performed at resisting damage caused by the blast. The FRC concrete performed better than the NWC, and the thickness of the panels proved to be equally important at resisting the shearing forces caused by the blast.

# TABLE OF CONTENTS

# LIST OF TABLES

# NOMENCLATURE

| | | |
|---|---|---|
| ANFO | - | Ammonium Nitrate Mixed with Diesel Fuel |
| ASTM | - | American Society for Testing Materials |
| C4 | - | Composition 4 |
| CFRP | - | Carbon Fiber Reinforced Polymer |
| CON | - | Control |
| ConWep | - | Conventional Weapon Effects |
| DIF | - | Dynamic Increase Factor |
| FRC | - | Fiber Reinforced Concrete |
| FRP | - | Fiber Reinforced Polymer |
| GFRP | - | Glass Fiber Reinforced Polymer |
| INL | - | Idaho National Laboratory |
| LVDT | - | Linear Variable Differential Transformer |
| MTS | - | Material Testing System |
| NSTR | - | National Security Test Range |
| NWC | - | Normal Weight Concrete |
| SRP | - | Steel Fiber Reinforced Polymer |
| TNT | - | Trinitrotoluene |

# ACKNOWLEDGEMENTS

I would like to thank my advisor Dr. Chris Pantelides, and committee members Dr. Larry Reaveley, and Dr. Pedro Romero. Their dedication to advise and meet with me was instrumental to the success of my education. They were always able to clarify any technical questions pertaining to my education. Without their help I would not be able to complete this thesis.

I would like to thank Bill Richins, Tom Larson, and Jeff Blakley from Idaho National Laboratories for initiating a project through which I could obtain my master's degree. They always had the patience and dedication to help me succeed throughout this project. Without their help I would not have been able to report the findings within this document.

I would also like to thank Mark Bryant for five years of help and counsel in all of my various research endeavors. His ability to point me in the right direction was paramount to my success in all of my projects.

I would also like thank my family and my wife, and I would also like to thank all of the individuals who helped me with equipment issues, data collection, and various other tasks. The individuals include, but are not limited to, Brett Raddon, Clayton Burningham, Michael Gibbons, and Erika Weber.

# 1. LITERATURE REVIEW

## 1.1. Introduction

Structural engineers are faced with many different challenges when designing structures especially when designing reinforced concrete buildings that could be subjected to a blast load. Reinforced concrete is a widely used construction material that is used around the world to build structures. Even though concrete is widely used, there is much that can still be learned about its performance under varying environmental conditions. Additionally there are constantly new reinforcement techniques and materials that require research to understand their interaction with concrete in resisting blast loads.

An explosion is a very fast chemical reaction that produces hot gases; the hot gases force the air around those gases outwards, these gases are the outer most or top layer of the blast wave. The outwards motion compresses the air that surrounds the gases; the compressed air contains energy as a form of pressure from the explosion. As this blast wave travels through the air it rapidly decreases in energy as it travels further from the center of the explosion. The momentum of the upper layer of gases causes the air to over-expand causing the pressure to decrease below atmospheric conditions at the tail end of the blast wave; this decrease causes a negative suction phase to occur. Mays et al. (2009) presented a figure similar to Figure 1.1 which is a typical pressure-time profile of an explosion that occurs in free air. Figure 1.2 shows the rapid increase in pressure ($p_s$) as

the explosive detonates at some time ($t_a$); then the positive pressure wave occurs over a time ($t_0$), and then the negative pressure wave occurs over a time ($t_0^-$).

Two types of common explosives are composition 4 (C4) and ammonium nitrate mixed with diesel fuel (ANFO). C4 is a plastic explosive that is primarily used in the military and government, because it is easy to transport, lightweight, very pliable, and can easily be shaped. C4 is also very stable; detonation can only occur under intense pressure or heat; when C4 detonates it does so with a detonation velocity of 26,550 ft./s. ANFO is a widely used high explosive that is used extensively through the world for mining, agriculture, and construction purposes. ANFO is formed into small pellets that are easily transported and it is typically very stable; to detonate ANFO a booster is required typically a stick of C4 is used. The detonation velocity of ANFO varies widely depending on the manufacture; a common assumption is that ANFO has a detonation velocity half the detonation velocity of C4 or a detonation velocity of 13,275 ft./s., Cooper and Kurowski (1996).

A common practice is to compare the energy of an explosive compound to the energy in trinitrotoluene (TNT); this is done because of the universal knowledge and availability of TNT. The ratio of TNT to another explosive is called the equivalent weight of TNT. C4 produces 1.37 times more energy than TNT; for example one pound of C4 has the equivalent energy of 1.37 pounds of TNT. ANFO produces 0.86 times more energy than TNT; for example one pound of ANFO has the equivalent energy of 0.86 pounds of TNT. These factors are variable depending on the source; the factors presented here were provided by the personnel at Idaho National Laboratory.

This thesis describes results of research conducted at the Idaho National Laboratory and the University of Utah. The primary research goal was to investigate and validate the performance of new materials used with reinforce concrete subjected to explosive blast or dynamic impact events. Various types of reinforced concrete panels were constructed and tested by detonating an explosive near the panel. The data collected from this research are being used to improve the knowledge of how structures will respond to a blast event, and improve finite element models for predicting the blast performance of concrete structures. In addition, the research investigates the postblast performance of reinforced concrete panels in terms of their remaining capacity under an applied static load.

## 1.2. Reinforced Concrete

Reinforced concrete is one of the most widely used construction materials. It is also known that the mechanical properties of reinforced concrete depend on the rate at which the load is applied to the material. The loading time for a typical compression test of a concrete cylinder, in the extreme case, can be as long as $1.8 \times 10^{3}$ s. A conventional weapon will load a concrete specimen for only $1.0 \times 10^{-4}$ s which is a much shorter rate than the duration of a compression test. This drastic difference in loading duration affects the mechanical properties of the concrete. Ross et al. (1995) conducted research on normal weight concrete with no reinforcement and found that concrete does indeed exhibit different tensile and compressive properties depending on the rate at which it is loaded. It was also determined that at high loading rates, concrete experienced a greater increase in tensile strength than in compressive strength of the specimen; this is shown in Figure 1.2.

Further research has been conducted on reinforced concrete to determine how reinforcement added to concrete would affect the behavior of concrete at high strain rates. Haifen et al. (2009) carried out tests by using a one-stage light gas gun and pressure sensors in the specimen; they were able to confirm what has been known for many years: that reinforced concrete in compression and tension is stronger at high strain rates than unreinforced (plain) concrete.

The ability of concrete to increase in strength as the strain rate increases is sometimes referred to as the dynamic increase factor (DIF). The DIF is a function of the compressive or tensile strength at high strain rates versus the compressive or tensile strength of the concrete at static testing strain rates. The DIF for compression is typically 1.1 to 1.5 and because of this it is usually ignored in most research; the tensile DIF is usually much greater than the compressive DIF and this is important because a concrete specimen will typically fail in tension under blast. Malvar and Ross (1998) conducted a research study and found a DIF of 7.0 when concrete is in tension at the highest measured strain rate of 157 $s^{-1}$. The same study by Malvar and Ross (1998) compared the DIF results from research reported in the open literature. They were able to develop a figure similar to Figure 1.2 from comparisons of existing research data. Weerheijm and Van Doormaal (2006) reported a DIF of 5.3; this was obtained at loading rates of 145,000 ksi/s. Zhang et al. (2009) report a maximum DIF for the peak load of 7.14 and a DIF of fracture energy of 32.23. Brara et al. (2001) reported that the tensile strength of concrete subjected to a dynamic load is 10 times the static strength.

### 1.3. Fiber Reinforced Concrete

When fibers are added to concrete the concrete then becomes a fiber reinforced concrete (FRC). Fibers are usually made of steel, glass, or synthetic materials. Fibers are added to help increase the tensile strength of concrete which is typically 10% the compressive strength of the concrete. Recently, many studies have been carried out to evaluate the performance of FRC in a blast event or under high strain rate loading event.

Naaman et al. (2007) reported that adding polyvinyl alcohol, polyethylene, or steel fibers to concrete increases the punching shear resistance of regular reinforced concrete. Their research determined that depending on the amount of fibers that were added to the mix, the concrete tensile strength could increase anywhere from 15% to as high as 100%; the highest increase was obtained by using steel fibers. It was also determined that when 1.75% to 2.00% by volume of fibers were added to the mix, the specimens experienced little to no spalling on the face of the specimen when large deformations were applied. Coughlin et al. (2009) conducted tests on concrete traffic barriers. The barriers were tested by placing an explosive near the concrete traffic barrier. The concrete barriers were constructed with different fiber volumes and different types of fibers; nylon, carbon, and synthetic/steel fibers were used. The results of their study were that the fibers increased the performance of typical reinforced concrete barriers; performance was defined by the author as reducing the damage, keeping the damaged concrete more intact, and reducing the amount of spalling. Their research found that the concrete with 3.8% fiber content performed as well as the 5.0% concrete showing that there is little increase in the performance with an increase in the fiber content.

Altoubat et al. (2007) tested reinforced concrete beams with macrosynthetic fibers and a span to depth ratio of 3.5; the beams contained no shear reinforcement. Their tests showed that the fibers improved the first diagonal shear crack strength and the ultimate shear capacity of the beams. The ultimate shear capacity increased anywhere from 12% up to 25% depending on the dosage of fibers in the concrete. Using embedded strain gauges they were also able to determine that the additional fibers increased the effectiveness of the concrete to evenly distribute the load. The fibers also improved the postdiagonal cracking stiffness and the toughness of the concrete beams and decreased the brittleness of the concrete during shear failure.

Behnood and Ghandehari (2009) conducted a study on the effects of high temperature on the strength of concrete with polypropylene fibers. The compressive strength of the concrete with fibers was higher than without fibers. As the temperature of the concrete increased, the compressive and tensile strengths decreased. As the temperature in the concrete increase to 100°C, the researchers were able to determine that the percentage of fibers was important: three different dosages were used and of the three dosages of 1.7, 3.4, and 5.1 lbs. per cubic yard, the dosage of 3.4 lbs. per cubic yard had the highest residual compressive strength after heating the specimen to 100°C. The lower performance of the other dosages is due to deterioration of the cement paste and a higher volume of voids.

Lan et al. (2004) conducted full scale blast experiments on 74 different concrete panels; the panels were tested with an amount of bare high explosives ranging between 18 lbs. and 220 lbs. at a standoff distance of 16.4 ft. Some of their panels were made from FRC by using two types of commercially available steel fibers; 0.5%, 1.0%, and 1.5%

fiber concentrations by volume were used in the concrete mix. Type A fibers had enlarged ends and were 0.75 in. long; type B fibers were hooked-ended fibers and two different lengths of type B fibers were used: 1.2 in. long and 2.4 in. long. The panels with the longer fibers performed better in resisting cracking and spalling of the concrete due to the blast load than the shorter fibers. Their test results also showed that adding 1.0% of fibers by volume was the optimum volume of fibers for protecting the concrete panels from the blast forces.

Wu et al. (2009) tested three concrete panels, two with Ultra High Performance Fiber Concrete (UHPFC) and one typical reinforced concrete panel; the panels were tested with a unidentified explosive of weights from 2.2 lbs. to 97.2 lbs. and standoff distances from 2.5 ft. to 9.8 ft. UHPFC has small steel fibers that are mixed in with the concrete at the time of batching; the authors do not mention the percentage of fibers by volume or the size and properties of the fibers. Of the two panels that were made from UHPFC, one panel contained reinforcement and the other panel contained no reinforcement other than the small steel fibers. The UHPFC panel with no reinforcement suffered less damaged than the typical reinforced concrete panel. The UHPFC panel that contained reinforcement performed the best of all the panels that were tested in their research.

### 1.4. Fiber Reinforced Polymer Laminates

Fiber reinforced polymers laminates have been shown to strengthen and stiffen structures. This section is concerned with work that has been published on various types of fiber reinforced polymer laminates used to improve the blast resistance of structures. Two important considerations in the design of a structure to resist blast loads are: (1) prevention of catastrophic failure (2) prevention of projectile-induced damage due to

fragmentation. The flexible nature of FRP laminates, their light weight, and ease of installation has led to an increased interest in how FRP laminates can improve the performance of a structure subjected to blast loads.

Razaqpur et al. (2006) conducted a study of reinforced concrete panels subjected to blast load with some of the panels reinforced with GFRP laminates. The laminates were applied externally in a crucifix form on the panels. The results from the study concluded that when a control and GFRP retrofitted panel were subjected to a blast load of 49 lbs. of ANFO at a standoff distance of 10 ft., the GFRP panel performed significantly better in residual strength than the control panel; this panel performed better because the postblast strength of the panel was 75% higher than that of the companion unretrofitted panel. In some cases the panel with GFRP laminates performed better than the control panels but in one case the panel with GFRP laminates completely disintegrated. Because of the decrease in performance of the GFRP panel that was subjected to a larger blast force it was difficult to draw a strong conclusion about the blast mitigation effectiveness of GFRP laminates.

Maji et al. (2008) conducted full scale blast tests on masonry walls shaped similar to a 20 ft. by 12 ft. mailroom. The east and west walls were 12 ft. long and the north and south walls were 20 ft. long. Instead of internal steel rebar reinforcement different quantities of GFRP laminates were placed on the wall surfaces, outside of the building. The walls were 13 ft. tall and made from 6 in. X 16 in. X 8 in. hollow masonry units and were tied together at the four corners. The charge, 2 lbs. of equivalent TNT, was placed at the center of the room on a table that was 2.5 ft. off the ground; the standoff distance varied depending on which wall was under consideration and was either 10 ft. for the

north and south walls or 6 ft. for the east and west walls. Two different types of GFRP fabrics were used: SikaWrap Hex 100 G, a unidirectional fabric, and SikaWrap Hex 106 G, a bidirectional fabric. Ten layers of the SikaWrap Hex 100 G were applied to a subset of the walls and 5 layers of SikaWrap Hex 106 G were applied to the remaining walls. The east and west walls had both types of laminates on each half of the wall. Maji et al. (2008) were able to determine that if the GFRP laminates are designed correctly, they could be an effective material in containing the forces generated by a blast load.

Muszynski and Purcell (2003) tested a bidirectional E-glass fabric as a retrofit on reinforced concrete walls and columns on a structure. The E-glass was subjected to large blast from relatively small standoff distances. Each blast was approximately 860 kg of TNT and the standoff distance on average was 15 m. It was concluded that the pressures caused by the blast should have catastrophically destroyed the structure; the columns failed but the wall did not fail even though it had suffered large displacements.

Lawver et al. (2003) tested the blast resistance of 20 ft. long reinforced concrete bridge decks. Four types of bridge decks were built: a typical reinforced deck, a deck built to current blast resistant standards, typical reinforced deck with carbon fiber reinforced polymer (CFRP) laminates, and a typical reinforced deck with GFRP laminates. The bridge decks were placed on columns to simulate a bridge deck section and a blast (weight and standoff distance was not reported) was placed below the deck. Their goal was to develop a simple model that could predict the behavior of panels using these overlays. Their full scale tests validated their simulation models and proved that composite retrofits could perform as well as current blast resistant standards.

Mosalam and Mosallam (2001) conducted research on reinforced concrete two-way slabs subjected to blast with CFRP laminates; one slab was not reinforced with CFRP laminates and the other slab was strengthened using CFRP laminates. Their research concluded that by adding the CFRP laminate system to a two-way slab system resulted in a 200% increase in load carrying capacity; the maximum displacement was also reduced by 40% to 70% when compared to the slab without CFRP laminate. They also determined that the CFRP laminates reduced the frequency of vibration of the slab and the damage in the slab.

Hosur et al. (2001) conducted a study to determine the effects that high strain rates have on the compression capacity of CFRP laminates. The samples were tested using a modified split Hopkinson Pressure Bar to apply a simple dynamic load on each specimen. Their research showed that the dynamic response of the laminates is highly dependent on the loading direction and the layup of the laminate. They tested specimens with a load that was applied through the thickness of the laminate and a load that was applied in the same plane as the laminates; it was determined that the strains at peak stress are three to four times higher when the load was applied to the laminates through the thickness. Finally, in all cases the stiffness increased as the strain rate increased in the laminates.

Silva and Lu (2006) conducted blast tests on one-way reinforced concrete slabs. The slabs were either covered with (CFRP) or steel fiber reinforced polymer (SRP) laminates; one of each slab type was covered only on one side and another of that same slab type was covered on both sides. The slabs were then tested at various standoff distances and varying weight of desensitized RDX which is a high explosive; the weights and distances were not disclosed in the research. The slabs that were only covered with the laminate on

one side were severely damaged by the blast. The slabs that were covered with the laminate on both sides displayed significant increase in blast resistance when compared to the panels that only had the laminate on one side; the slabs failed under concrete shear failure. The authors recommended that concrete slabs should be laminated on both sides; the two types of laminates performed the same when compared; the SRP laminate is much cheaper than the CFRP laminates thus being the economically better choice.

### 1.5. GFRP Bars

No studies were found that examine the performance of GFRP bars used as reinforcement in concrete to mitigate the effects of a blast in the open literature.

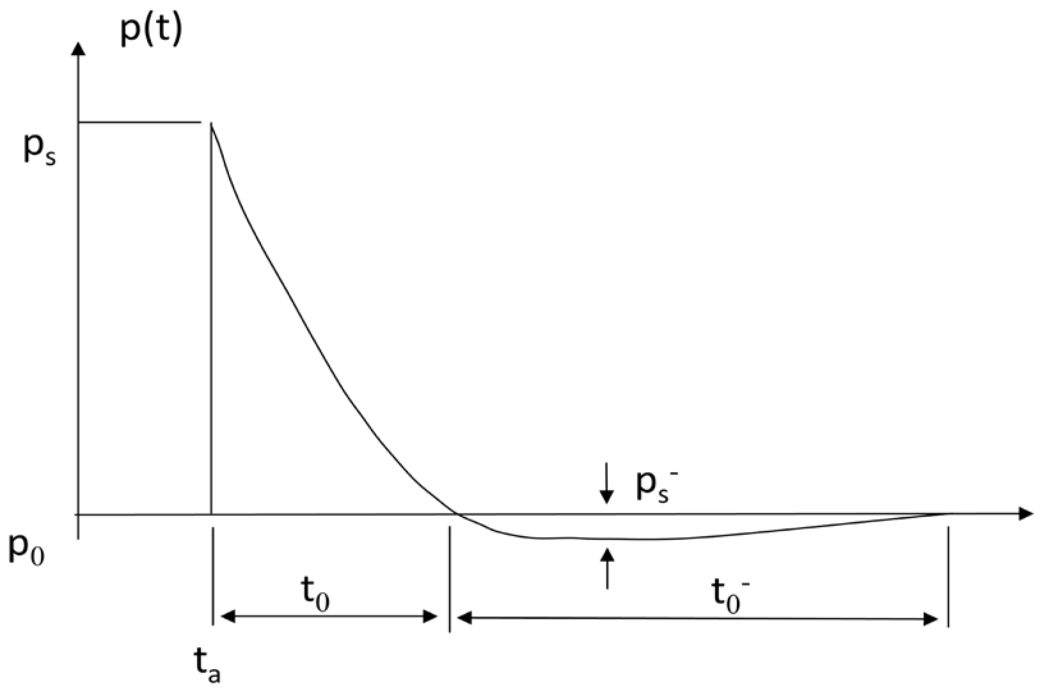


**Figure 1.1 Typical pressure-time diagram for a blast wave**

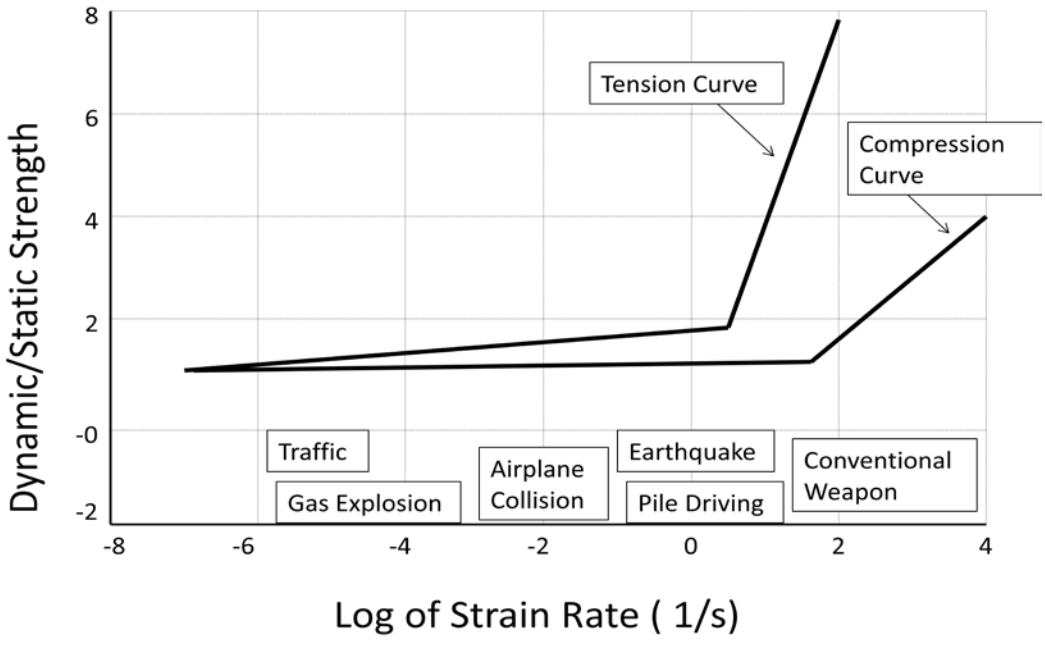


**Figure 1.2 Normalized concrete strength as a function of the strain rate**

# 2. PROJECT SCOPE

## 2.1. Purpose

The purpose of this research is to provide experimental data and observations that can be used to investigate the behavior of concrete structures subjected to blast loading.

## 2.2. Concrete Panel Experiments

This portion of the research is comprised of 4 ft. X 4 ft. concrete panels of different thickness and reinforcement types. The reinforcement types used were: 1) steel rebar, 2) mixed in macrosynthetic fibers, 3) GFRP rebar, and 4) GFRP composite laminates. The different thicknesses were 6, 10, and 14 in. thick. From these different reinforcements and thicknesses 20 panels were made and then subjected to a blast load that was generated by either C4 or ANFO. The weight of the explosive increased as the thickness of the panel increased.

The panels that survived the blast testing were then tested with a hydraulic actuator; the panels were loaded until failure. During this testing each concrete panel was tested one at a time and the force and displacement were measured. The load was measured by the load cell built into the hydraulic actuator and the displacement was measured with a linear variable displacement transducer attached to the bottom side in the center.

## 2.3. Project Objectives

This project will be used to further develop the understanding of how concrete and various reinforcement materials interact during a blast. To develop this understanding full scale testing was done to determine the following objectives:

1. Determine the performance of reinforced concrete panels that use materials pertaining to new construction and materials that pertain to rehabilitating existing concrete walls.
2. Determine the effects of the below variables:
    a. Wall thickness.
    b. Type of concrete in particular normal weight concrete (NWC) and fiber reinforced concrete (FRC).
    c. Internal and external reinforcement types, spacing, and reinforcement ratio. The types of reinforcement in particular are: steel rebar, glass fiber reinforced polymer (GFRP) bars, and GFRP composite laminates under blast loads.
    d. Reinforcement spacing and ratio.
3. Determine the performance of blast damaged panels when subjected to a hydraulically applied load.
4. Determine the tensile strength of FRC and NWC cylinders using the method outlined in, ASTM C 496/C 496M – 04 (ASTM 2004) Standard Test Method for Splitting Tensile Strength of Cylindrical Concrete Specimens.
5. Determine a performance level for each type of panel that is related to the damage of the panel that is caused by the blast.

6. Analytical predictions for capacity of panels under blast loads and postblast static loads.

Chapter 3 defines the specimens, test setup, and instruments used to record data. Chapter 4 explores the experimental results of the research. Chapter 5 defines analytical models developed to explore the analytical results. Chapter 6 summarizes the findings and the conclusions of this research.

## 2.4. Limitations

This project was conducted under a larger project that is supported by Idaho National Laboratory (INL). Their objectives are to develop better finite element models to predict the behavior of reinforced concrete during a blast load. The University of Utah does not have the means to do extensive finite element modeling as INL is able to. Because of this the University of Utah has different objectives than INL.

# 3. EXPERIMENTAL INVESTIGATION

## 3.1. Test Setup

3.1.1 Idaho National Laboratory (INL). Explosive testing was conducted at the National Security Testing Range (NSTR) on the INL property west of Idaho Falls, Idaho. The panels were constructed at Hanson Structural Precast in Salt Lake City and transported to Idaho Falls. During testing, the concrete panels were arranged in a square pattern with a centrally located charge, as shown in Figure 3.1. One panel was placed on each of three sides of the square layout, while the fourth side was left open for working space. The layout provided an equal standoff distance from the center of the explosive to the face of each panel. The panels were placed on the ground and two concrete blocks measuring 2 ft. X 2 ft. X 6 ft. were placed on each side behind each specimen to provide a one-way simply support system for the panel, as shown in Figure 3.2. A chain was attached to the blocks and wrapped around the top half of the panels to prevent the panel from falling forward and causing additional damage following the blast. The charge (C4 or ANFO) was placed on a small wooden table at the center of the test layout with the height adjusted to position the explosive at the midheight of the specimen.

A flexible mylar break screen, located at the bottom of the table holding the explosive, acted as the trigger for the data acquisition system. The break screen works by passing a current through a printed continuous conductive circuit that is laminated between two pieces of mylar plastic. The force of the explosive breaks the continuous

circuit and once the current stops the data acquisition system is triggered to start recording.

Twenty panels were constructed for blast testing and are described in more detail in Section 3.5; a summary of each panel type is shown in Table 3.1. A series of nine blast tests were carried out, in which 18 panels were tested. Two of the original 20 panels were not tested for blast loads because of budget and time constraints. C4 was originally planned for each test but quantities were limited and ANFO was used as a substitute at an equivalent amount. Blasts varied in charge size depending on the thickness of the panels being tested. Table 3.2 summarizes the following information for each panel: panel type, date of blast, standoff distance, type of charge, weight of charge, and weight of charge expresses as a mass of equivalent TNT.

3.1.2 University of Utah. Postblast strength testing of the panels was conducted at the University of Utah, in Salt Lake City. The panels were loaded into a steel frame containing a Material Testing Systems (MTS) hydraulic actuator positioned at the center of each panel; the panel was supported by two concrete blocks one on each side; between the concrete panels and the concrete support blocks an elastomeric pad that was 6 in. X 48 in. X 1 in. was used, as shown in Figures 3.3 and 3.4. The straps were added for extra safety to capture the panel in case it broke into pieces during the test.

## 3.2. Data Acquisition System

3.2.1 INL system. INL used a National Instruments PXI system to record strain, acceleration, and pressure during the blast. The system was powered by generators and an uninterruptable power supply as a backup. Data from accelerometers and free-field blast pressure transducers were digitized at $10^5$ data points per second. Data from strain gauges

were digitized at $10^4$ data points per second. INL supplied all this instrumentation and the instrumentation varied greatly from test to test depending on what was available. The accelerometers had a nominal maximum capability to record from 5g to 5000g. The free field blast pressure transducers had a nominal maximum capability to record from 5 psi to 500 psi.

During testing two Phantom V7.1 computer controlled high speed cameras were used, which had the capability to record anywhere between 250,000 frames per second up to 1,000,000 frames per second. The cameras were placed away from the blast at a safe distance and protected from fragmentation by bullet proof glass. One camera was placed to record the back of a panel and the other was placed to record the entire blast setup. The camera recording the back of the panel was able to capture the panel as it cracked. The camera recording the entire setup showed the blast wave hitting each panel and how the pressure waves moved through the air.

3.2.2. University of Utah system. During the postblast testing the University of Utah used MTS hardware to control the hydraulic actuator capable of applying a compressive load of 500 kips. Loading was displacement controlled at a rate of 0.125 in. per minute. Strain gauges were installed in each panel and on the external face of each panel for blast testing at INL as shown in Figure 3.2; the gauges that were still in working order when the panels were returned to the University of Utah for postblast testing were used to record data digitized at two points per second. A linear variable differential transformer (LVDT) was attached at midspan of the panel to measure vertical deflection. A Vishay micro-measurement system was used to record strain and LVDT data; LVDT data was also digitized at two points per second.

## 3.3. ConWep Predictions

The free field blast pressure transducers that were used during the experiments were placed further from the center of the blast than the front face of the panels. This was done because the pressure gauges on earlier tests reached their maximum capacity and the data points were cut off, requiring the location to be moved further from the center of the blast to reduce the pressure. Because the pressure transducers were not at the same distance from the blast as the front face of the panel, predictions were needed to estimate the blast pressure the panels experienced. To make these predictions the Army Corps of Engineers has developed a program known as Conventional Weapon Effects (ConWep). This program is based from the application of TM 5-855-1, 'Fundamentals of Protective Design for Conventional Weapons', a document that was developed by the Army Corps of Engineers before the development of computer programs.

Access to ConWep is strictly regulated and allowed for government officials that meet the requirements. Idaho National Laboratory has access to ConWep and was able to provide predicted pressure on the face of the panels for each blast. The program requires the following variables: environmental conditions, charge type and weight, and standoff distance; these variables are summarized in Table 3.2. Table 3.3 is the predicted charge pressure for each panel from ConWep.

## 3.4. Materials

3.4.1. Concrete. Two types of concrete mixes were used in this project: (i) normal weight concrete (NWC) and (ii) NWC with the addition of macrosynthetic fibers referred to herein as fiber reinforced concrete (FRC). Fifteen pounds of the 2 in. long polypropylene fibers per cubic yard of concrete was used in the FRC mixture, which

resulted in 1% of fibers by volume in the concrete mixture. The fibers were added to NWC while the concrete was mixing in the concrete mixer and allowed to mix for a minimum of 5 minutes.

The concrete was all mixed at the onsite concrete plant at Hanson Structural and Precast yard in Salt Lake City, Utah. Since a large amount of concrete was needed to create the number of specimens required by this research a series of three different batches were mixed, over a period of 2 weeks. The first batch was FRC and panel types B, C, and CON-5 were cast at this time, with a water to cement ratio of 0.46. The second batch was NWC and panel types A, D, and E were cast at this time; the water to cement ratio of this batch was 0.47. It is important to note that there was more water in the FRC mixture than the NWC mixture. The final batch was for the remaining CON specimens; the water to cement ratio of this batch was 0.453. Multiple 4 in. diameter by 8 in. long and 6 in. diameter by 12 in. long concrete cylinders were created from the first two batches for material testing purposes; the cylinders were made according to the American Society for Testing Materials (ASTM 2010) procedure C31 / C31M -10 Standard Practice for Making and Curing Concrete Test Specimens in the field. The average static 28 day compressive strength of NWC was 7,400 psi and 6,600 psi for the FRC. The average static tensile strength of NWC was 587 psi and 619 psi for the FRC. Testing procedures used to determine the compressive and tensile strengths are discussed in detail in Section 4.8.

3.4.2. Reinforcing bars. Steel and GFRP reinforcing bars were used in this research. The steel bars were a standard grade 60 rebar with a nominal tensile strength of 60 ksi and a modulus of elasticity of 29,000 ksi. The #5 GFRP bars had a tensile strength of 104

ksi and a modulus of elasticity of 6,280 ksi, for the specific lot of the bars used for this research; the #3 GFRP bars had a guaranteed tensile strength of 110 ksi and a modulus of 5,920 ksi. The GFRP properties were provided by Hughes Brothers who manufactures the GFRP bars.

3.4.3. GFRP composite fabric. SikaWrap Hex 100 G unidirectional glass fabric was adhered to both sides of panel Type E. The fabric has a tensile strength of 330 ksi and a modulus of elasticity of 10,500 ksi. The fabric weighed 27 ounces per square yard with a nominal thickness of 0.014 inches. Sikadur 300, a high-modulus high-strength impregnating two part epoxy was used to attach the GFRP composite fabric to the concrete. The epoxy was allowed to fully cure at least 7 days.

Sika USA assisted with the installation of the GFRP overlays. To install the fabric, the panels were first prepared using a diamond tipped grinder to create a rough surface. The Sikadur 300 resin was mixed for 5 minutes, and each side of the panel was painted with a thin coat of resin. The fabric was then cut to size and impregnated with the resin until the fabric was completely saturated. Once the fabric was fully saturated, it appeared to transmit light through itself. The fabric was applied to each side and pressed firmly to the concrete; a squeegee was used to help adhere the fabric to the panel and remove any excess resin. Two layers of fabric were applied to each side; the layers were applied perpendicular to each other, one at zero deg. and one at 90 deg. with respect to the horizontal axis.

3.4.4. Macrosynthetic fibers. Enduro 600 Macro-Synthetic Fibers manufactured by Propex was used in the FRC. The fibers are 2 in. long, made of polypropylene, and have a unique sinusoidal wavelike shape that increases the anchorage of the fiber in the

concrete, as shown in Figure 3.5. The fibers have a tensile capacity of 49 ksi and a modulus of elasticity of 435 ksi and a specific weight of 0.91.

### 3.5. Specimen Details

Twenty 4.0 ft. square wall panels were built with various reinforcement types and thicknesses. Specimens were built in April 2010 and Figure 3.6 shows the panels being constructed.

Five different types of concrete panels were constructed: Type A panels were NWC and contained steel rebar, Type B panels were only FRC and contained no additional reinforcement, Type C panels were FRC with steel rebar, Type D panels were NWC and contained GFRP bars, and Type E panels were NWC and contained steel rebar and two layers of GFRP overlays applied externally as a rehabilitation method on each side of the panel, before the panel was tested. Three panels were constructed from each panel type using three thicknesses: 6 in., 10 in., and 14 in. Five control (CON) panels were constructed to calibrate the testing equipment and standoff distance. The CON panels were 6 in. thick Type D panels. Table 3.1 includes a summary of each specimen.

Rebar mats were constructed for each panel type, except panel Type B which contained no reinforcement other than the synthetic fibers included in the FRC. Each panel contained two mats, with varied rebar spacing and size. In panel types A, E and CON, the rebar was spaced at 12 in. on center; in panel types C and D the rebar was spaced at 6 in. on center. The size of the bar increased as the panel thickness increased; the 6 in., 10 in., and 14 in. panels used a No. 3, No.4, and No.5, rebar, respectively. Panel type D did not follow this convention; instead a No.5 bar spaced at 9 in. was used in panel D4-10 instead of the above prescribed No.4 bar; the 9 in. spacing was used because

obtaining No.4 GFRP bars was difficult, and the spacing was adjusted to maintain as close as possible a constant reinforcement ratio. The clear cover to the mats was approximately 1 in. Figure 3.7 shows an example of the rebar layout for panel types C and D. The reinforcement ratio was calculated for each panel type according to the following: (i) the American Concrete Institute (ACI) 318 – 08 (ACI 318 2008) Building Code and Commentary for the panels with steel rebar; (ii) the ACI Committee 440.2 R-08 (ACI 440.2 2008) Guide for the Design and Construction of Externally Bonded FRP Systems for Strengthening Concrete Structures for the panels with GFRP composite laminates; and (iii) the ACI Committee 440.1 R-06 (ACI 440.1 2006) Guide for the Design and Construction of Structural Concrete Reinforced with FRP Bars for the panels with internal GFRP bars. Table 3.5 summarizes each reinforcement ratio for each panel. The reinforcement in the transverse direction and the longitudinal direction is equal and thus only one reinforcement ratio is listed for each.

Internal strain gauges were installed at the center of the rebar mat. On each mat, one gauge was installed in the horizontal x-direction and one in the vertical y-direction (perpendicular to x-direction), for a total of two gauges per mat and four gauges per panel. Figure 3.8 shows how the strain gauges were installed on a specimen with steel rebar as reinforcement. The grey paste is a protective covering for the gauges. In addition to the internal strain gauges, two external concrete strain gauges were installed on the exterior face of each test panel away from the blast, as shown in Figure 3.2.

Fifteen 2 ft. X 2 ft. specimens with the same varying thickness and reinforcement details as the 4 ft. X 4 ft. panels were also built to test the resistance of reinforced concrete to a high speed projectile. This is not covered in this thesis, but because the

panels were designed and built at the same time as the 4 ft. square wall panels a summary is provided. The 2 ft. square panels were created using the same reinforcement and details as the 4 ft. square wall panels. Table 3.6 shows a summary of the projectile panels. None of the 2 ft. square specimens contained strain gauges.

**Table 3.1 Summary of blast panels**

| 4 ft. X 4 ft. panels | | Thickness | | |
|---|---|---|---|---|
| Notation | Type | 6 in. | 10 in. | 14 in. |
| A4 | Plain Concrete with Steel Rebar | #3 @ 12" A4-6 | #4 @ 12" A4-10 | #5 @ 12" A4-14 |
| B4 | Concrete with Macrosynthetic Fibers Only | No Rebar B4-6 | No Rebar B4-10 | No Rebar B4-14 |
| C4 | Concrete with Macrosynthetic Fibers and Steel Rebar | #3 @ 6" C4-6 | #4 @ 6" C4-10 | #5 @ 6" C4-14 |
| D4 | Concrete and GFRP Rebar | #3 @ 6" D4-6 | #5 @ 9" D4-10 | #5 @ 6" D4-14 |
| E4 | Concrete Steel Rebar and 2 layers of GFRP Jacket on each face | #3 @ 12" E4-6 | #4 @ 12" E4-10 | #5 @ 12" E4-14 |
| CON | Control Panels with GFRP Rebar | #5 @ 12'' CON - 1 | N/A | N/A |
| CON | Control Panels with GFRP Rebar | #5 @ 12'' CON - 2 | N/A | N/A |
| CON | Control Panels with GFRP Rebar | #5 @ 12'' CON - 3 | N/A | N/A |
| CON | Control Panels with GFRP Rebar | #5 @ 12'' CON - 4 | N/A | N/A |
| CON | Control Panels with Only Fibers | CON - 5 | N/A | N/A |

**Table 3.2 Characteristics of blast for each panel**

| Panel | Date of Blast | Standoff Distance (in.) | Type of Charge | Weight of Charge (lbs.) | Equivalent Weight of TNT (lbs.) |
|---|---|---|---|---|---|
| A4-6 | 9/28/2010 | 40.0 | C4 | 10.0 | 13.7 |
| A4-10 | 10/27/2010 | 38.0 | ANFO | 34.0 | 29.2 |
| A4-14 | | | | | |
| B4-6 | 9/29/2010 | 40.0 | C4 | 10.0 | 13.7 |
| B4-10 | 9/29/2010 | 40.0 | C4 | 21.0 | 28.8 |
| B4-14 | | | | | |
| C4-6 | 9/28/2010 | 40.0 | C4 | 10.0 | 13.7 |
| C4-6 | 9/30/2010 | 41.0 | C4 | 10.0 | 13.7 |
| C4-10 | 10/27/2010 | 38.0 | ANFO | 34.0 | 29.2 |
| C4-14 | 10/28/2010 | 38.0 | ANFO | 34.0 | 29.2 |
| D4-6 | 9/30/2010 | 41.0 | C4 | 10.0 | 13.7 |
| D4-10 | 10/27/2010 | 38.0 | ANFO | 34.0 | 29.2 |
| D4-14 | 10/28/2010 | 38.0 | ANFO | 34.0 | 29.2 |
| E4-6 | 9/29/2010 | 40.0 | C4 | 10.0 | 13.7 |
| E4-10 | 9/29/2010 | 40.0 | C4 | 21.0 | 28.8 |
| E4-14 | 10/28/2010 | 38.0 | ANFO | 34.0 | 29.2 |
| CON-1 | 9/29/2010 | 40.0 | C4 | 10.0 | 13.7 |
| CON-2 | 9/27/2010 | 120.0 | C4 | 12.0 | 16.4 |
| CON-2 | 9/28/2010 | 120.0 | C4 | 25.0 | 34.3 |
| CON-2 | 9/28/2010 | 40.0 | C4 | 1.25 | 1.7 |
| CON-3 | 9/28/2010 | 40.0 | C4 | 10.0 | 13.7 |
| CON-4 | 9/29/2010 | 40.0 | C4 | 21.0 | 28.8 |
| CON-5 | 9/30/2010 | 41.0 | C4 | 10.0 | 13.7 |

**Table 3.3 ConWep predictions**

| Panel | Type of Charge | Blast Pressure CON-WEP (psi) | Blast Force (kip) |
|---|---|---|---|
| A4-6 | C4 | 447.3 | 1031 |
| A4-10 | ANFO | 798.4 | 1840 |
| A4-14 | Not Tested | | |
| B4-6 | C4 | 447.3 | 1031 |
| B4-10 | C4 | 704.3 | 1623 |
| B4-14 | Not Tested | | |
| C4-6 | C4 | 447.3 | 1031 |
| C4-6 | C4 | 426.4 | 982 |
| C4-10 | ANFO | 798.4 | 1840 |
| C4-14 | ANFO | 798.4 | 1840 |
| D4-6 | C4 | 426.4 | 982 |
| D4-10 | ANFO | 798.4 | 1840 |
| D4-14 | ANFO | 798.4 | 1840 |
| E4-6 | C4 | 447.3 | 1031 |
| E4-10 | C4 | 704.3 | 1623 |
| E4-14 | ANFO | 798.4 | 1840 |
| CON-1 | C4 | 447.3 | 1031 |
| CON-2 | C4 | 46.99 | 108 |
| CON-2 | C4 | 82.08 | 189 |
| CON-2 | C4 | 103.0 | 237 |
| CON-3 | C4 | 447.3 | 1031 |
| CON-4 | C4 | 704.3 | 1623 |
| CON-5 | C4 | 426.4 | 982 |

**Table 3.4 Reinforcement material properties**

| Material | Tensile Capacity (ksi) | Modulus of Elasticity (ksi) |
|---|---|---|
| Steel Rebar | 60 | 29,000 |
| #5 GFRP Bar | 104 | 6,280 |
| #3 GFRP Bar | 110 | 5,920 |
| Macro-Synthetic Fibers | 49 | 435 |
| GFRP Overlays | 88.8 | 3,791 |

**Table 3.5 Reinforcement ratio**

| Specimen | Reinforcement | Reinforcement Ratio (%) |
|---|---|---|
| A4-6 | No. 3 Steel Rebar at 12 in. | 0.199 |
| A4-10 | No. 4 Steel Rebar at 12 in. | 0.192 |
| A4-14 | No. 5 Steel Rebar at 12 in. | 0.207 |
| B4-6 | Only Synthetic Fibers | No Bar Reinforcement |
| B4-10 | Only Synthetic Fibers | |
| B4-14 | Only Synthetic Fibers | |
| C4-6 | No. 3 Steel Rebar at 6 in. and Synthetic Fibers | 0.398 |
| C4-10 | No. 4 Steel Rebar at 6 in. and Synthetic Fibers | 0.385 |
| C4-14 | No. 5 Steel Rebar at 6 in. and Synthetic Fibers | 0.413 |
| D4-6 | No. 3 GFRP bars at 6 in. | 0.398 |
| D4-10 | No. 5 GFRP bars at 9 in. | 0.382 |
| D4-14 | No. 5 GFRP bars at 6 in. | 0.413 |
| E4-6 | No. 3 Steel Rebar at 12 in. and GFRP Laminates | 0.199 |
| E4-10 | No. 4 Steel Rebar at 12 in. and GFRP Laminates | 0.192 |
| E4-14 | No. 5 Steel Rebar at 12 in. and GFRP Laminates | 0.207 |

**Table 3.6 High speed projectile specimens**

| All 2'-0" X 2'-0" slabs | | Thickness (in.) | | |
|---|---|---|---|---|
| Notation | Type | 6 | 10 | 14 |
| A2 | Plain Concrete With Steel Rebar | #3 @ 12" A2-6 | #4 @ 12" A2-10 | #5 @ 12" A2-14 |
| B2 | Concrete with Macro-Synthetic Fibers Only | B2-6 | B2-10 | B2-14 |
| C2 | Concrete with Macro-Synthetic Fibers and Steel Rebar | #3 @ 6" C2-6 | #4 @ 6" C2-10 | #5 @ 6" C2-14 |
| D2 | Concrete and GFRP Rebar | #3 @ 6" D2-6 | #5 @ 9" D2-10 | #5 @ 6" D2-14 |
| E2 | Concrete Steel Rebar and 2 layers of GFRP Jacket on each face | #3 @ 12" E2-6 | #4 @ 12" E2-10 | #5 @ 12" E2-14 |
| CON | Concrete with Only Fibers | CON - 6 | N/A | N/A |
| CON | Concrete and GFRP Rebar | #5 @ 12" CON-7 | N/A | #5 @ 12" CON-9 |
| CON | Concrete and GFRP Rebar | #5 @ 12" CON-8 | N/A | #5 @ 12" CON-10 |
| CON | Concrete and GFRP Rebar | N/A | N/A | #5 @ 12" CON-11 |
| CON | Concrete and GFRP Rebar | N/A | N/A | #5 @ 12" CON-12 |
| CON | Concrete and GFRP Rebar | N/A | N/A | #5 @ 12" CON-13 |

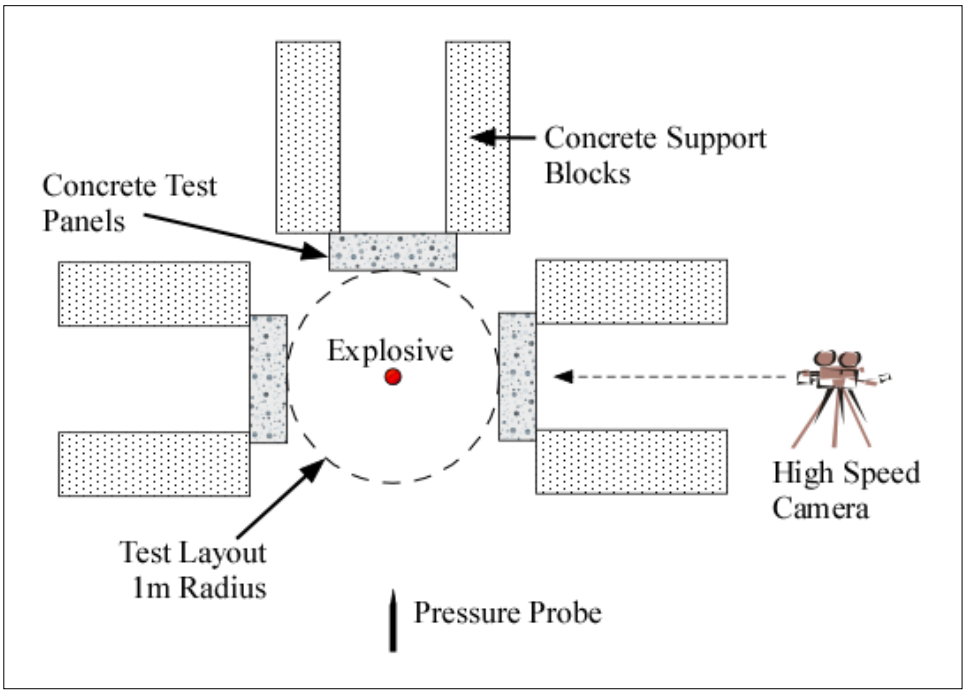


**Figure 3.1 Test layout plan**

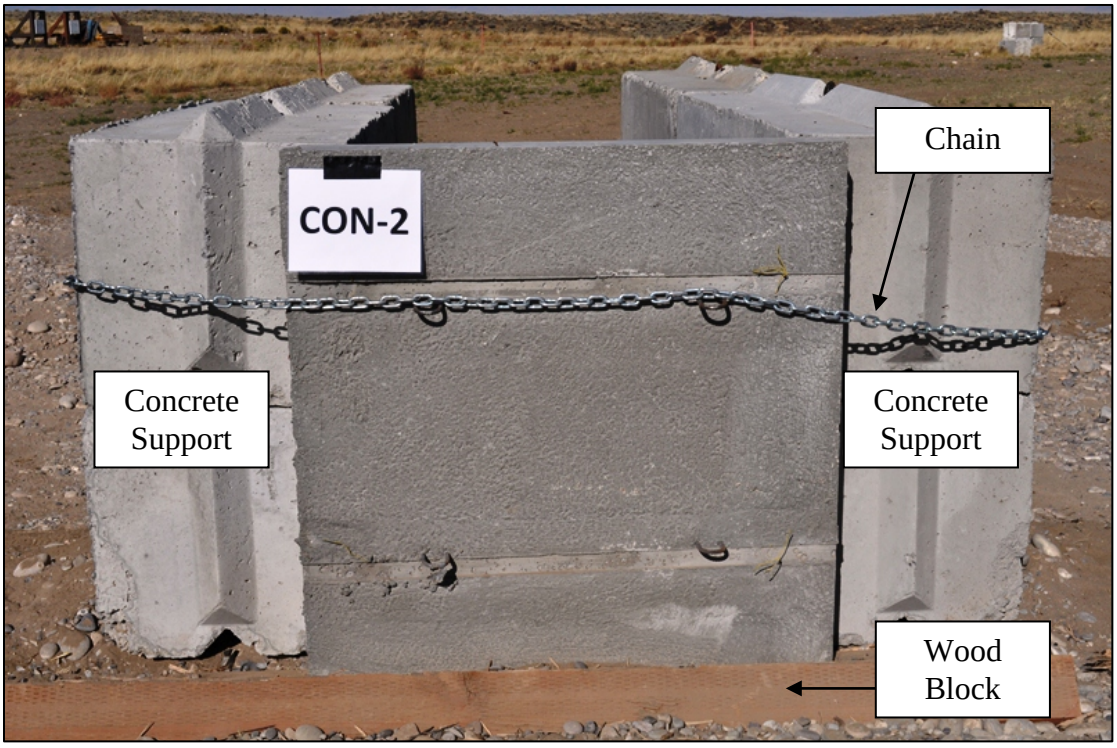


**Figure 3.2 Support details**

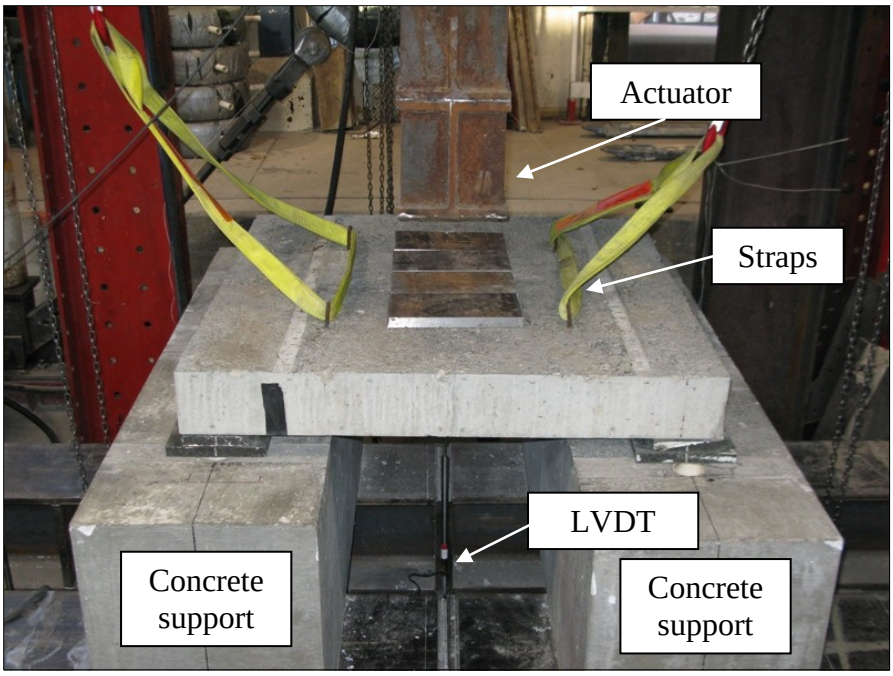


**Figure 3.3 Postblast test setup**

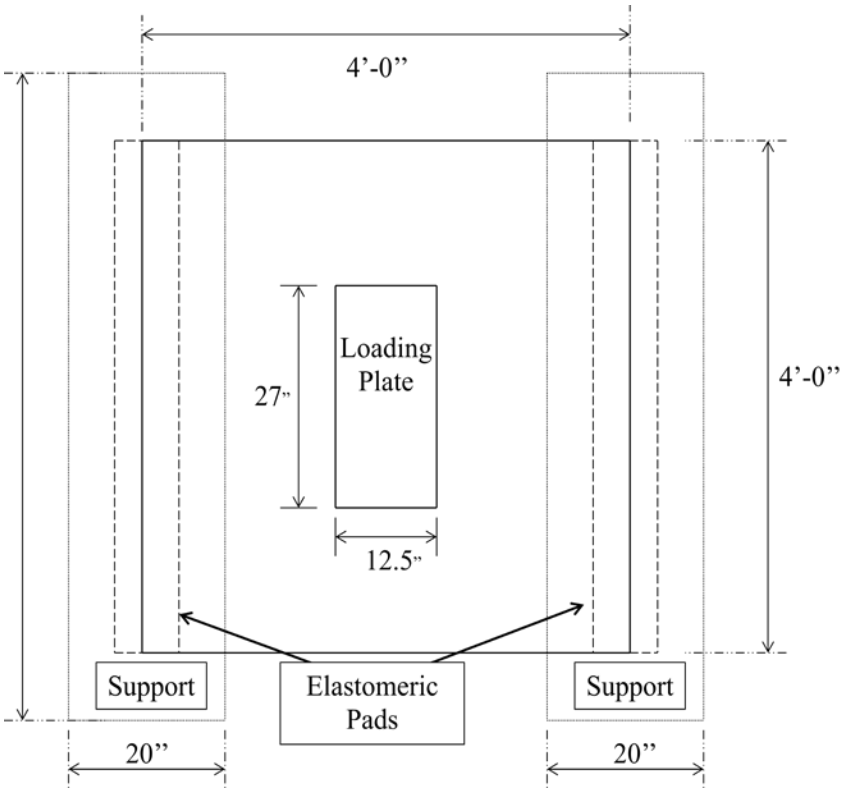


**Figure 3.4 Loading dimensions**

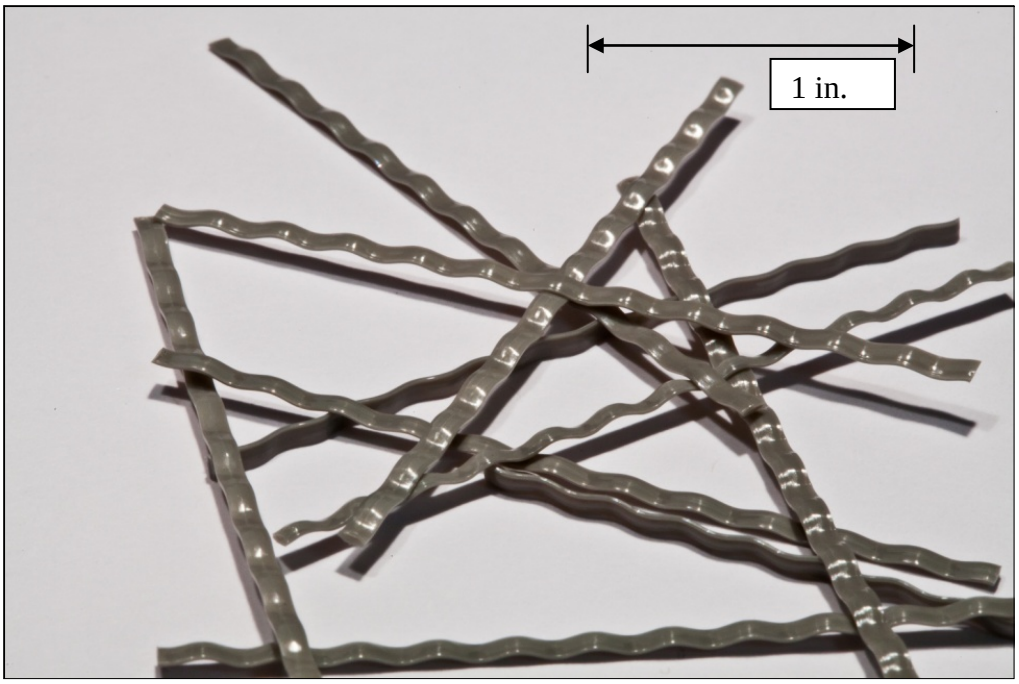


**Figure 3.5 Polypropylene macrosynthetic fibers**

**Figure 3.6 Construction of panels**

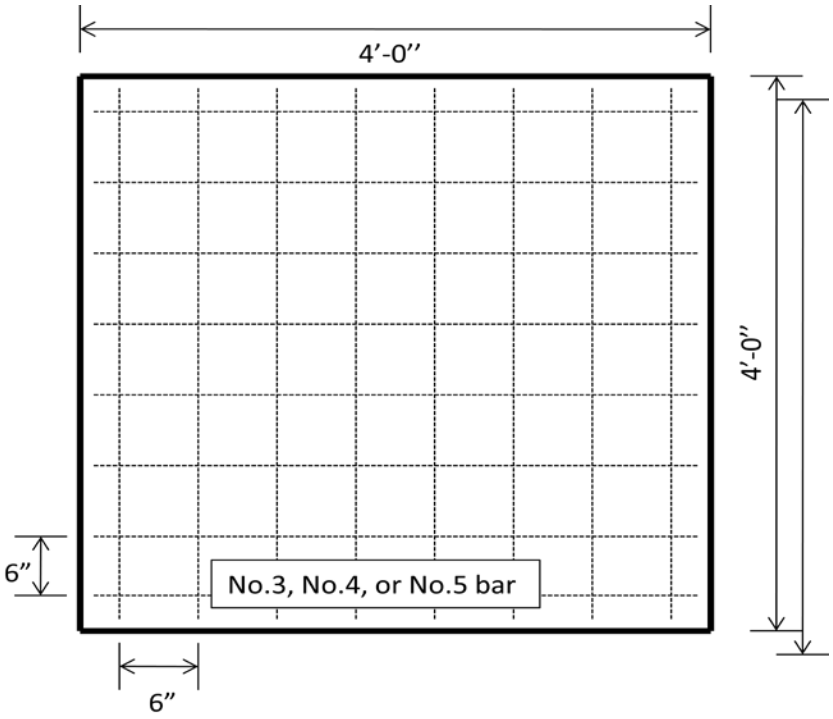


**Figure 3.7 Example rebar layout**

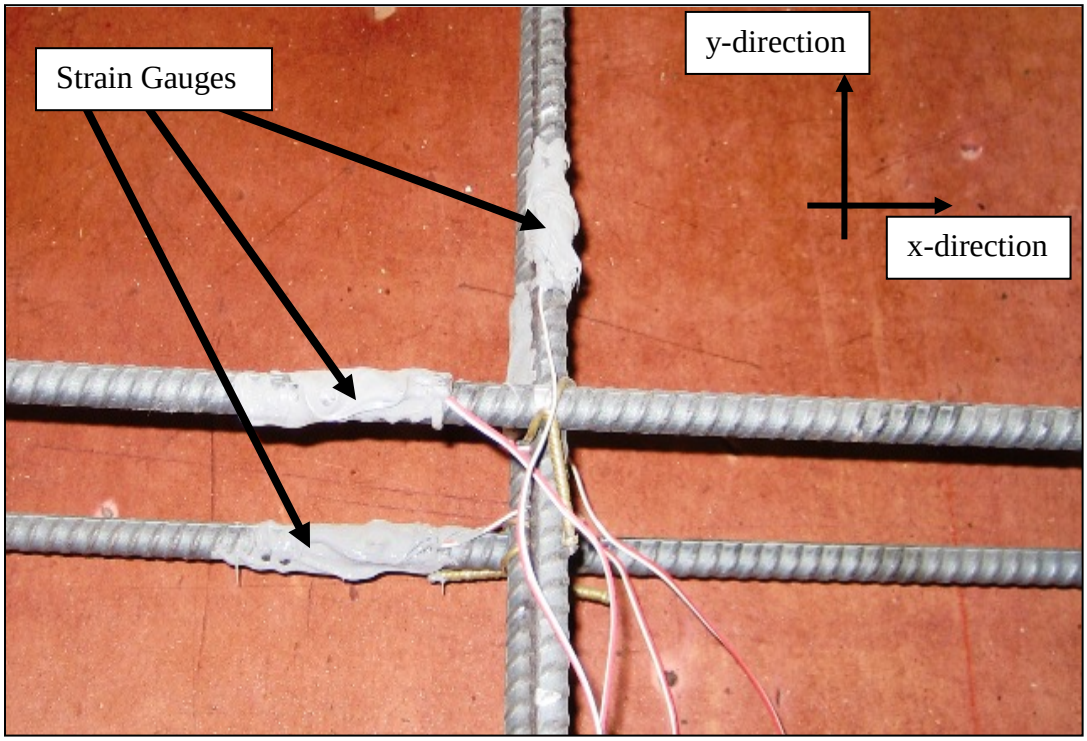


**Figure 3.8 Strain gauge location**

# 4. EXPERIMENTAL RESULTS

## 4.1. Panel Performance

4.1.1. Introduction. Defining the blast load is important for describing the damage from each blast and predicting how a panel will respond. To define a blast load Tedesco (1998) presented a ratio called the normalized standoff distance, shown in Eq. (4.1):

$$Z = \frac{R}{W^{\frac{1}{3}}} \tag{4.1}$$

where Z=normalized standoff distance, R=standoff distance, and W= weight of the explosive charge. This ratio normalizes the blast standoff distance to the weight of the charge. The weight of the charge for this research was presented in equivalent weight of TNT, because two types of explosives were used in testing; the ratios are computed for each panel and listed in each section and in Table 4.1 as a summary. The smaller the value of Z, the greater the damage is expected to be.

4.1.2. Panel type A. Panel type A was designed to replicate a typical reinforced concrete wall that was constructed without any enhancements to resist a blast. Panel A4-6 was tested with 10 lbs. of C4 at a standoff distance of 40 in.; the normalized standoff distance was 1.4. This panel experienced complete loss of structural integrity, as shown in Figure 4.1. The explosion created large spalling of concrete in the center of the panel

and flexural cracks that propagated radially outwards; as a result of the radial cracks, severe damage was caused in the panel and concrete fragmented as shown in Figure 4.2. The explosion also caused large flexural cracking on the side of the panel as shown in Figure 4.3.

Panel A4-10 was tested with 34 lbs. of ANFO at a distance of 38 in.; the normalized standoff distance was 1.0. Because this panel was cracked from the top to the bottom and lost large chunks of concrete it was considered a complete loss of structural integrity, meaning that the panel was so badly damaged the panel can no longer perform its original structural design. This panel experienced two large vertical cracks with an average width of 0.375 in., which separated the panel into thirds; the maximum crack width on this panel was 0.5 in. on the side of the panel. The entire left side of the panel was also damaged heavily near the support; the front of panel A4-10 is shown in Figure 4.4, and the back of the panel is shown in Figure 4.5. The cracks on the back of the panel are located very close to the location of internal reinforcement; Figure 4.6 shows the panel with dotted lines representing the location of the rebar, and the solid lines representing the cracks. The back of the panel was so heavily damaged that the rebar was exposed as shown in Figure 4.7, which also shows the side of the panel where two flexural cracks and one shear crack can be seen. For panel type A it is clear that when the normalized standoff distance is equal to 1.4 the panels are damaged more than when the standoff distance to 1.0; this is caused by the different thicknesses. The 6 in. thick panels are thinner and because of this they have less mass to absorb and distribute the destructive energy caused by the explosion. Therefore they are more heavily damaged. Also, the moment of inertia of the panel is less for the thinner panels than the thicker panels and

the inertia is directly related to the deflection. The more a panel deflects the more damage the panel experienced. A4-14 was not tested because of time and budget c.

4.1.3. Panel type B. This type of panel was designed to determine the effects of the macrosynthetic fibers as the only reinforcement. Panel B4-6 was tested with 10 lbs. of C4 at a distance of 40 in.; the normalized standoff distance was 1.4. The explosion caused the panel to break into two separate pieces, shown in Figure 4.8. Panel B4-10 was tested with 21 lbs. of C4 at 40 in.; the normalized standoff distance was 1.1. The result of the blast for this panel was the same as panel B4-6; the panel was completely broken into two pieces, as shown in Figure 4.9. For panel type B it is clear that panels were easily destroyed by a minimal amount of pressure when compared to the other panel types. Panel B4-14 was not tested because of time constraints.

4.1.4. Panel type C. This type of panel was designed to determine the effects of using the macrosynthetic fibers in addition to traditional steel rebar as reinforcement. Panel C4-6 was tested with 10 lbs. of C4 at a distance of 40 in.; the normalized standoff distance was 1.4. The panel experienced minimal damage as shown in Figures 4.10, 4.11, and 4.12. The crack locations relative to the internal reinforcement can be seen in Figure 4.13, where the dotted lines represent the location of the rebar and the solid lines represent the cracks. The side of the panel experienced a few small radial cracks as shown in Figure 4.14. The largest measured crack width in the panel was 0.04 in. Because the panel was not visibly damaged, it was actually tested a second time with 10 lbs. of C4 at 41 in.; the normalized standoff distance was again 1.4. The panel again experienced minimal damage as shown in Figures 4.15, 4.16, and 4.17. As a result of the second blast, the largest measured crack width was 0.065 in.; thus, the second blast allowed the cracks to

propagate and open only by 0.025 in., while creating only a few new cracks in the specimen. Because the concrete did not crack significantly more by the second explosion the ductility of the steel reinforcement must have carried the additional load from the second blast. The crack locations relative to the internal reinforcement can be seen in Figure 4.18, where the dotted lines represent the location of the rebar and the solid lines represent the cracks.

Panel C4-10 was tested with 34 lbs. of ANFO at a distance of 38 in.; the normalized standoff distance was 1.0. The panel experienced no damage as shown in Figures 4.19, 4.20, and 4.21. The largest measure crack width in the panel was 0.05 in. The blast also caused two radial cracks on the side of the panel approximately 0.050 in. wide, as shown in Figure 4.22. The crack locations relative to the internal reinforcement can be seen in Figure 4.23, where the dotted lines represent the location of the rebar and the solid lines represent the cracks.

Panel C4-14 was tested with 34 lbs. of ANFO at a distance of 38 in.; the normalized standoff distance was 1.0. The panel did not experience significant damage as shown in Figures 4.24, 4.25, and 4.26. The maximum measured crack width was 0.002 in; the crack locations relative to the internal reinforcement can be seen in Figure 4.27, where the dotted lines represent the location of the rebar and the solid lines represent the cracks. Figure 4.28 shows the side of panel C4-14 with no visible cracks.

For panel type C it is clear that when the normalized standoff distance is equal to 1.4 for the 6 in. thick panel it was cracked much more than when the standoff distance was equal to 1.0 for the 10 in. and 14 in. panels; this is again caused by the different

thicknesses, and the fact that the 6 in. panels cannot absorb and distribute the energy as well as the thicker panels.

4.1.5. Panel type D. This type of panel was designed to determine the effects of using GFRP bars as internal reinforcement. Panel D4-6 was tested with 10 lbs. of C4 at 40 in.; the normalized standoff distance was 1.4. The panel experienced spider web like cracks that started at the center of the panel and propagated radially outwards. The cracks were traced with a black marker as shown in Figure 4.29; the panel showed no signs of spalling. Figure 4.30 shows the front of the panel after the blast, and Figure 4.31 shows the side of the panel where very little cracking was apparent. The crack locations relative to the internal reinforcement can be seen in Figure 4.32, where the dotted lines represent the location of the rebar and the solid lines represent the cracks. The maximum measured crack width was 0.0625 in.

Panel D4-10 was tested with 34 lbs. of ANFO at 38 in.; the normalized standoff distance was 1.0. Recall that this panel has a No. 5 rebar spaced at 9 in. The front face of the panel after the blast is shown in Figure 4.33. This panel experienced two large vertical cracks splitting the panel into thirds as shown in Figure 4.34; the maximum measured crack width was 0.5 in. The crack locations relative to the internal reinforcement can be seen in Figure 4.35, where the dotted lines represent the location of the rebar and the solid lines represent the cracks. The side of the panel was also very heavily damaged as a result of the cracks propagating completely through the thickness of the panel, as shown in Figure 4.36. The blast also caused minor spalling of concrete exposing the GFRP bar on the back face of the panel as shown in Figure 4.37.

Panel D4-14 was tested with 34 lbs. of ANFO at 38 in.; the normalized standoff distance was 1.0. The front face of the panel after the explosion is shown in Figure 4.38. This panel experienced two small vertical cracks in the middle of the panel as shown in Figure 4.39; the maximum measured crack width was 0.25 in. It was observed that the boundary condition at the bottom of the panel caused some additional resistance as indicated by the cracks in Figure 4.40. The crack locations relative to the internal reinforcement can be seen in Figure 4.40, where the dotted lines represent the location of the rebar and the solid lines represent the cracks. The sides of the panel did not experience much damage; only two small cracks were measured at 0.06 in. and 0.040 in., as shown in Figure 4.41. The panel had a portion of the concrete spall off in the lower left corner of the back face, as shown in Figure 4.42.

For panel type D the normalized standoff distance results are not as clear. For panel D4-6 the normalized standoff distance was 1.4 and this panel cracked less than panel D4-10 where the normalized standoff distance was 1.0. Then panel D4-14 which had a normalized standoff distance of 1.0 (which is the same as panel D4-10) experienced much less cracking than panel D4-10, but more cracking than Panel D4-6. This confusion is caused by the rebar spacing. In the other panel types, the rebar spacing did not change as the panel thicknesses increased. In this panel type the spacing did change from 6 in. for the 6 in. and 14 in. thick to 9 in. thick for the 10 in. thick panel. This change in the spacing caused more damage for the 10 in. thick panel when compared with the other thicknesses for this panel type.

4.1.6. Panel type E. This type of panel was designed to determine the effects of retrofitting a typical reinforced concrete wall that contained typical steel rebar with GFRP

overlays. Panel E4-6 was tested with 10 lbs. of C4 at 40 in.; the normalized standoff distance was 1.4. The explosion caused the panel to fall forward onto the ground. The panel had some cracking that was on the edges of the panel with a maximum measured crack width of 0.125 inches, as shown in Figure 4.43. There was also some flexural and radial cracking on the side of the panel, as shown in Figure 4.44. The GFRP composite laminate overlay that was bonded to the back face of the panel debonded in the explosion; the laminate was easily removed, as shown in Figure 4.45. The GFRP laminate that was bonded on the front face sustained minimal damage and was still bonded to the front of the panel as shown in Figure 4.46.

Panel E4-10 was tested with 21 lbs. of C4 at 40 in.; the normalized standoff distance was 1.1. Panel type E was the same as panel type A except for the GFRP laminates. After seeing how panel type A reacted to a blast it could be assumed that panel type E would perform similar to panel type A. The panel experienced some damage, because the GFRP overlay acted as a jacket protecting the concrete. On one side of the panel one shear crack and one flexural crack formed, as shown in Figure 4.47. The backside GFRP overlay debonded from most of the concrete surface except at the dark spots shown in Figure 4.48. For this panel type the dark spots were assumed to be negligible because the area was so small. The GFRP laminate debonded because the strain in the surface of the concrete exceeding the strain capacity of the resin was used to bond the laminate to the face of the concrete. The overlay was then easily removed for further inspection of the panel. The dark spots were assumed to still be bonded because as the GFRP cures with the impregnated resin, the fabric becomes somewhat transparent; the dark spots are actually the darkness of the concrete showing through the GFRP laminate. The largest

measured crack was radial in shape, 0.5 in. wide and was located on the bottom side of the panel at 45 degrees from the front of the panel to the back face of the panel, shown in Figure 4.49.

Panel E4-14 was tested with 34 lbs. of ANFO at 38 in.; the normalized standoff distance was 1.0. The panel had very little signs of damage. The front face GFRP laminate sustained no visible damage and did not debond from the concrete, as shown in Figure 4.50. The back face GFRP overlay debonded from the concrete surface except where dark spots are shown in Figure 4.51. The only sign of cracking was on the side panel; the crack was visible starting from the back face and progressively closing as the crack propagated to the front face of the panel as seen in Figure 4.52; the maximum measured crack width was 0.125 in. The top side of the panel, shown in Figure 4.53, shows minor cracking with only one shear crack that was easily visible.

For panel type E it is clear that when the normalized standoff distance is equal to 1.4 for the 6 in. thick panel it was cracked much more than when the standoff distance was equal to 1.0 and 1.1 for the 10 in. and 14 in. panels, respectively; this is again caused by the different thicknesses.

4.1.7. Panel type CON. This type of panel was used to calibrate the blast test setup and the instrumentation used. All CON panels used GFRP bars as reinforcement with spacing of 12 in., they were 6 in. thick, and used a No.5 internal reinforcement bar; the CON panels are presented here for comparison to panel type D which used GFRP bars as internal reinforcement as well.

Panel CON-3 was tested with 10 lbs. of C4 at 40 in. standoff distance; the normalized standoff distance was 1.4. This panel was heavily damaged and as a result of the blast

large pieces of the concrete panel were missing; the maximum crack width was 0.625 in. The back face and front face of the panel are shown in Figures 4.54 and 4.55, respectively. It is also noticed that this panel experienced a progressive failure, meaning that the damage was cumulative. The panel will first crack and as the cracks spread the concrete will then spall and fragment. As the fragmentation progresses the cracks will propagate further through the panel and open until the cracks reach the bottom of the panel.

Panel CON-4 was tested with 21 lbs. of C4 at 40 in. standoff distance; the normalized standoff distance was 1.1. This panel was completely broken into many fragments as a result of the explosion. Large fragments of concrete were found behind the panel; one in particular was approximately 7 in. X 3 in. X 1 in. and was found 4 ft. behind the back face of the panel; the explosive also sheared many of the GFRP bars used as internal reinforcement. The back face and front face of the panel is shown in Figures 4.56 and 4.57, respectively.

For the two CON panels presented here as the normalized standoff distance decreased the damage increased. This is because the thickness was constant for both panels tested but the weight of the charge increased. This is important to note: GFRP bars performed poorly in the control panels because they were spaced at 12 in. apart on center. If we compare this to panel type D where the reinforcing bars were spaced at 6 in. on center there is a big difference in visible damage.

In the test setup portion of this thesis it was mentioned that each panel was supported by concrete blocks on the side and placed directly on the ground; it was also assumed that this setup provided a simple supported system. It was determined after the testing that the

ground does provides some amount of resistance on the bottom of the panel. How much resistance it is not known but it was determined that this test setup does not provide a true one-way support system. For this testing this resistance was ignored but the effect that the ground has on the support system needs to be studied more.

### 4.2. Normalized Standoff Distance

For panel types A, B, C, and E as the normalized standoff distance increased, so did the damage that the panel experienced as a result of the blast. This trend can be attributed to the increasing thickness for each panel type. For panel type D when the normalized standoff distance was 1.4 for the panel D4-6 the damage was less than panel D4-10 which had a normalized standoff distance of 1.0. For panel D4-14, which had a standoff distance of 1.0, experienced less damage than panel D4-10 but more damage than panel D4-6. This change in behavior of panel type D was caused by the spacing and the elastic behavior of the GFRP bars used as reinforcement.

### 4.3. Effect of Panel Thickness

In the blast experiments, the 10 in. and 14 in. thick panels were tested with the same blast charge and standoff distance. This was done to examine the effect concrete thickness has on the performance of the panel. It is known that as the thickness of the panel increases so does the moment of inertia of the panel. It is obvious that if the thickness of the panel is increased the shear capacity of the panel will increase. It was shown for this research that this is true. However this is only true if the thickness is the only thing that is changed in the panel, for example if the reinforcement type and/or spacing is changed then the result is no longer true. This was proven in this research by examining panel type D where the reinforcement spacing was changed from 6 in. for D4-

6 to 9 in. for D4-10, because of this D4-10 performed much worse than D4-6. Increasing the thickness does typically add capacity, but as the wall thickness increases so do the negative impacts of having a thicker wall, for example increased dead weight, increased seismic effects, increased material costs, and decreased useable space. It was also observed that the 14 in. panels had significantly less cracking as a result of the panel being able to form better strut action.

### 4.4. Effect of Concrete Type

From the experimental results obtained in this study, the FRC concrete panels that contained steel rebar (panel type C) visibly performed better than the NWC panels (panel type A, D, and E). From panel type C it can be observed that FRC will limit the damage by limiting the amount of fragmentation from the panel, and the crack widths caused by the explosion. FRC with no additional reinforcement (panel type B) was found to be an ineffective way to provide additional blast resistance because the panel completely broke in half. When no internal reinforcement is used the concrete has no ductility and therefore cannot flex under the blast loading and will have a brittle failure. But the two halves produced no shrapnel which is the same result as panel type C. The failure of panel type B can be considered a global failure from lack of global reinforcement; the fibers in the FRC can be thought of as local reinforcement because the length of the fibers is much smaller than the length of the panel. Unfortunately there is not an exact comparison of FRC panels with steel rebar and NWC panels because the rebar spacing is different, but it can be seen from the blast experiments that FRC panels with steel rebar performed the best; the performance was good enough that panel C4-6 was actually tested twice and still maintained structural integrity under the same normalized standoff distance.

### 4.5. Effects of Internal and External Reinforcement Type

Three types of reinforcement were used in the concrete in this research: steel rebar, GFRP bars, and GFRP composite laminates. The steel rebar was used in three different panel types: A, C, and E. Once the steel rebar yields it deforms but does not break; instead it allows the panel to create a hinge by bending and permanent yielding as shown in Figure 4.58. GFRP bars were used in panel type D. GFRP bars are brittle and when the ultimate strain is reached, bars shear, as shown in Figure 4.59. GFRP composite laminates were used in panel type E; the GFRP laminate adds additional compressive and tensile reinforcement to the concrete. The overlays can only provide this additional reinforcement as long as the layers are still bonded to the specimen. During testing, the tensile side of the overlays always became debonded as a result of the blast, because once the strain in the extreme tensile fiber of the concrete is greater than the strain capacity of the resin, the GFRP laminate will debond.

Adhesive anchors have been used in the past to attach the FRP composite to a concrete surface as was done by McMullin et al. (2003). These anchors are known to resist out of plane loads and reduce crack growth near the concrete surface. However because of the size of the panel these anchors were not used; it was assumed that for a large concrete wall with FRP composite laminates the anchors would be spaced apart more than 4 ft.

This research found that the best type of internal reinforcement to resist a blast depends on the concrete type and the spacing of the reinforcing bars. For most cases the steel reinforcement is the best, because of the high ductility; this does not mean that GFRP bars do not have good engineering properties as well. The GFRP bars are non-

corrosive, nonmagnetic, and because of their linear behavior can be rehabilitated much more easily than steel if the ultimate load is not reached. The linear behavior of the GFRP means that if the ultimate load of the bar is not reached the material will behave plastically and return to their original position. Therefore the panel could be repaired easier than steel which will yield at lower loads and bend making it much harder to rehabilitate.

### 4.6. Effects of the Spacing of the Internal Reinforcement

Internal reinforcement is used with concrete to increase the tensile capacity of the reinforced concrete member. The more reinforcement embedded in the concrete, the better the concrete can perform when subjected to tensile forces; to a certain degree, adding too much reinforcement can be detrimental to the performance of the concrete. Essentially as long as the same amount of reinforcement area is used the reinforcement could be a smaller diameter and distributed more evenly across the panel. Cracking of the concrete is also related to the arrangement of the reinforcement and its spacing; the cracks tend to follow the pattern of the reinforcement and the smaller the reinforcement spacing, the shorter the cracks are.

The panels in this research that had internal reinforcement at 6 in. (type C and D) performed better to blast than the panels with reinforcement at 12 in. spacing, when other things were equal. Panel type D which had GFRP as an internal reinforcement did not perform as well as panel type C (internal steel reinforcement), because GFRP reinforcement has a fifth of the modulus of elasticity of the steel reinforcement. Panel type D also had variable reinforcement spacing as the panels increased in overall thickness.

## 4.7. Static Postblast Strength

A portion of the concrete panels that were tested under blast at the INL site were shipped back to the University of Utah for further testing; some panels were too damaged to be shipped back. At the University of Utah the panels were loaded into a testing frame as simply supported slabs. The panels were then loaded by a hydraulic actuator through a 12.5 in. X 27 in. X 1in. thick steel plate located at the center of the panel; the orientation of the plate is shown in Figure 4.60. The panels that were shipped back to the University were the following: A4-14, B4-14, C4-6, C4-10, C4-14, D4-6, D4-14, E4-6, E4-10, and E4-14. Panels E4-6 and E4-14 GFRP laminates had debonded as a result of the blast load; the laminates for panels E4-6 and E4-14 were just laid back on the tensile side of the panels and then the panels were post-blast tested with the laminate being clamped between the elastomeric pads and the concrete panel. The laminates were not bonded to the tensile side of the concrete in any way during the postblast tests. The laminate for panel E4-10 was lost in transportation and could not be used during the postblast testing. Therefore panel E4-10 test results are not valid.

Each specimen was tested in the frame as shown in Figure 3.3. Table 4.2 shows the data obtained from the load cell and external LVDT for each panel that was postblast tested. During testing it was observed that the load applied by the actuator was causing the cracks formed during the blast testing to open up further and to propagate. Because of this, it was concluded that the loading did not cause any new significant cracks, and the load applied by the actuator was transferred through the already present cracks. As an example, panel C4-6 was examined before the postblast load was applied, shown in Figure 4.61, and then after the postblast load was applied, shown in Figure 4.62. The

crack size for panel C4-6 went from a maximum measured crack of 0.0625 in. caused by the blast to a maximum measured crack of 0.75 in. caused by the static load. Table 4.3 lists the maximum measured crack widths during blast loading and the maximum measured postblast crack widths under static load for the rest of the panels.

The force and deflection data were graphed based on panel thickness as shown in Figures 4.63 through 4.64 and 4.66. From each graph it is possible to estimate the stiffness of each panel after the blast. The stiffness is important to consider because the cracking that the panel experienced during the blast loading decreased the initial stiffness; the smaller the cracks caused by the blast loading, the stiffer the panel was during postblast testing, and the better the panel performed at negating the effects of the blast.

The force that each panel broke at was compared to the blast force applied to the panel presented in the form of a ratio of the postblast strength divided by the applied blast load; the ratios are given in Table 4.4. This ratio expresses the amount of postblast load capacity when compared to the blast load. The loading force caused by the blast is very large making the ratio very small, but it is important to note that the load duration is only a few milliseconds since the loading was an impulse type force.

The performance of the 6 in. thick panels is shown in Figure 4.63. Panel C4-6 had the best performance out of the 6 in. panels reaching a maximum load of 67.9 kips, and a maximum deflection of 2.36 in.; this panel also had the greatest stiffness (67.5 kip/in.) of all the 6 in. panels. Panel type D4-6 for up to 1.25 in. of deflection had close to the same stiffness as panel C4-6 until there was a sudden drop in the load; this sudden drop is caused by GFRP bars deflecting to their maximum strain and breaking. This resulted in the panel failing at a maximum deflection of 1.42 in. Panel E4-6 and panel CON-1 had a

similar performance to each other and failed in the same range of a load of 40 kips and 1.60 in. deflection. The reinforcement ratios for each of the 6 in. thick panels are shown in Figure 4.63. The reinforcement ratio for Panel C4-6 was 0.296% and this panel had the best performance; panel CON-1 had a reinforcement ratio of 0.584% and this was one of the worst performers. When the reinforcement ratios are compared, the highest reinforcement ratio is not an indicator as to which panel will perform the best; an indicator to the best performance is the ductility and spacing of the reinforcement, and the type of concrete (NWC or FRC).

The performance of the 10 in. thick panels is shown in Figure 4.64. Panel C4-10 performed the best out of the two 10 in. panels tested with a maximum force of 181.1 kips, a maximum deflection of 2.04 in., and a stiffness of 200 kip/in. Panel C4-10 was also much stiffer than panel E4-10 by 97 kip/in. The large drop in load in panel C4-10 at 1.8 in. of deflection is the point the macrosynthetic fibers began to fail in rupture, as shown in Figure 4.65; the first drop occurred when only a few fibers ruptured, the second drop was when more fibers ruptured, and finally the third drop was when the remaining fibers that were resisting crack propagation ruptured. The reinforcement ratios for each of the 10 in. thick panels are shown on Figure 4.64.

The performance of 14 in. panels is shown in Figure 4.66. Because panels A4-14 and B4-14 were not tested with an explosive, they will not be compared with the other panels. Panel C4-14 performed the best out of the 14 in. panels tested, with a maximum force of 399 kips, a maximum deflection of 1.71 in., and the greatest stiffness of 266 kip/in. when compared to the rest of the 14 in. panels. Panel type E4-14 performed the second best; it had the second highest stiffness of 252 kip/ in. and achieved a maximum force of 341.1

kips, and a maximum deflection of 1.40 in. Panel D4-14 performed very poorly with a sudden loss of strength once the GFRP reached the maximum strain causing the bars to break; this shows the large drop in load on the graph. The reinforcement ratios for each of the 14 in. thick panels are shown in Figure 4.66. The reinforcement ratio for the panel C4-14 which had the best performance was 0.413%; this is also the highest reinforcement ratio for the 14 in. thick panels. The reinforcement ratio for the panel D4-14 was also 0.413% but it had the worst performance during the postblast testing when compared to all the other 14 in. thick panels.

The 6 in. thick panels were compared to panel C4-6; this was done because panel A4-6 was too damaged to be postblast tested and panel C4-6 performed the best of the 6 in. thick panels. The following are percentages of peak break loads that were less than panel C4-6; panel D4-6 broke at 5% less than C4-6 and panel E4-6 broke at 28% less than panel C4-6.

Since only one 10 in. thick panel was in good enough shape to be postblast tested the 10 in. thick panels could not be compared; it would have been valuable to compare them to panel type A as was done for the 14 in. panels, but the A4-10 was too damaged to perform any postblast testing.

The 14 in. thick panels were compared to the panel A4-14. This was done because panel type A was designed to replicate a wall that is standard wall in a previously constructed building. The following are percentages of peak break load for panels B4-14, C4-14, D4-14, and E4-14 when compared to the peak break load of panel A4-14; panel B4-14 broke at 55% less, panel C4-14 broke at 80% greater, panel D4-14 broke at 36% less, and panel E4-14 broke at 54 % greater.

From the information obtained from the postblast loading it can be concluded that panel type C performed the best of all the other types of panels in postblast residual strength. Panel type C consistently had a higher displacement at static failure, and panel type C broke at the highest static forces of all the other panel types. These comparisons were made across panel types and same thicknesses of the panel. For the 6 in. thick panels C4-6 was able to hold on average 11% more load than the other 6 in. thick panels. For the 10 in. thick panels C4-10 was able to hold 30% more load than panel E4-10. For the 14 in. thick panels C4-14 was able to hold on average 40% more load than the other 14 in. thick panels. When compared across all the panel types and thicknesses panel type C was able to reach 27% greater peak load than the other panel types.

### 4.8. Static Concrete Properties

During the construction of different types of panels, concrete cylinders were also constructed to determine the tensile and compressive static strengths of the concrete; both 4 in. and 6 in. diameter cylinders were made. The compressive and splitting tensile strengths were determined using equipment at the University of Utah.

The static compressive strengths were determined using 4 in. diameter by 8in. long concrete cylinders and in accordance with the ASTM C 39/C 39M – 10 (ASTM 2010) Standard Test Method for Compressive Strength of Cylindrical Concrete Specimens. The static tensile strengths were determined using 4 in. diameter by 8in. long concrete cylinders and in accordance with the ASTM C 496/C 496M – 04 (ASTM 2004) Standard Test Method for Splitting Tensile Strength of Cylindrical Concrete Specimens. The results for the static, compressive and tensile strengths are summarized in Figures 4.67 and 4.68. FRC was able to reach higher loads in splitting tension than the NWC concrete,

but FRC was not able to reach higher load in the compressive strength when compared to the NWC. On average FRC was 10% stronger than NWC in splitting tension test, and FRC was 11% lower compressive strength. Small beams approximately 4 in. X 4 in. X 14 in. were also built and tested to obtain strain data for each type of concrete: NWC, FRC, and NWC with GFRP laminates.

During the compression tests each cylinder was capped with a steel cap that had a rubber pad placed inside the ring to allow the specimen to properly seat inside the cylinder as the load was applied. The specimen was then loaded into the frame with the steel cap on the top and bottom and loaded at 500 lbs./s until failure was reached, as shown in Figure 4.69. This failure shows a typical compression test for a FRC cylinder.

During the split cylinder tension test each cylinder had to be placed into a jig to ensure the cylinder was perfectly in-line with the applied load; the test setup is shown in Figure 4.70. The jig was specially fabricated from steel to meet the specifications in the ASTM standard. The jig was reused each test except for the pieces of wood, which were replaced with new each time a new specimen was tested. The specimen was loaded at a rate of 125 lbs./s until failure was reached. Failure during this test was very sudden and usually violent with shrapnel flying in various directions. Depending on the type of concrete, failure would consist of a crack at the center of the cylinder which caused the cylinder to break into two separate pieces; an NWC failure is shown in Figure 4.71 (in this figure there are four pieces; the smaller breaks are from the two pieces falling on the ground and breaking). When the concrete was made from FRC, failure was similar except that fibers would keep the cylinder from breaking into two separate pieces; an FRC failure is shown in Figure 4.72.

Six NWC and six FRC concrete beams approximately 4 in. square by 14 in. long were constructed to evaluate flexural performance; two NWC beams were covered with the GFRP composite laminate, referred to from here on as a GFRP laminated beam; Figure 4.73 shows the various beams with strain gauges attached. The beams were tested according to a modified ASTM 1609/C1609M – 10 (ASTM 2010) Standard Test Method for Flexural Performance of Fiber-Reinforced Concrete.

The beams were tested in the same frame as the postblast testing. The load was applied to one of NWC, FRC, and two GFRP beams very fast and another load was then applied to one NWC and one FRC beam slowly. The fast loading was applied at 0.205 in./s and the slow loading was applied at 0.00208 in./s. This was done to try to determine the differences in the behavior of the beams when experiencing two different strain rates.

The NWC beam when loaded slowly reached a maximum strain of $1.48 \text{ X } 10^{-4}$ in./in. and when loaded fast reached a maximum strain of $1.45 \text{ X } 10^{-4}$ in./in. The fact that the NWC beams that were loaded slowly, reached a higher strain than the NWC beams that were loaded fast, means that the load was not applied fast enough to cause dynamic properties to affect the materials. The NWC beams broke by shearing perpendicular to the direction of the tension fiber. The FRC beam when loaded slowly reached a maximum strain of $2.05 \text{ X } 10^{-4}$ in./in. and when loaded fast reached a maximum strain of $1.57 \text{ X } 10^{-4}$ in./in. The FRC beams also broke by shearing perpendicular to the direction of the tension fiber. Because the maximum strain results are not significantly different from each other, the loading rate was not fast enough to impose a dynamic increase on the concrete. Strain vs. time plots are shown in Figures 4.74 and 4.75 for each of the NWC and FRC small beams loaded slowly and fast.

The NWC beams with the GFRP composite laminates were both tested with a fast load. These beams were able to deflect to a greater amount than the other beams because of the GFRP laminates on each side of the beam. This is known because the testing was set up to apply a load as fast as the hydraulic actuator could, but the actuator was to stop after the actuator had displaced 0.5 in. The first GFRP laminated beam tested was loaded as fast as possible up to 0.5 in. and was not broken; the other NWC and FRC beams without the GFRP laminates all broke within the 0.5 in. limit. The beam was then retested with the limit of the actuator set to 0.75 in.; this allowed the beam to deflect enough and to break. The GFRP laminate on the NWC beams reached a maximum strain of 3.58 X $10^{-3}$ in./in. and 6.03 X $10^{-3}$ in./ in. Strain vs. time plots are shown in Figure 4.76 for the GFRP laminated beams loaded fast.

From Figures 4.76 the strain rate was determined for each GFRP laminated beam by finding the slope of the line from the start of the strain data to the peak strain. This was significant for the GFRP laminated beams, because the peak strain of each beam was the strain when the beam broke and also was assumed to be the debonding strain of the laminate to the concrete. The strain rates and peak strains for each beam were then used to obtain Figure 4.77 where the effective debonding strain of the concrete can be predicted depending on the applied strain rate. To obtain the values on Figure 4.77 the strain rate was used from the testing of the two beams and the strain rate from a blast done at the National Security Testing Range (NSTR) at INL. The effective strain values were used from the peak strain values from the two GFRP laminated beam tests and 90% of the effective strain capacity of the GFRP composite laminates, as recommended by ACI Committee 440.2 R-08 (ACI 2008) - Guide for the Design and Construction of

Externally Bonded FRP Systems for Strengthening Concrete Structures. Table 4.5 shows the calculated values that were used to create Figure 4.77.

**Table 4.1 Normalized standoff distance**

| Panel | Standoff Distance (in.) | Type of Charge | Weight of Charge (lbs.) | Equivalent Weight of TNT (lbs.) | Normalized Standoff Distance Z, (ft./lbs$^{1/3}$) |
|---|---|---|---|---|---|
| A4-6 | 40.0 | C4 | 10.0 | 13.7 | 1.4 |
| A4-10 | 38.0 | ANFO | 34.0 | 29.2 | 1.0 |
| A4-14 | | | | | |
| B4-6 | 40.0 | C4 | 10.0 | 13.7 | 1.4 |
| B4-10 | 40.0 | C4 | 21.0 | 28.8 | 1.1 |
| B4-14 | | | | | |
| C4-6 | 41.0 | C4 | 10.0 | 13.7 | 1.4 |
| C4-10 | 38.0 | ANFO | 34.0 | 29.2 | 1.0 |
| C4-14 | 38.0 | ANFO | 34.0 | 29.2 | 1.0 |
| D4-6 | 41.0 | C4 | 10.0 | 13.7 | 1.4 |
| D4-10 | 38.0 | ANFO | 34.0 | 29.2 | 1.0 |
| D4-14 | 38.0 | ANFO | 34.0 | 29.2 | 1.0 |
| E4-6 | 40.0 | C4 | 10.0 | 13.7 | 1.4 |
| E4-10 | 40.0 | C4 | 21.0 | 28.8 | 1.1 |
| E4-14 | 38.0 | ANFO | 34.0 | 29.2 | 1.0 |

**Table 4.2 Summary of postblast results**

| Specimen | Reinforcement | Static Peak Force (kip) | Displacement at Static Failure (in.) | Maximum Recorded Displacement (in.) |
|---|---|---|---|---|
| A4-14 | Steel rebar at 12" | 221.7 | 1.14 | 1.890 |
| B4-14 | ONLY Synthetic Fibers | 98.8 | 0.19 | 0.504 |
| C4-6 | Steel rebar at 6" & Synthetic Fibers | 67.9 | 1.42 | 2.346 |
| C4-10 | Steel rebar at 6" & Synthetic Fibers | 181.1 | 1.60 | 2.042 |
| C4-14 | Steel rebar at 6" & Synthetic Fibers | 399.0 | 1.14 | 1.712 |
| D4-6 | GFRP bar at 6" | 64.6 | 1.24 | 1.416 |
| D4-14 | GFRP bar at 6" | 141.9 | 0.59 | 1.001 |
| E4-6 | Steel rebar at 12" & GFRP Laminate | 49.0 | 1.64 | 1.790 |
| E4-10 | Steel rebar at 12" & GFRP Laminate | 72.8 | 0.96 | 1.478 |
| E4-14 | Steel rebar at 12" & GFRP Laminate | 341.4 | 0.90 | 1.397 |
| CON-1 | GFRP bar at 12" | 44.5 | 1.16 | 1.583 |

**Table 4.3 Summary of blast and postblast crack widths**

| Specimen | Reinforcement | Blast Crack Width (in.) | Post-Blast Crack Width (in.) |
|---|---|---|---|
| A4-14 | Steel rebar at 12" | N/A | 0.688 |
| B4-14 | ONLY Synthetic Fibers | N/A | 0.375 |
| C4-6 | Steel rebar at 6" & Synthetic Fibers | 0.063 | 0.750 |
| C4-10 | Steel rebar at 6" & Synthetic Fibers | 0.050 | 1.500 |
| C4-14 | Steel rebar at 6" & Synthetic Fibers | 0.000 | 0.875 |
| D4-6 | GFRP bar at 6" | 0.063 | 0.250 |
| D4-14 | GFRP bar at 6" | 0.250 | 1.750 |
| E4-6 | Steel rebar at 12" & GFRP Laminate | 0.125 | 0.313 |
| E4-10 | Steel rebar at 12" & GFRP Laminate | 0.500 | 0.750 |
| E4-14 | Steel rebar at 12" & GFRP Laminate | 0.125 | 0.438 |
| CON-1 | GFRP bar at 12" | 0.375 | 0.375 |

**Table 4.4 Postblast force ratios**

| Specimen | Peak Postblast Force (kip) | Estimated Applied Blast Force (kip) | Ratios |
|---|---|---|---|
| A4-14 | 221.7 | NA | NA |
| B4-14 | 98.8 | NA | NA |
| C4-6 | 67.9 | 982 | 6.91% |
| C4-10 | 181.1 | 1840 | 9.84% |
| C4-14 | 399.0 | 1840 | 21.7% |
| D4-6 | 64.6 | 982 | 6.58% |
| D4-14 | 141.9 | 1840 | 7.71% |
| E4-6 | 49.0 | 1031 | 4.75% |
| E4-14 | 341.4 | 1840 | 18.6% |
| CON-1 | 44.5 | 1031 | 4.32% |

**Table 4.5 Values used to create Figure 4.77**

| Specimen | Strain Rate (1/s) | Effective Strain (in./in.) |
|---|---|---|
| GFRP Beam 1 | 0.0120 | 0.004 |
| GFRP Beam 2 | 0.2000 | 0.006 |
| Explosion | 3.0000 | 0.021 |


**Figure 4.1 Front of panel A4-6 after 10 lbs. of C4 at 40 in.**


**Figure 4.2 Back of panel A4-6 after 10 lbs. of C4 at 40 in.**

**Figure 4.3 Side of panel A4-6 after 10 lbs. of C4 at 40 in.**


**Figure 4.4 Front of panel A4-10 after 34 lbs. of ANFO at 38 in.**

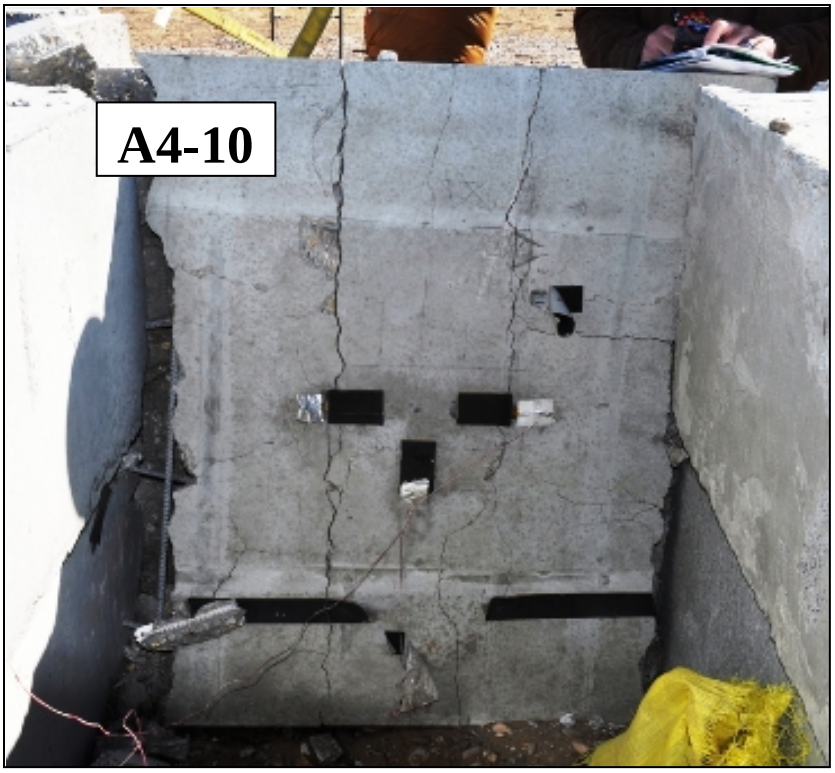


**Figure 4.5 Back of panel A4-10 after 34 lbs. of ANFO at 38 in.**

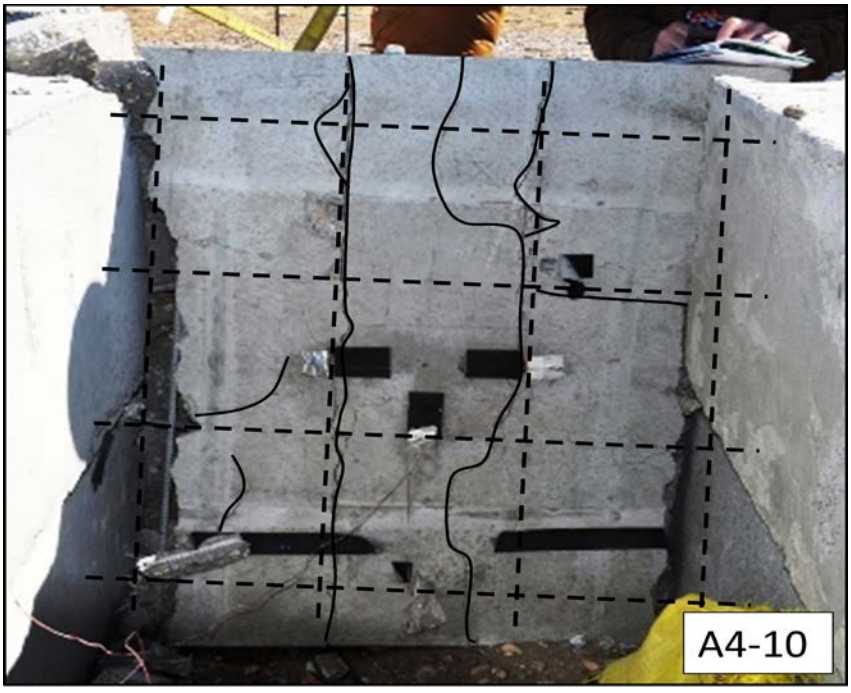


**Figure 4.6 Cracks relative to reinforcement for panel A4-10**

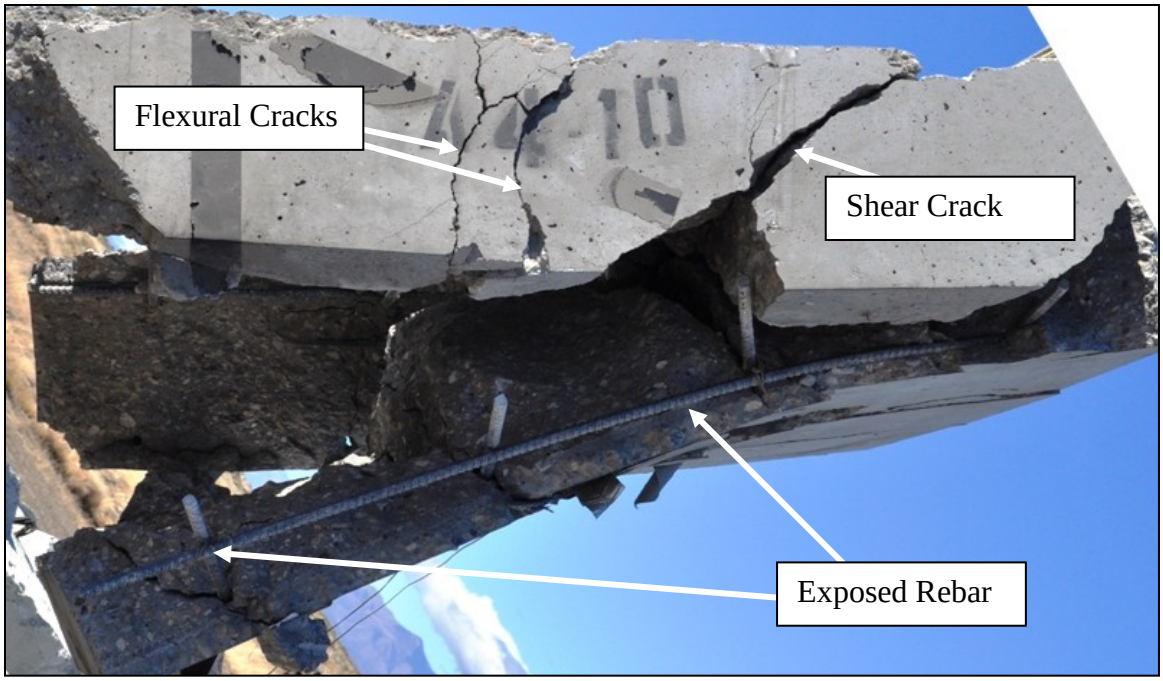


**Figure 4.7 Side of panel A4-10 after 34 lbs. of ANFO at 38 in.**


**Figure 4.8 Panel B4-6 after 10 lbs. of C4 at 40 in.**


**Figure 4.9 Panel B4-10 after 21 lbs. of C4 at 40 in.**

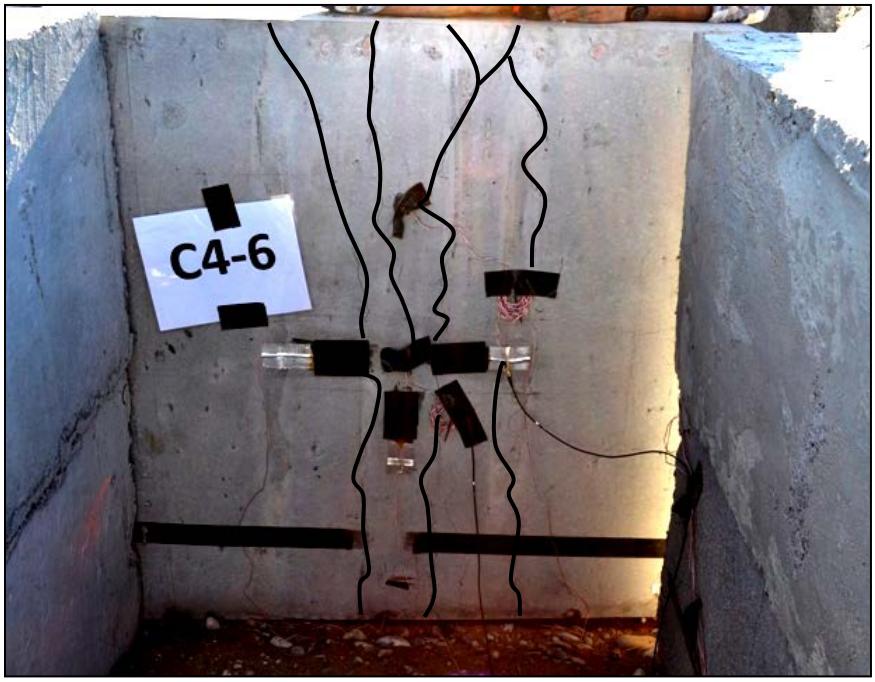


**Figure 4.10 Back of panel C4-6 after 10 lbs. of C4 at 40 in. (1st blast)**


**Figure 4.11 Cracks on back of panel C4-6 after 10 lbs. of C4 at 40 in. (1st blast)**


**Figure 4.12 Front of panel C4-6 after 10 lbs. of C4 at 40 in. (1st blast)**


**Figure 4.13 Cracks relative to reinforcement for panel C4-6 (1st blast)**

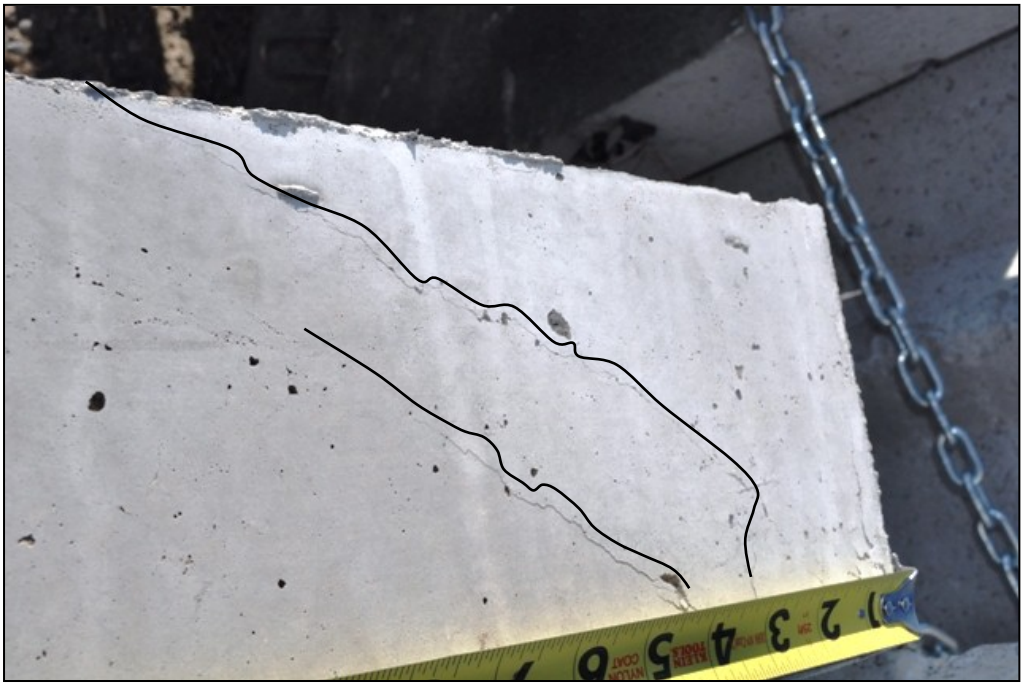

**Figure 4.14 Side of C4-6 after 10 lbs. of C4 at 40 in. (1st blast)**

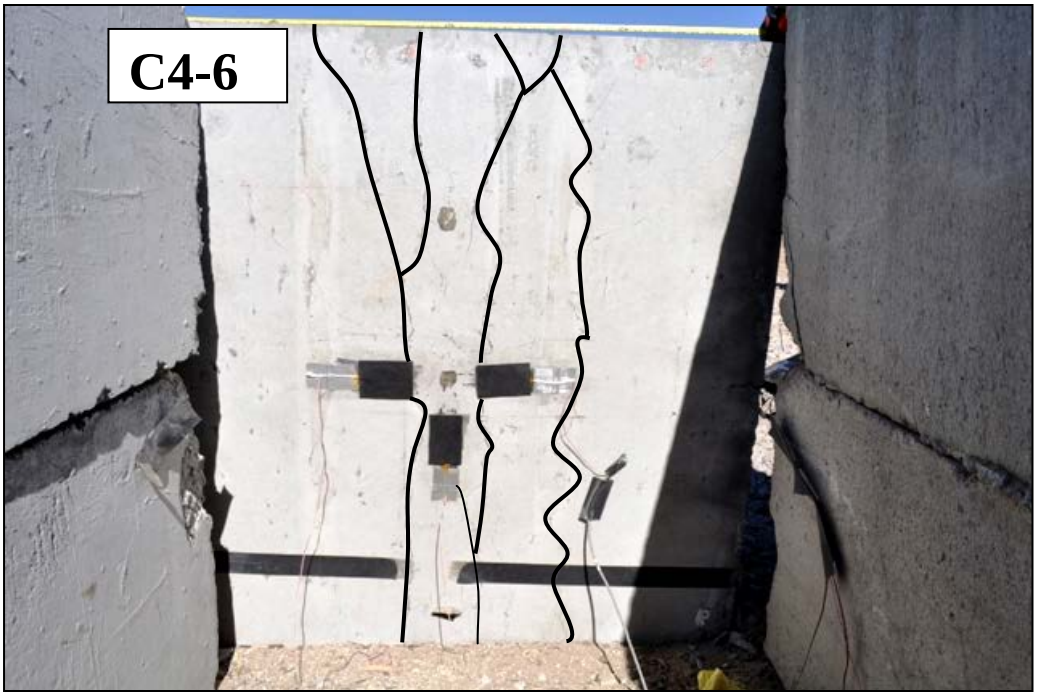


**Figure 4.15 Back of panel C4-6 after 10 lbs. of C4 at 41 in. (2nd blast)**


**Figure 4.16 Cracks on panel C4-6 after 10 lbs. of C4 at 41 in. (2nd blast)**


**Figure 4.17 Front of panel C4-6 after 10 lbs. of C4 at 41 in. (2nd blast)**

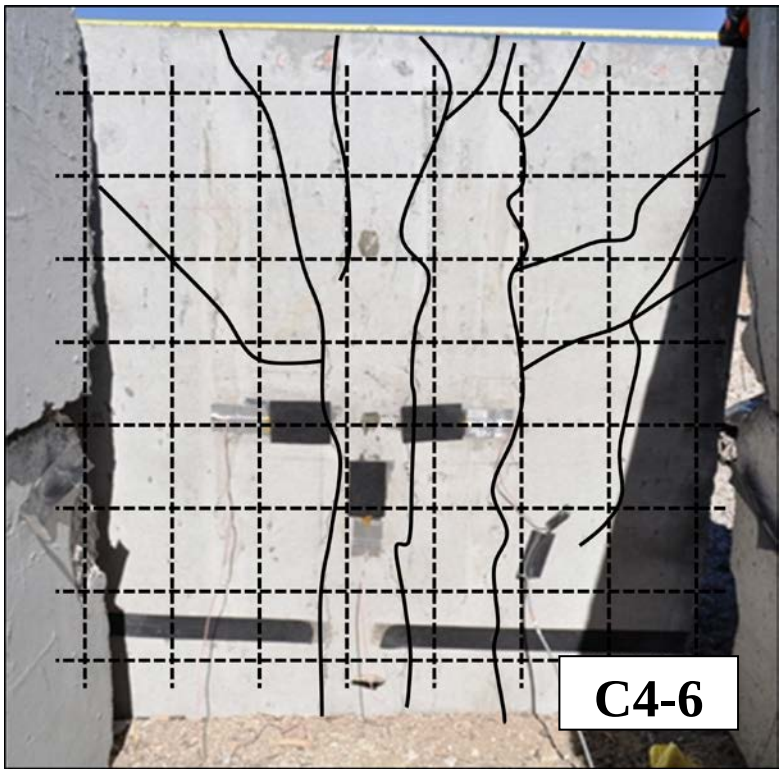


**Figure 4.18 Cracks relative to reinforcement for panel C4-6 (2nd blast)**


**Figure 4.19 Front of panel C4-10 after 34 lbs. of ANFO at 38 in.**

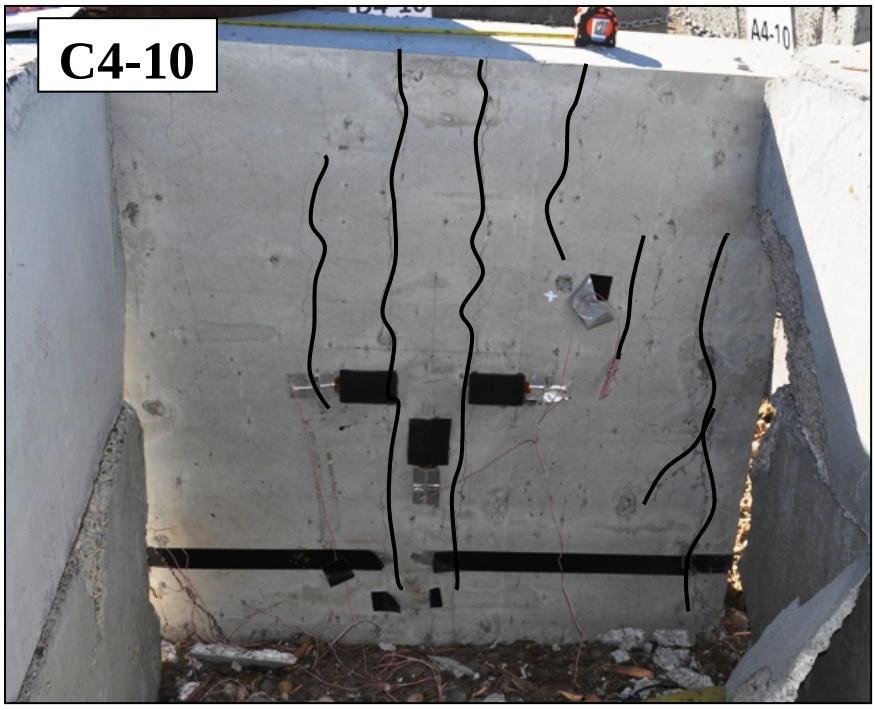


**Figure 4.20 Back of panel C4-10 after 34 lbs. of ANFO at 38 in.**


**Figure 4.21 Cracks on panel C4-10 after 34 lbs. of ANFO at 38 in.**


**Figure 4.22 Side of panel C4-10 after 34 lbs. of ANFO at 38 in.**

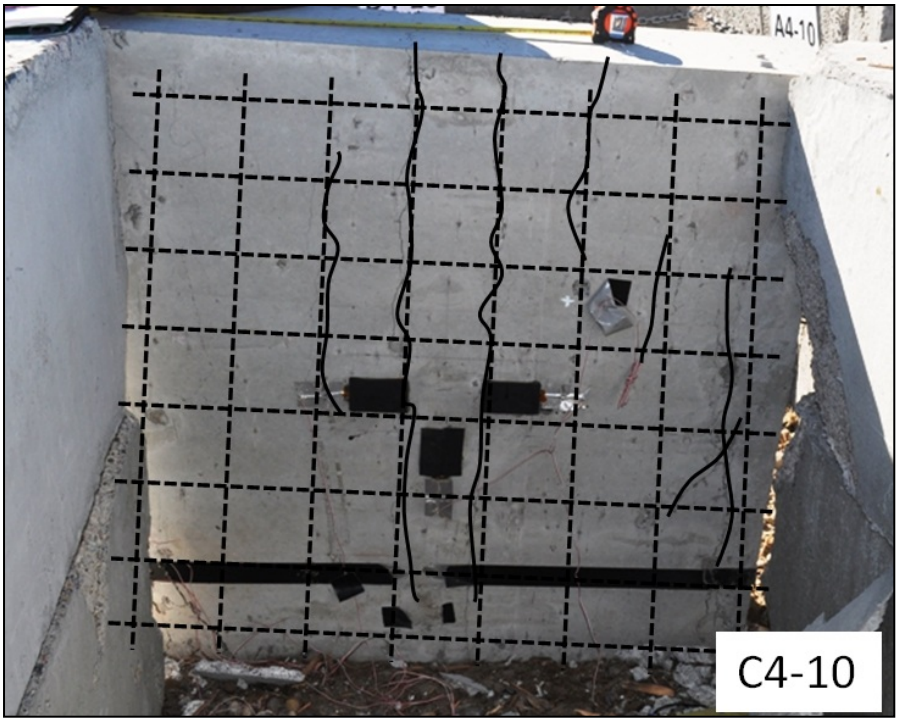


**Figure 4.23 Cracks relative to reinforcement for panel C4-10**


**Figure 4.24 Front of panel C4-14 after 34 lbs. of ANFO at 38 in.**


**Figure 4.25 Back of panel C4-14 after 34 lbs. of ANFO at 38 in.**


**Figure 4.26 Cracks on panel C4-14 after 34 lbs. of ANFO at 38 in.**

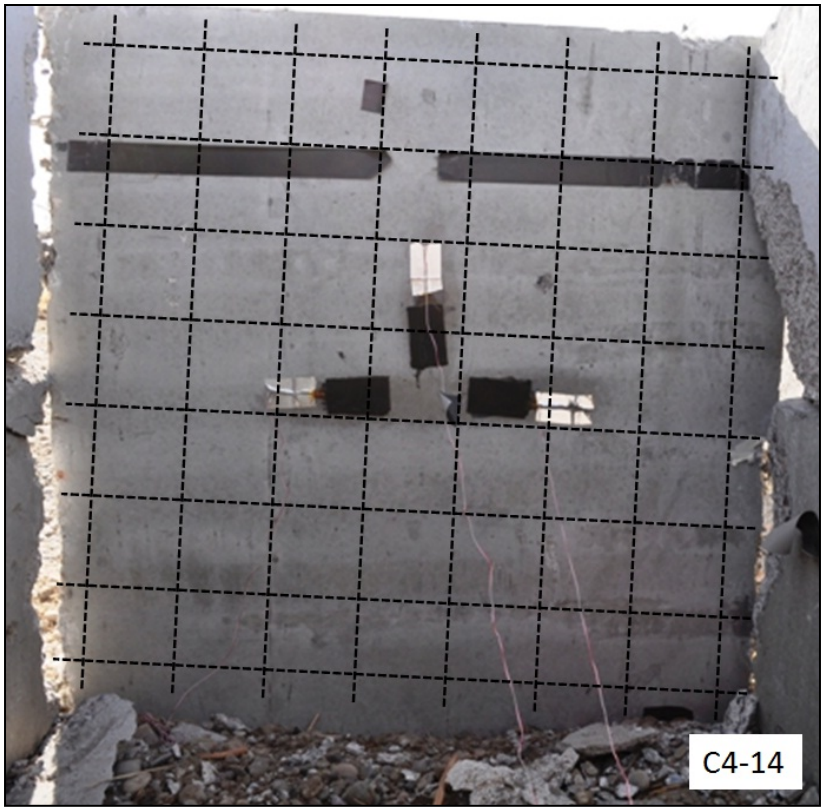


**Figure 4.27 Cracks relative to reinforcement for panel C4-14**

**Figure 4.28 Side of panel C4-14 after 34 lbs. of ANFO at 38 in.**


**Figure 4.29 Back of panel D4-6 after 10 lbs. of C4 at 41 in.**

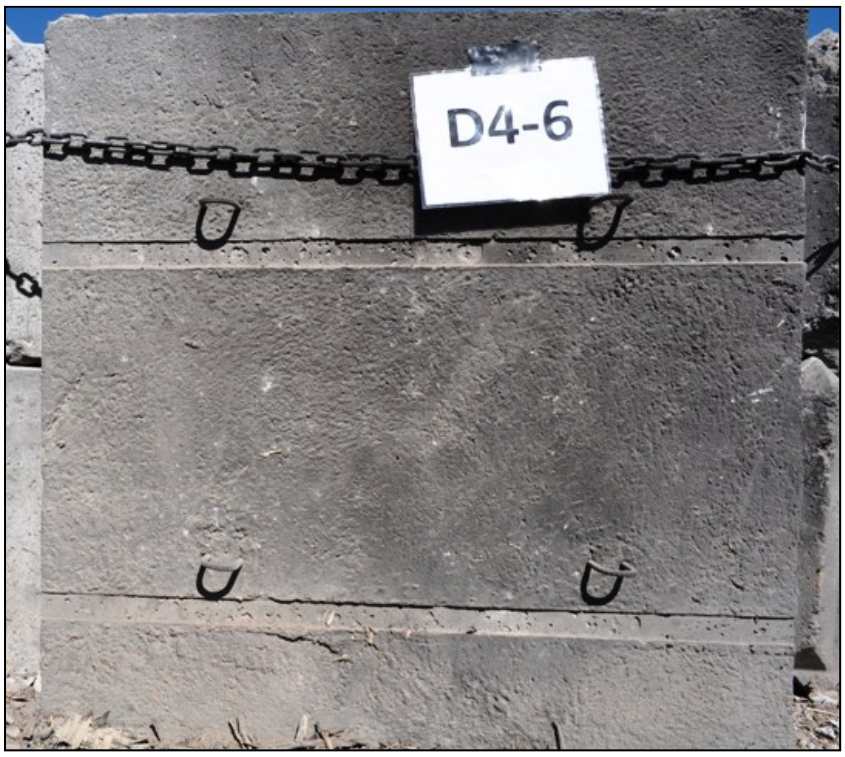


**Figure 4.30 Front of panel D4-6 after 10 lbs. of C4 at 41 in.**

**Figure 4.31 Side of panel D4-6 after 10 lbs. of C4 at 41 in.**

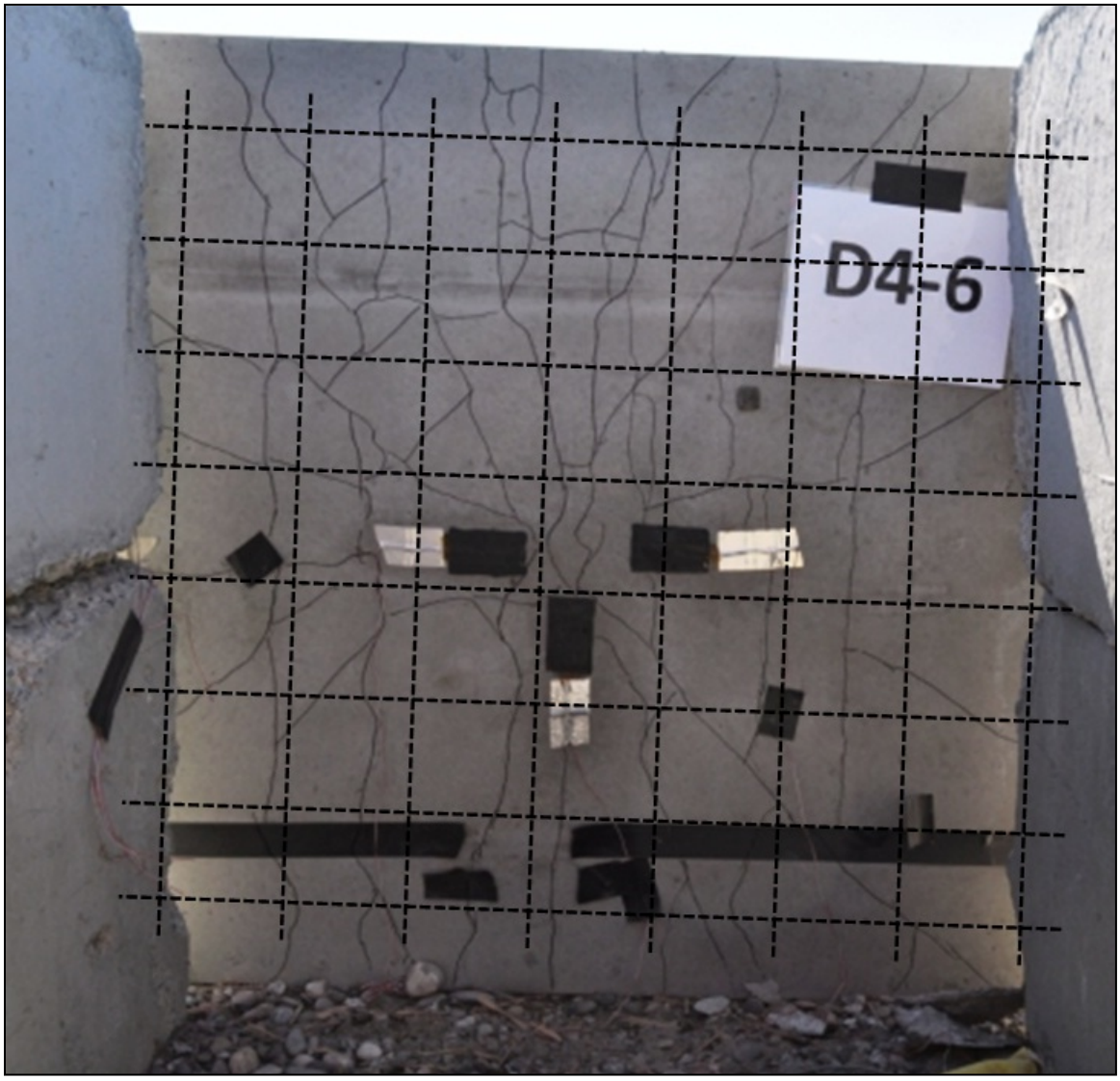


**Figure 4.32 Cracks relative to reinforcement for panel D4-6**

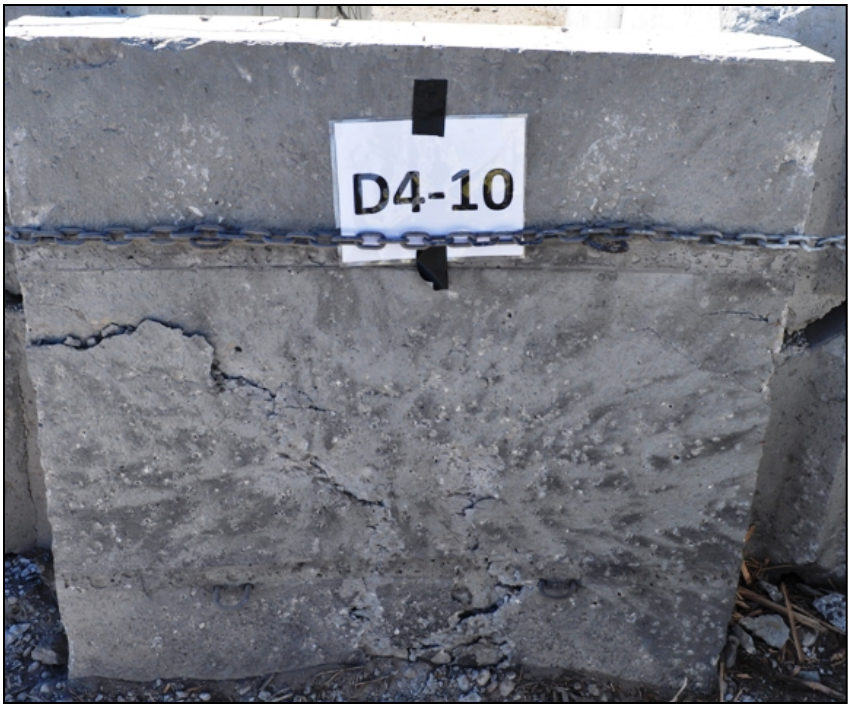


**Figure 4.33 Front of panel D4-10 at 34 lbs. of ANFO at 38 in.**

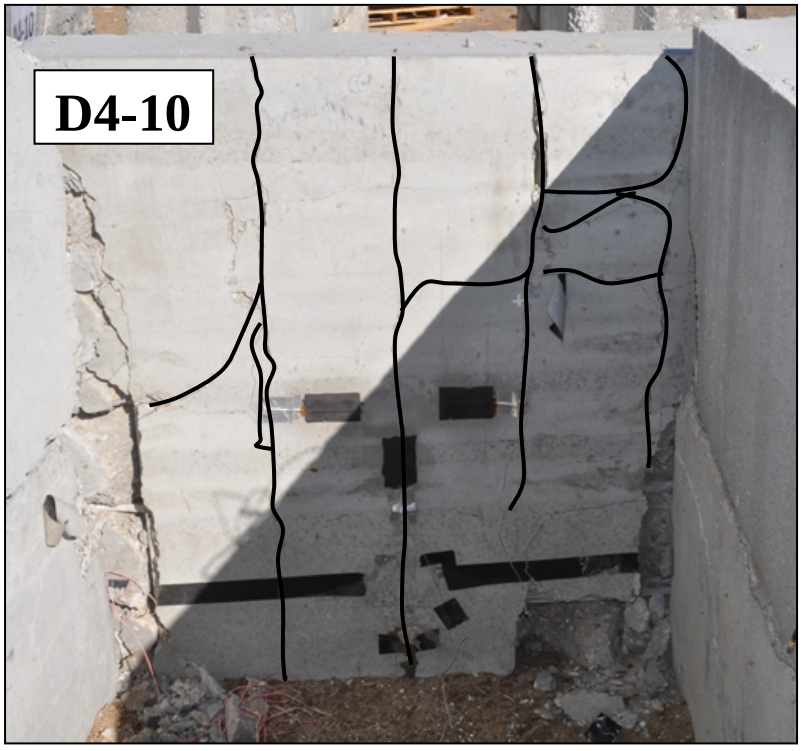


**Figure 4.34 Back of panel D4-10 at 34 lbs. of ANFO at 38 in.**

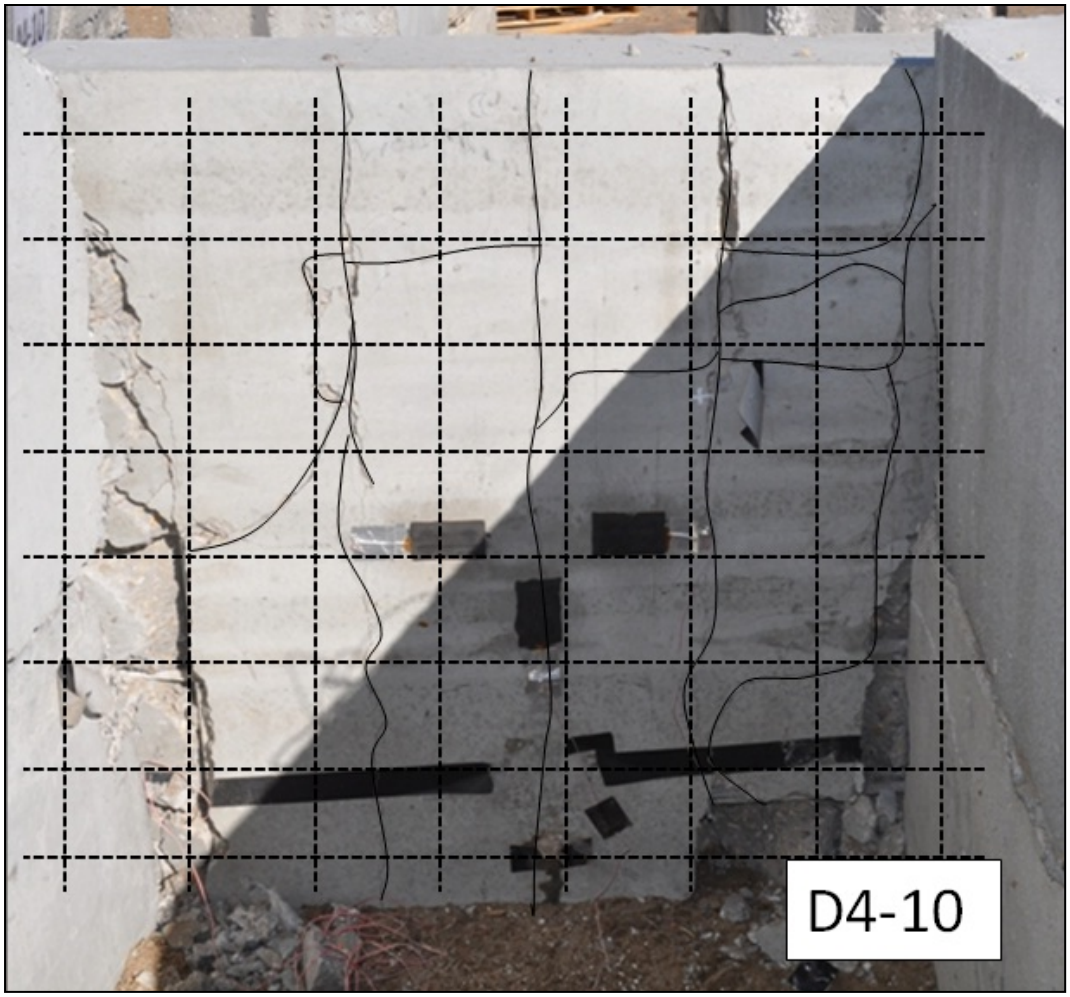


**Figure 4.35 Cracks relative to reinforcement for panel D4-10**

**Figure 4.36 Side of panel D4-10 at 34 lbs. of ANFO at 38 in.**

**Figure 4.37 Exposed rebar on panel D4-10 after 34 lbs. of ANFO at 38 in.**

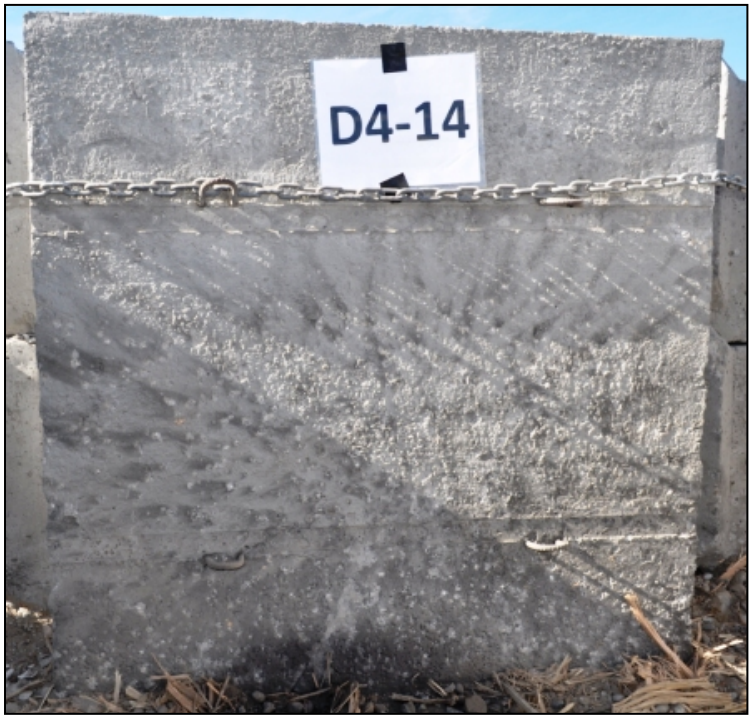


**Figure 4.38 Front of panel D4-14 after 34 lbs. of ANFO at 38 in.**

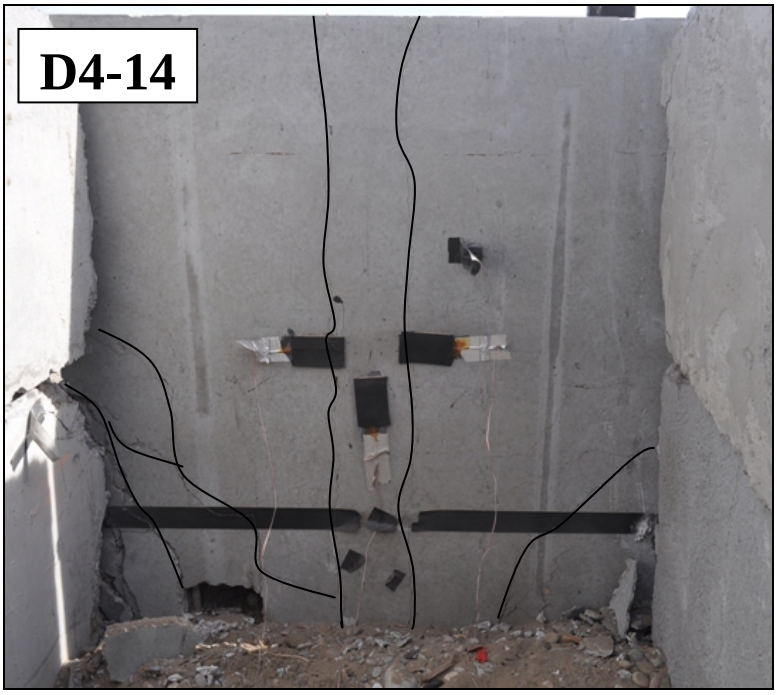


**Figure 4.39 Back of panel D4-14 after 34 lbs. of ANFO at 38 in.**

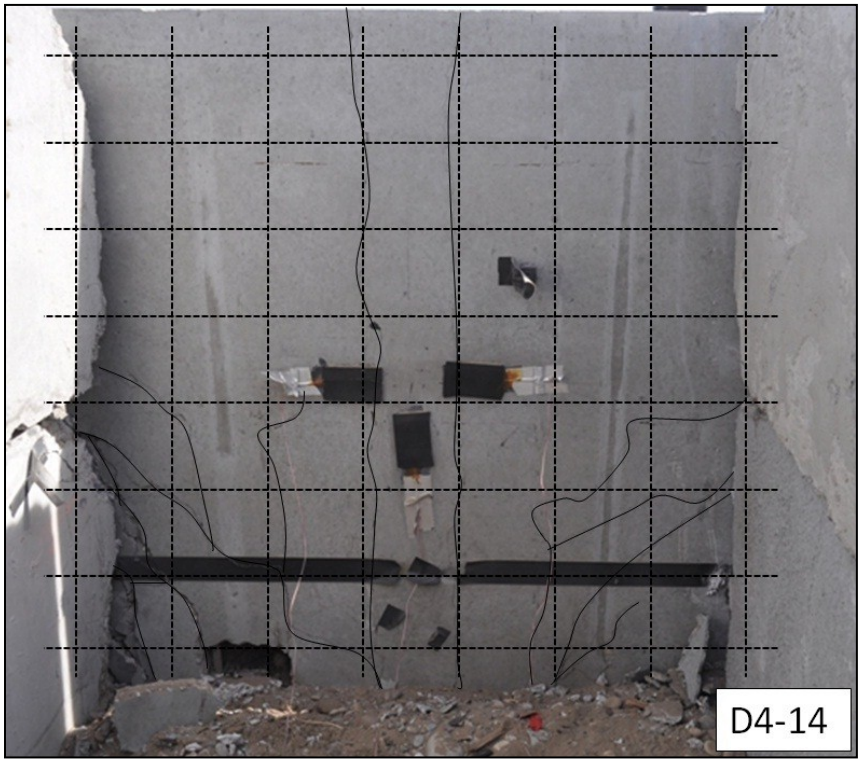


**Figure 4.40 Cracks relative to reinforcement for panel D4-14**

**Figure 4.41 Side of panel D4-14 after 34 lbs. of ANFO at 38 in.**

**Figure 4.42 Bottom left corner of panel D4-14 after 34 lbs. of ANFO at 38 in.**


**Figure 4.43 Back of panel E4-6 after 10 lbs. of C4 at 40 in.**

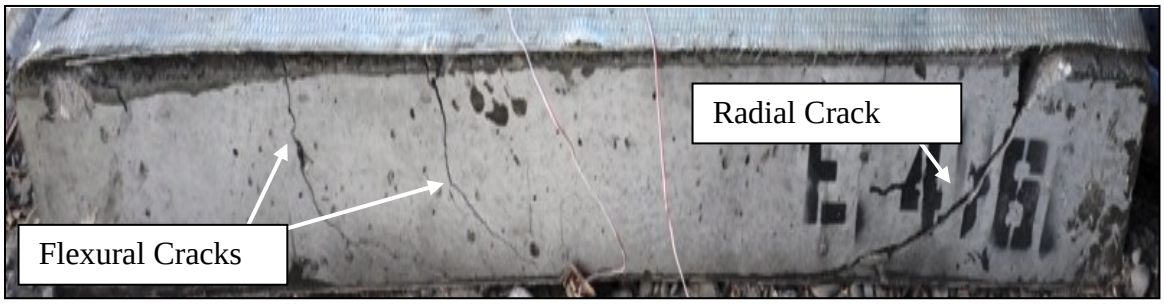


**Figure 4.44 Side of panel E4-6 after 10 lbs. of C4 at 40 in.**

**Figure 4.45 Panel E4-6 debonding of the tensile GFRP laminate**


**Figure 4.46 Front of panel E4-6 after 10 lbs. of C4 at 40 in.**

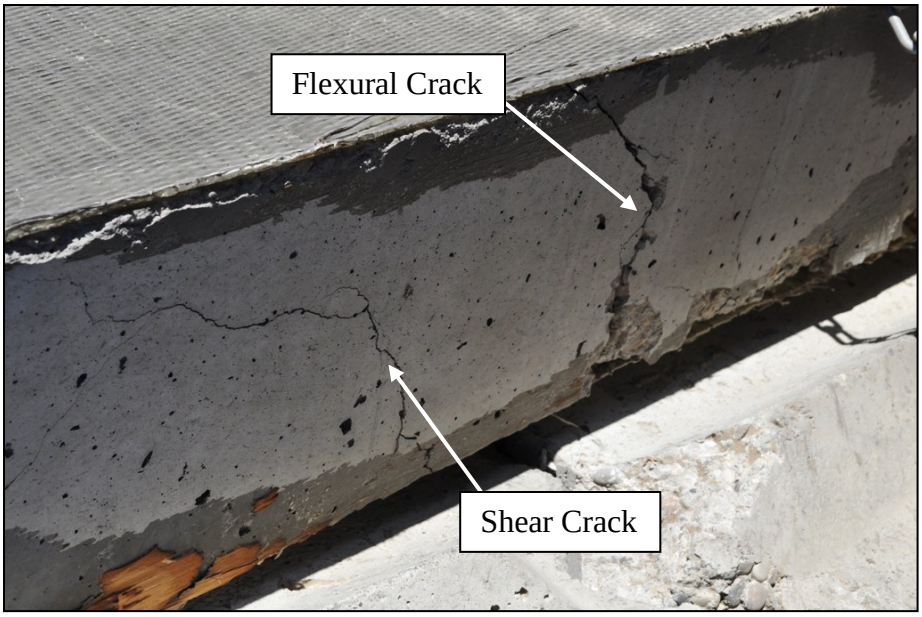


**Figure 4.47 Side of panel E4-10 after 21 lbs. of C4 at 40 in.**

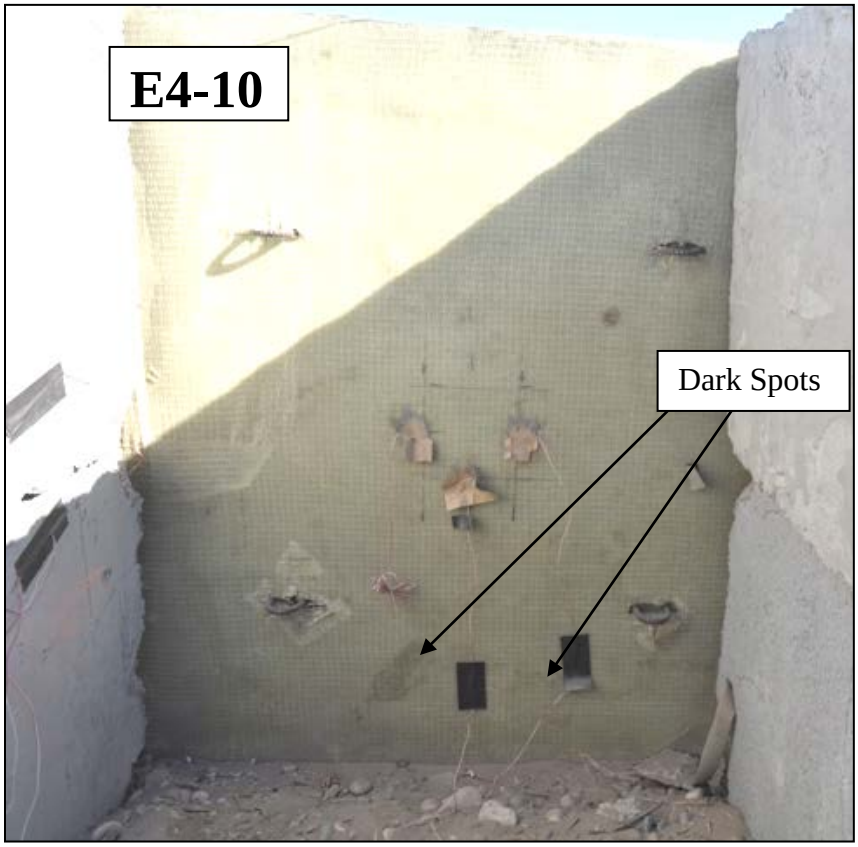


**Figure 4.48 Back of panel E4-10 after 21 lbs. of C4 at 40 in.**

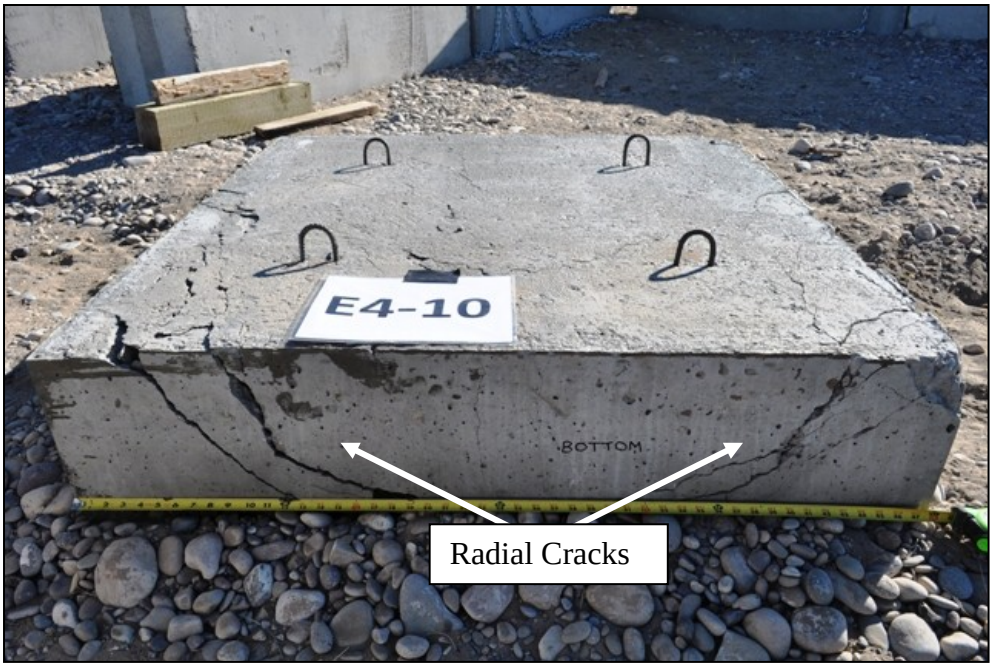


**Figure 4.49 Panel E4-10 tensile side after the fabric had been removed**


**Figure 4.50 Front of panel E4-14 after 34 lbs. of ANFO at 38 in.**

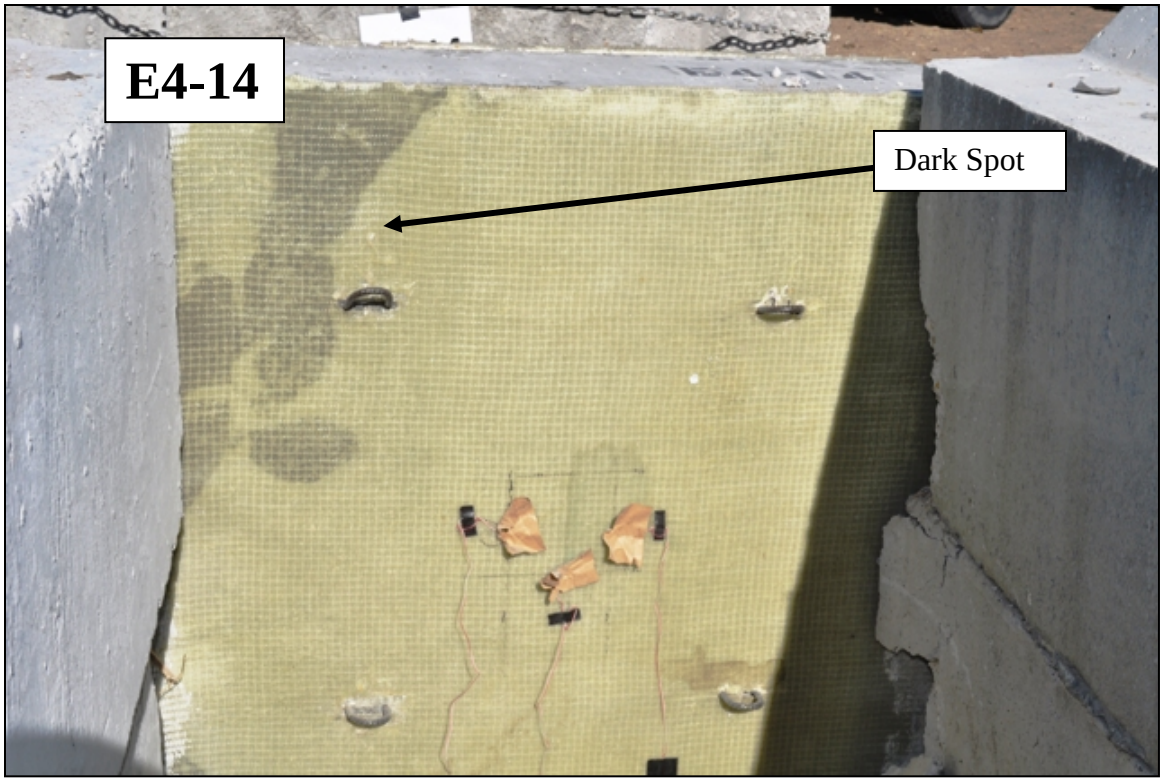


**Figure 4.51 Back of panel E4-14 after 34 lbs. of ANFO at 38 in.**

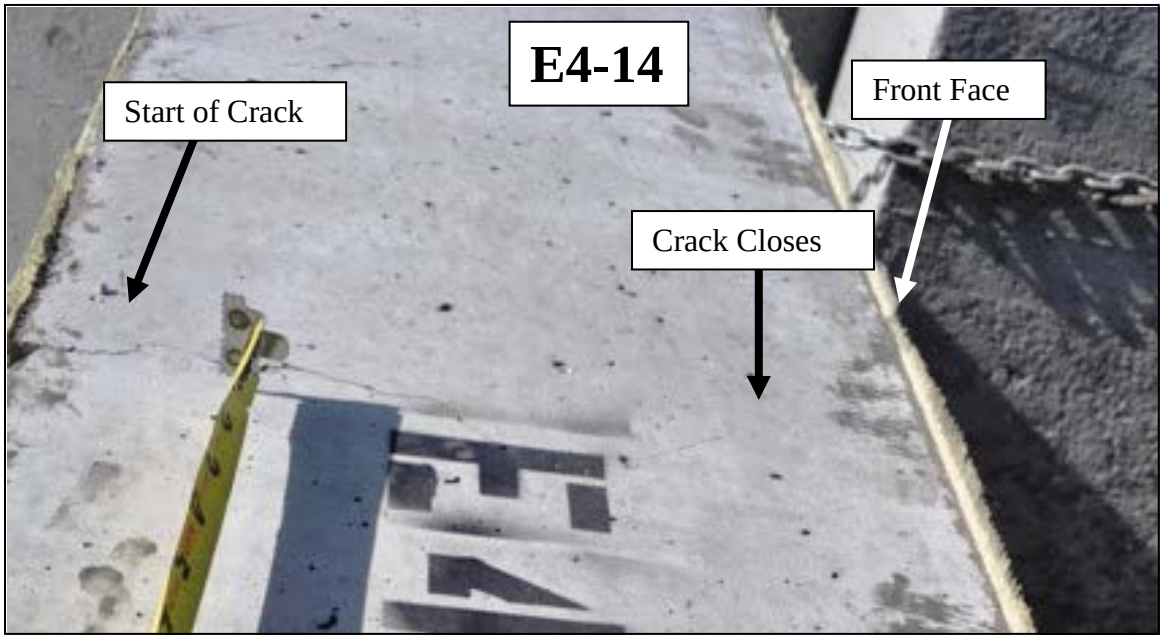


**Figure 4.52 Cracks on panel E4-14 after 34 lbs. of ANFO at 38 in.**


**Figure 4.53 Side of panel E4-14 after 34 lbs. of ANFO at 38 in.**


**Figure 4.54 Back of panel CON-3 after 10 lbs. of C4 at 40 in.**


**Figure 4.55 Front of panel CON-3 after 10 lbs. of C4 at 40 in.**


**Figure 4.56 Back of panel CON-4 after 21 lbs. of C4 at 40 in.**


**Figure 4.57 Front of panel CON-4 after 21 lbs. of C4 at 40 in.**


**Figure 4.58 Steel rebar hinge point**

**Figure 4.59 GFRP bars sheared**

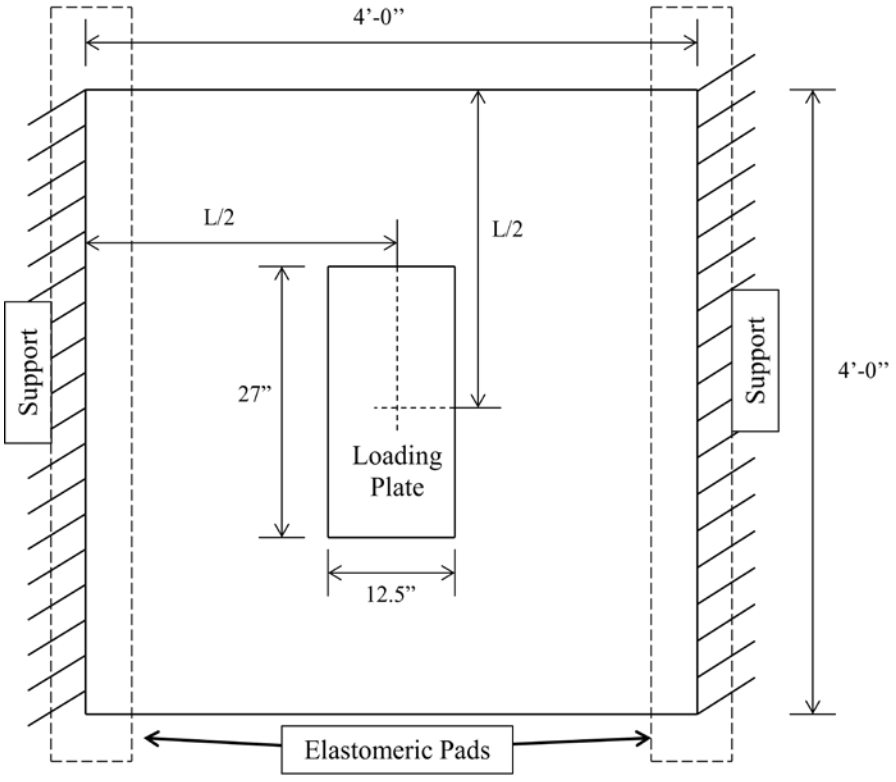


**Figure 4.60 Orientation of loading plate**

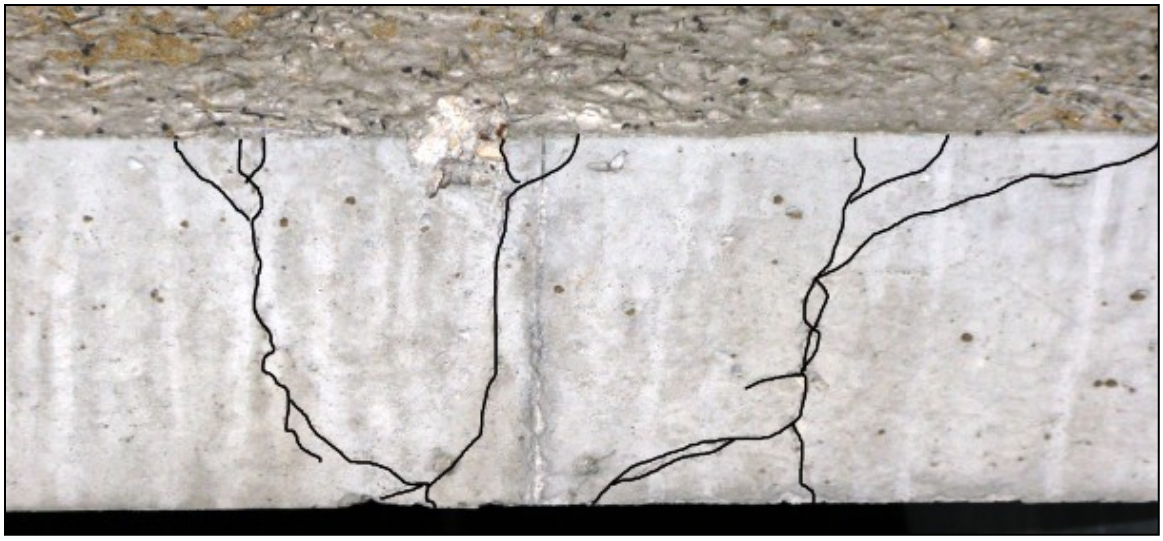

**Figure 4.61 Center of panel C4-6 before postblast loading**


**Figure 4.62 Center of panel C4-6 after postblast loading**

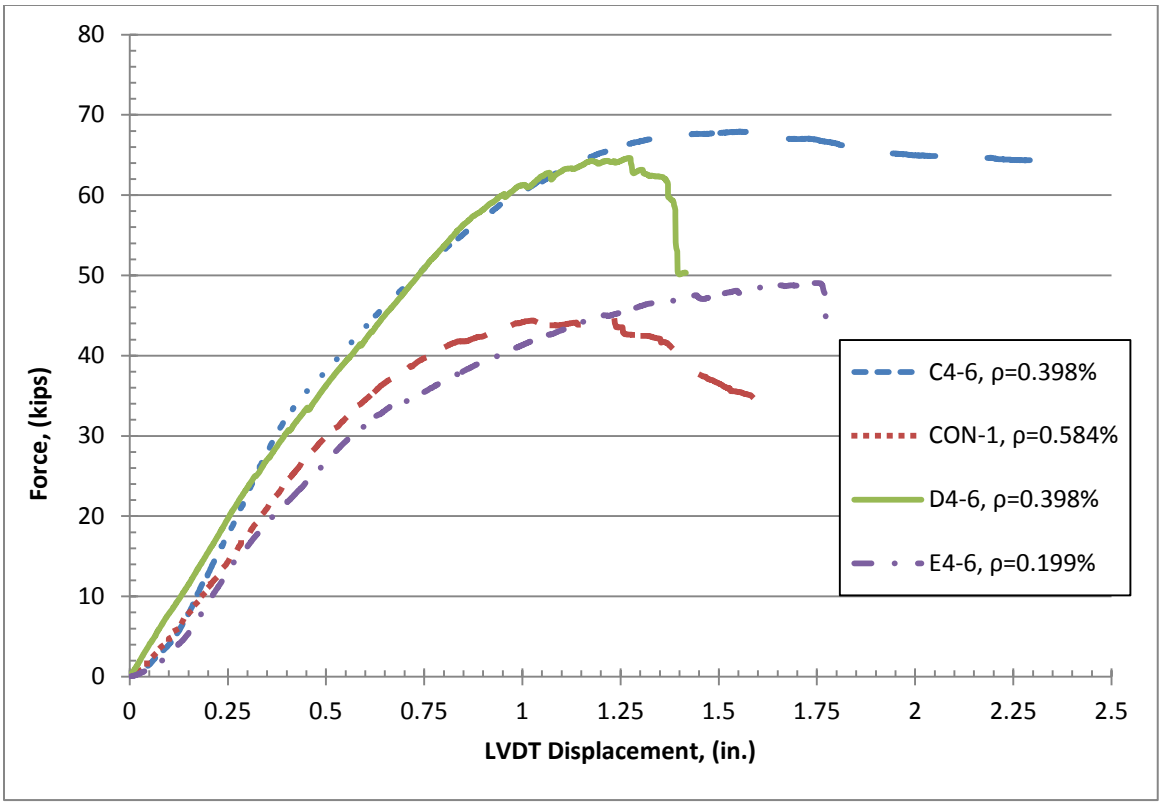


**Figure 4.63 Performance of 6 in. panels**

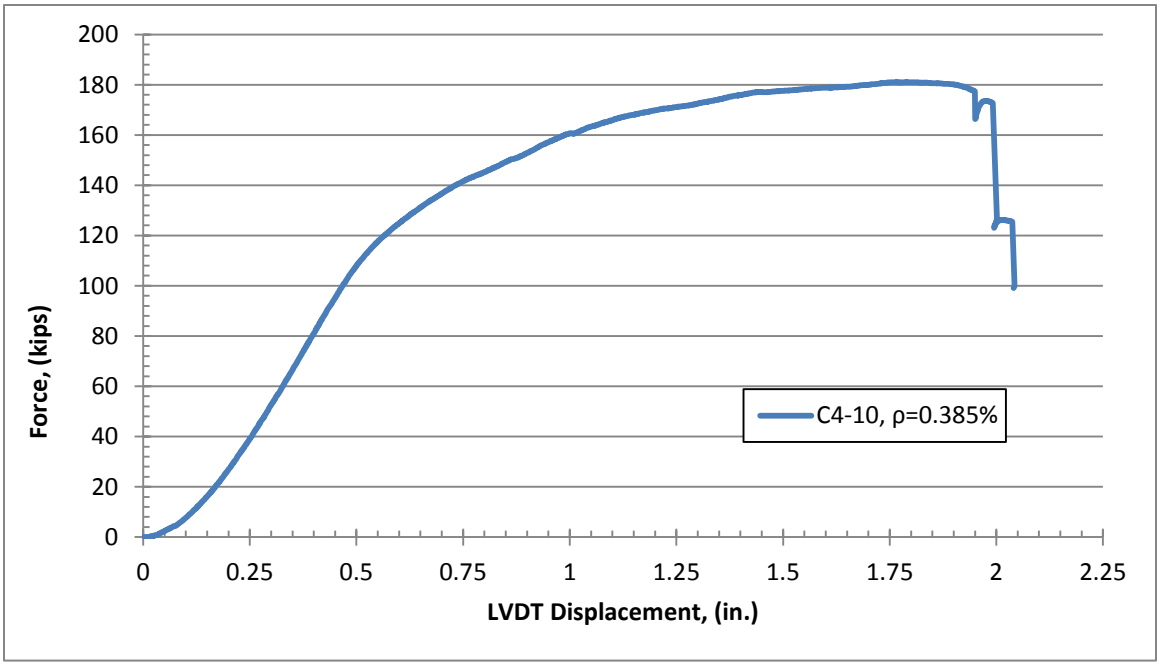


**Figure 4.64 Performance of 10 in. panels**

**Figure 4.65 Rupture of the macrosynthetic fibers**

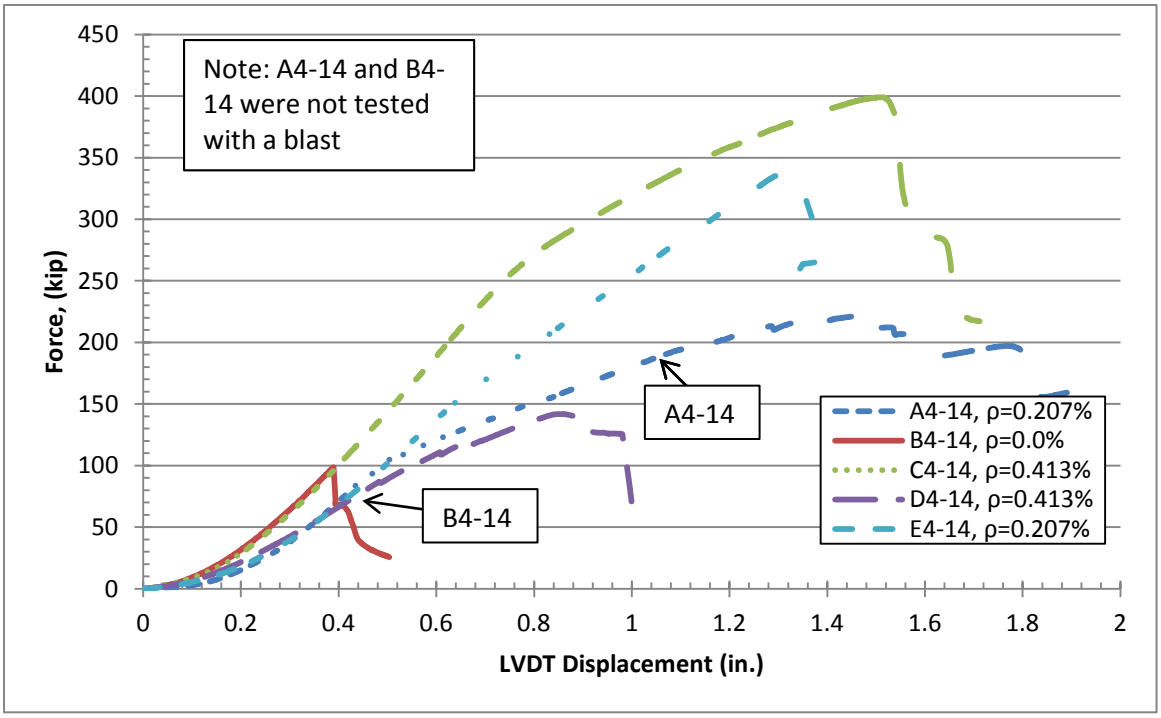


**Figure 4.66 Performance of 14 in. panels**

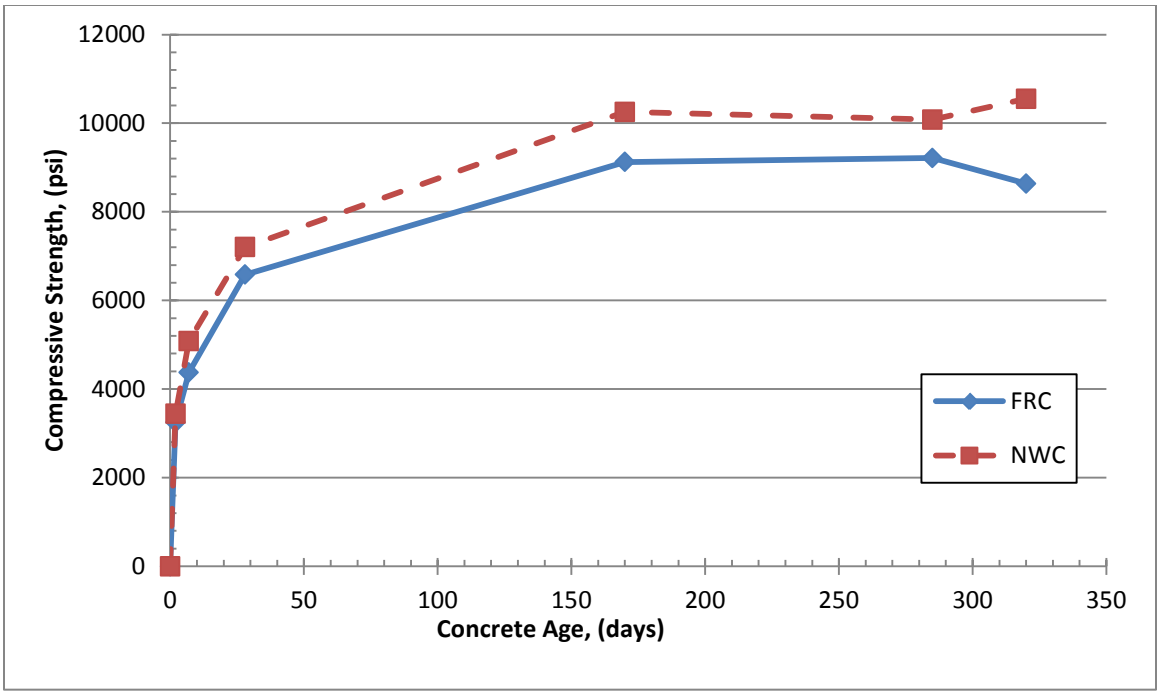


**Figure 4.67 Compressive cylinder strengths**

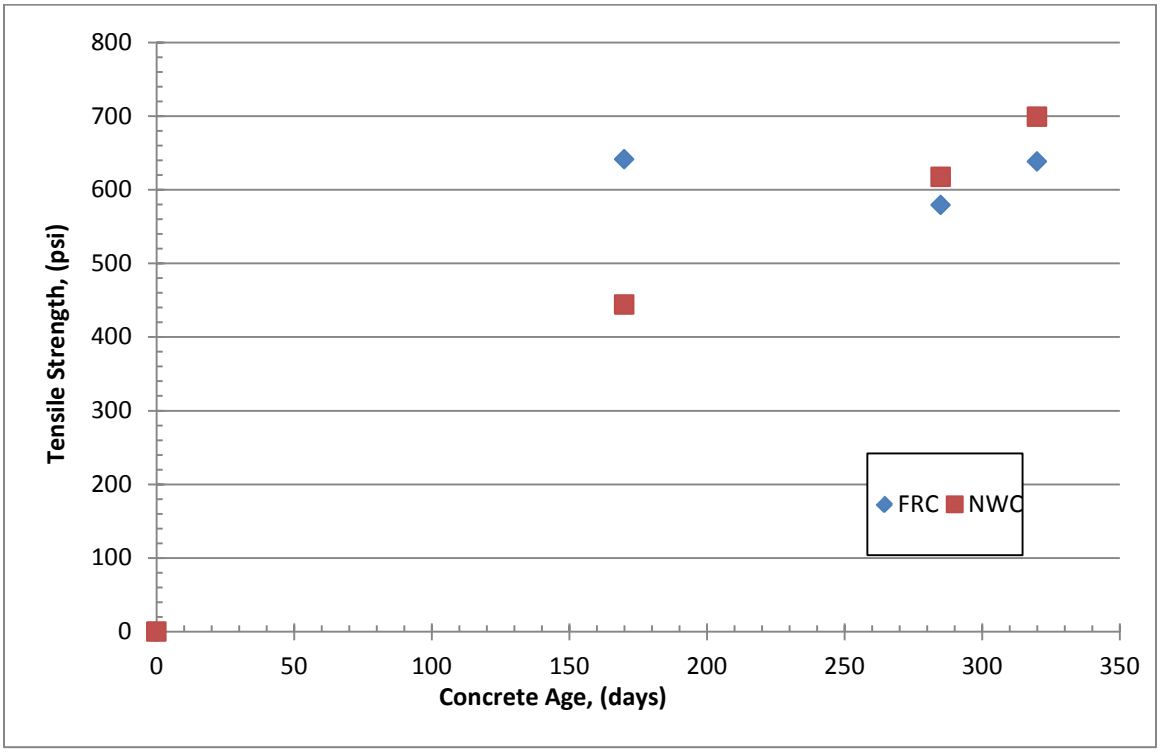


**Figure 4.68 Splitting tensile cylinder strengths**

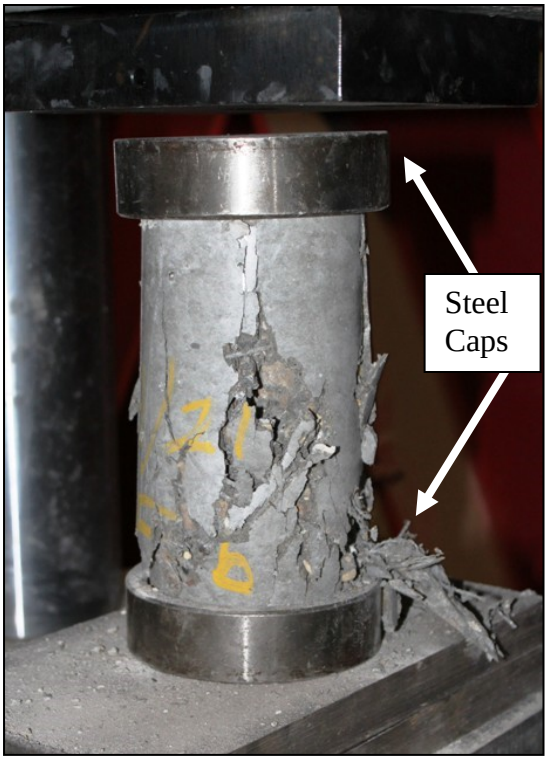


**Figure 4.69 FRC cylinder loaded to failure**

**Figure 4.70 Split tension jig**


**Figure 4.71 NWC failure from split tension test**

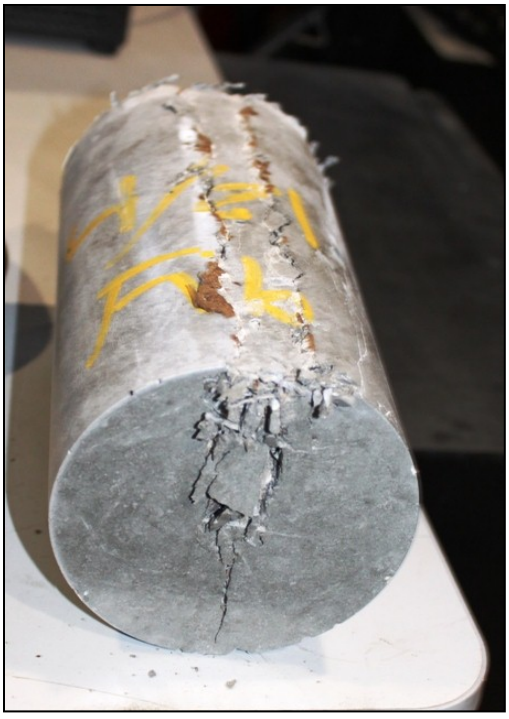

**Figure 4.72 FRC failure from split tension test**

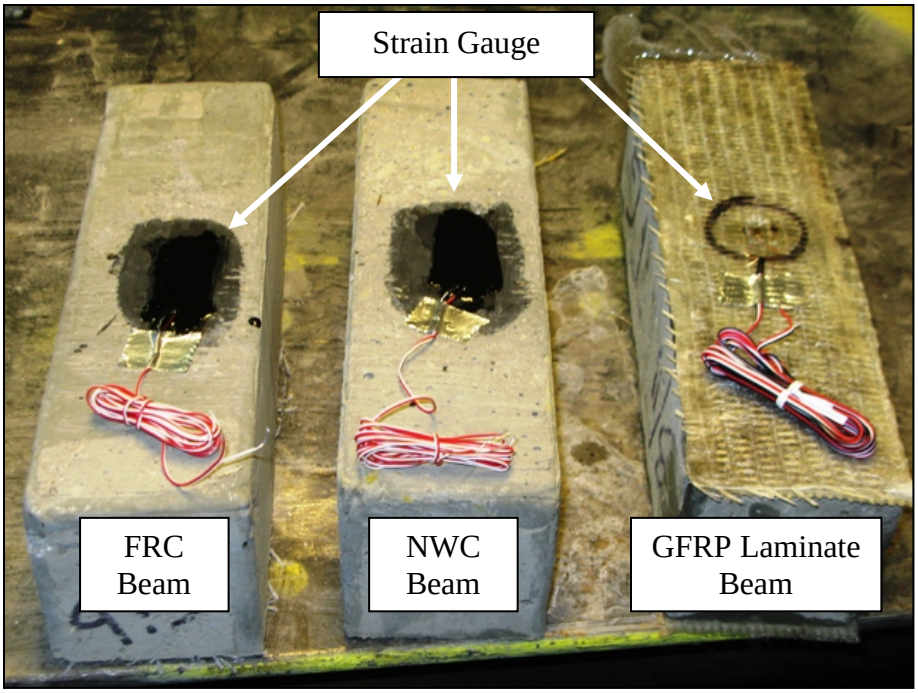


**Figure 4.73 Example of small beams**

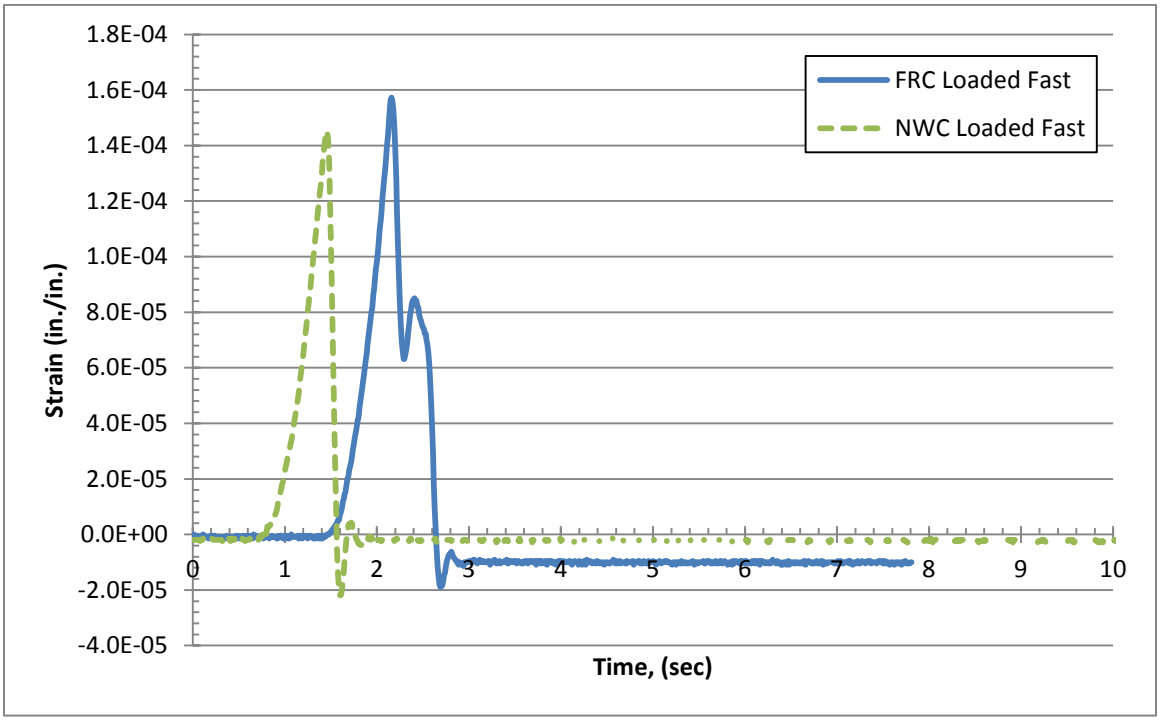


**Figure 4.74 Results of small beams when loaded fast**

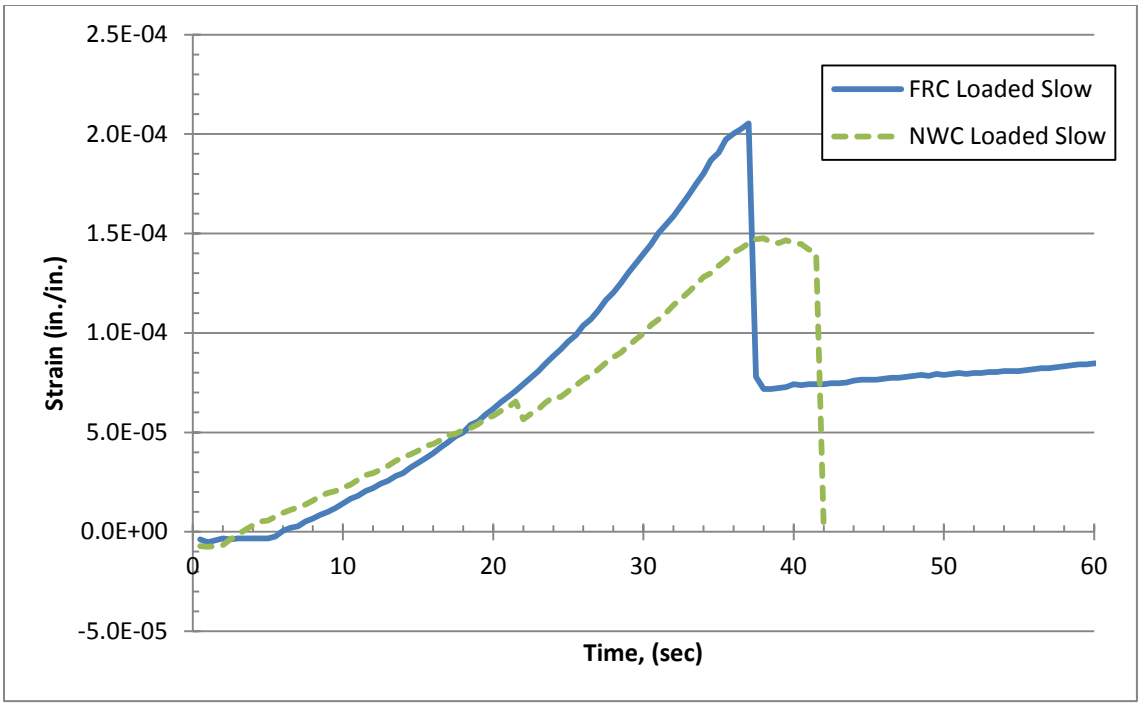


**Figure 4.75 Results of small beams when loaded slow**

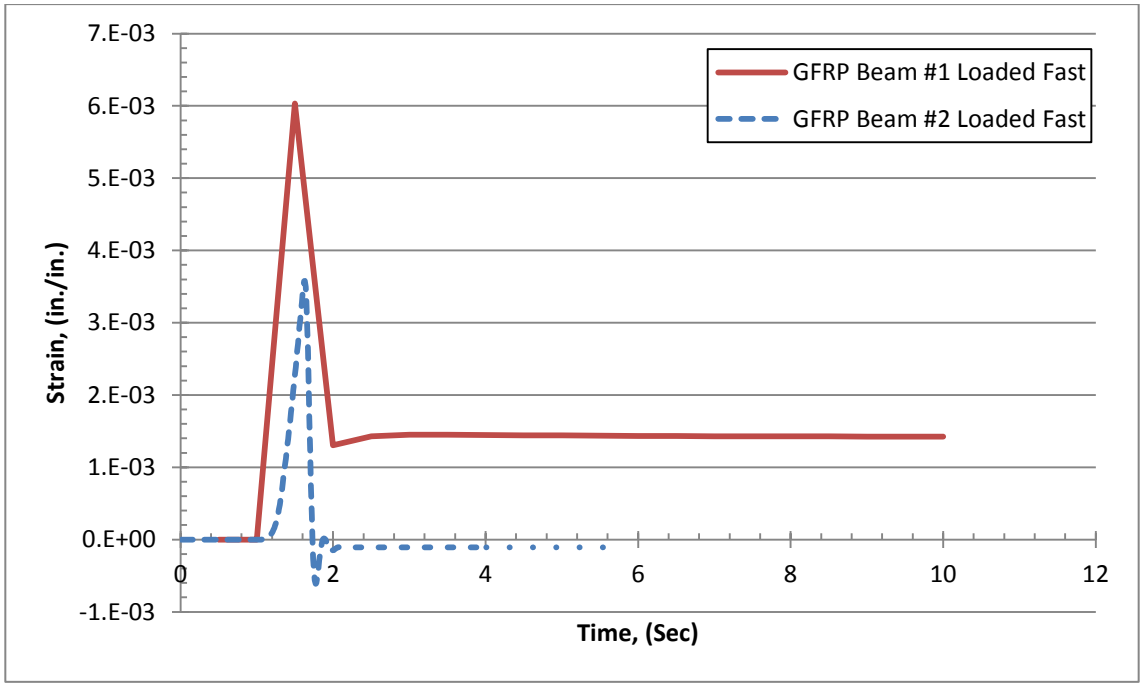


**Figure 4.76 Results of small GFRP beam when loaded fast**

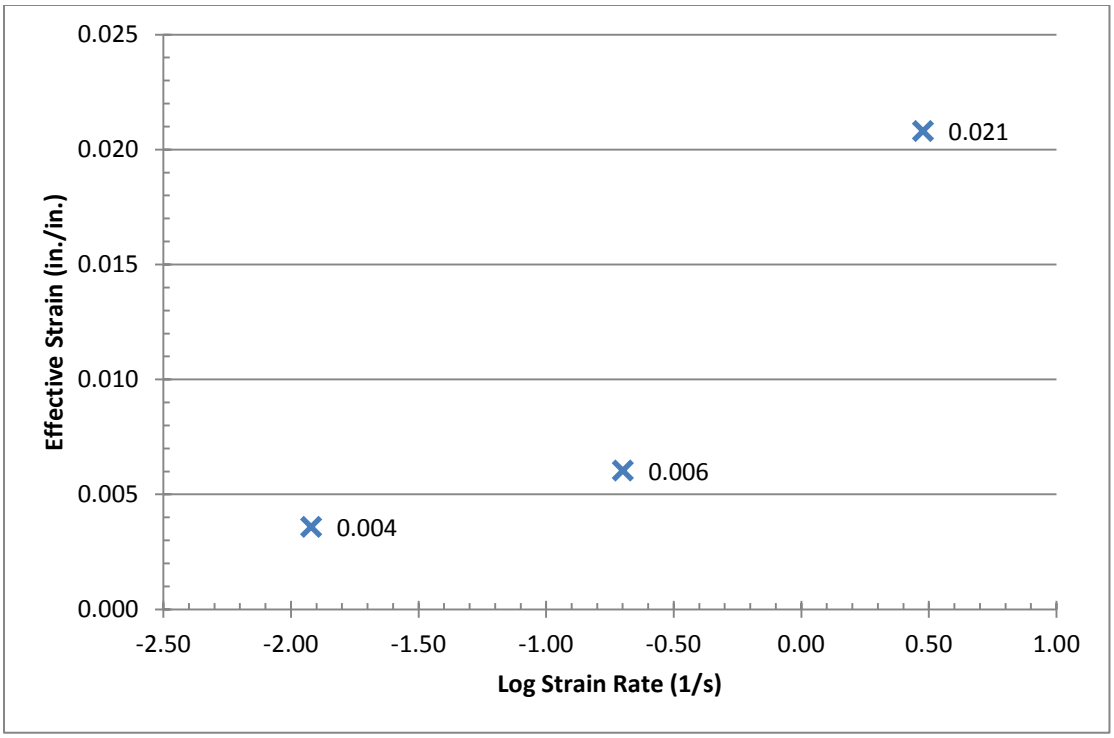


**Figure 4.77 Effective strain vs. the applied strain rate**

# 5. ANALYTICAL RESULTS

## 5.1. Model Development

5.1.1. Introduction. In order to draw conclusions about the experimental results it was important to quantitatively estimate how the panels should behave, and compare that with how they actually behaved. The deflection, moment capacity, and shear capacity were all calculated for each type of panel. Since the methods used were based on static conditions, to get the dynamic behavior of the panels the dynamic increase factor (DIF) was applied to each result, where appropriate, to determine the dynamic behavior of the panel. The DIF values were obtained from Figure 1.2 which was formulated from the open literature mentioned earlier in this thesis. None of the type B panels were analyzed in this section because of their poor performance under blast conditions.

5.1.2. Failure mode. Because the panels do not contain stirrups, failure of each panel depends on the strength of the concrete, the longitudinal steel ratio, and the thickness of the panel. The panel can fail in shear or flexure, or a combination of both flexure and shear. To predict which way a panel will fail the ratio of the shear span ($a$) to the effective depth ($d$) is computed; the variables are defined in Figure 5.1.

To predict whether a panel will fail in flexure or shear simple ratios have been developed from past research. MacGregor and Wight (2005) report, if the $a/d$ ratio is between 0 and 1 then a panel will form a compression arch and will fail in shear. If the $a/d$ ratio is between 1 and 2.5 the panel develops inclined cracks and would be expected

to fail in shear. If the *a/d* ratio is greater than 2.5 the panel would likely fail in a combination of flexure and shear. If the *a/d* ratio is greater than 4 then the panel would likely fail in flexure.

The shear span (*a*) is 21 in. for each of the tests and only the effective depth (*d*) changes for each panel type. Therefore one can estimate the possible panel failure mode. Table 5.1 shows a summary of how the panels might fail according to the *a/d* ratio. From this table it is seen that the 10 in. thick panels are on the boundary line of shear failure and flexure failure. To evaluate whether the 10 in. panel will fail in flexural and shear combination a more detailed analysis is performed in Section 5.4.

5.1.3. Assumed loading. In order to properly predict how the panels will react to a blast load it is necessary to understand how the blast pressures are applied to the panel. The blast applies a distributed load across the area of the panel; it was assumed that the applied blast pressure is greater in the center of the panel and then decreases outwards from the center. For this research, it was assumed that the loading applied to the specimen from the blast was similar to that shown in Figure 5.2. This shape was developed based on evidence of how the panels were damaged after the blast event, and from simplifying the shape used by Silva and Lu (2006). The actual values of the load were determined by using the known total pressures from ConWep and finding how those pressures were distributed on the panel. The load ratios at the two outer quarter points of the span and at midspan were determined by setting the total applied load equal to that of the load from ConWep.

The shear, moment, and curvature shapes along the length of the panel would be the same for each panel because the applied pressure was assumed to be the same for each

panel. For example, the shape of the shear, moment, and curvature about the centerline along the length of panel A4-6 is shown in Figures 5.3 to 5.5.

## 5.2. Deflection Model

5.2.1. Introduction. The deflection of the panel during the blast event was difficult to measure by instrumentation because of how fast the blast event occurs. Because of this, a model was developed to predict the deflection of the panel at midspan. After the blast events, some panels had permanently deflected shapes for which deflections could be measured. These measurements were then used to help calibrate the results and ensure the model was valid. To predict the dynamic deflection of the model the dynamic increase factor (DIF) was applied to the model.

5.2.2. Assumptions. In designing concrete panels, the moment of inertia decreases as the panel cracks. Before the panels were tested, they were first moved and transported many times using equipment; during this movement some minor cracking occurred within the panels. The gross moment of inertia is used to calculate the deflection of a structural member, but if the member has been cracked or damaged then the cracked moment of inertia must be used to calculate the deflection. The standard method for calculating the cracked moment of inertia is not always the most accurate method to determine the effective value.

Depending on the type of panel, the effective moment of inertia used in the deflection model was changed to match the amount of damage that was seen after the blast; for example panel type C was much less cracked than panel type A. This means that panel type C should have a higher effective moment of inertia in the model than panel type A. After the blast, it was determined that the middle third of the panel was typically more

cracked than the outer thirds of the panel. The observation made here is that the moment of inertia in the middle third of the panel was actually less than the moment of inertia in the outer thirds of the panel, as seen in Figure 5.6. This assumption results in a greater midspan deflection and a change in the slope of the curvature shape in the center of the curvature diagram. Table 5.2 shows the fully cracked moment of inertia, and moment of inertia that was assumed for each type of panel in each section of the panel.

The final assumption is that the dynamic deflection is equal to the static deflection times some factor (alpha, α), as shown in Eq. (5.1). Alpha was determined by computing the deflection of the panel using the DIF and observing that on average the deflection of the panel using the DIF was half of the static deflection. Assuming that the dynamic deflection was greater than the static deflection in the tests it was determined that the alpha could be determined according to Eq. (5.2).

$$\Delta_{dynamic} = \alpha * \Delta_{static} \quad \textbf{(5.1)}$$

$$\alpha = 1 + \frac{\Delta_{static}}{\Delta_{DIF}} \quad \textbf{(5.2)}$$

5.2.3. Methodology. The deflection model was created in a computer program using the following steps:

1. Define the known properties of the panel, and determine the transformed properties using the modular ratio shown in Eq. (5.3). The modulus of elasticity of the concrete was calculated by using Eq. (5.4) as reported by ACI committee 363, since the concrete used in this research is high strength concrete.

$$\eta = \frac{E_R}{E_C} \tag{5.3}$$

$$E_C = \left(40{,}000\sqrt{f_c^{`}} + 10^6\right)\left(\frac{W_c}{145}\right)^{1.5} \quad (psi) \tag{5.4}$$

where, $E_R$=modulus of elasticity of the reinforcement, $E_C$= modulus of elasticity of the concrete, $f`_c$=compressive strength of the concrete, and $W_c$=unit weight of the concrete.

2. Assume a loading shape (Figure 5.2) and determine the reactions of the simply supported panel.
3. Write equations for the assumed loading along the length of the panel as a function of the distance from the left support, Eq. (5.5).

$$Loading = w(x) \tag{5.5}$$

4. Determine the shear along the panel by taking the integral of the loading along the beam, Eq. (5.6).

$$V(x) = -\int w(x)dx \tag{5.6}$$

5. Determine the Moment along the beam by taking the integral of the shear along the beam, Eq. (5.7).

$$M(x) = \int V(x)dx \tag{5.7}$$

6. Using the moment equations along the beam determine the curvature along the beam using Eq. (5.8).

$$\phi(x) = \frac{M(x)}{EI(x)} \quad \textbf{(5.8)}$$

where, ϕ(x)=the curvature along the length of the panel, M(x)=applied moment along the length of the panel, E=modulus of the concrete, I(x)=moment of inertia. The moment of inertia will vary depending on where in the panel the curvature is being calculated, as discussed above.

7. The midspan deflection is the area under the curvature curve; this area can be found by using Eq. (5.9).

$$\Delta = \int_0^{0.5L} \phi(x) x dx \quad \textbf{(5.9)}$$

where, ϕ(x)=the curvature along the length of the panel, x=distance along the panel, and L=length of the panel.

8. Apply the DIF of 4 to only the concrete strength to compute the deflection using the DIF values, by repeating steps 3 through 7. Since this method does not account for the reinforcement that may or may not be in the panel a DIF was not applied to the reinforcement.
9. To determine the total deflection, using Eqs. (5.1) and (5.2).

5.2.4. Deflection model results. The deflection of two panels was measured after the blast, panel A4-6 and panel C4-6. Panel A4-6 had a permanent deflection of 3.5 in. and panel C4-6 had a permanent deflection of 0.125 in. The model predicted that panel A4-6 deflected 3.24 in. and that panel C4-6 deflected 0.18 in.; the actual measure deflections were 3.5 in. for A4-6 and 0.125 in. for C4-6. The model was able to predict within an average value of 19% to the actual deflection of these two panels. The results for each panel deflection from the model are shown in Table 5.3. The panels that failed because of the blast were listed in the last column of Table 5.3; the deflection model accurately depicted which panels would and would not fail as a result of the blast.

## 5.3. Bending Moment Capacity

5.3.1. Introduction. The bending moment capacity of each panel was calculated using the moment curvature method. As the compressive strain in the compression fiber of the concrete increases from $\varepsilon_c$=0.000 to $\varepsilon_c$=0.003 so does the curvature of the section. When the curvature increases, the bending moment that is required for equilibrium also increases. The relationship between the bending moment and curvature is very important; the bending moment is proportional to the flexural rigidity of the section times the curvature of the section. This means that the flexural stiffness of a section is equal to the slope of the moment-curvature curve, as shown in Figure 5.7.

The moment curvature method is an iterative process in which the strain in the extreme compression fiber of the concrete is defined, and then the tensile strain is solved for each value of compressive strain and when the axial load is set to a fixed value. A computer program was developed to perform the iterative processes.

5.3.2. Assumptions. The moment curvature method uses the stress-strain relationship for concrete to calculate the stress in the concrete at a particular strain. The stress is typically calculated using the equation presented by Todeschini et al. (1964), and assumes that the concrete has no tensile strength. Equation (5.10) is Todeschini's stress-strain relationship:

$$f_c = \frac{2\left(0.9f_c^{`}\right)\left(\frac{\varepsilon}{\varepsilon_0}\right)}{1+\left(\frac{\varepsilon}{\varepsilon_0}\right)^2} \quad \textbf{(5.10)}$$

where f`$_c$=the compressive strength of concrete, $\varepsilon_0$=strain at the inflection point of the stress-strain curve, and ε=strain at the point of interest. However, FRC is able to carry tensile load. The stress-strain relationship is different for FRC and thus new equations are needed to account for the tensile strength of the concrete. The stress-strain relationship presented by Hamoush et al. (2010) was used in the moment curvature method instead of the Todeschini's relationship to determine the moment capacity of only the FRC panels. The differences in the relationships are shown graphically in Figure 5.8.

Equations (5.11) to (5.15) are the stress-strain relationships presented by Hamoush et al. (2010):

(i) For concrete in tension,

$$\sigma = f_t\left(\frac{\varepsilon_c}{\varepsilon_0}\right), \qquad for\ 0 < \varepsilon_c < \varepsilon_0 \quad \textbf{(5.11)}$$

$$\sigma = f_t - 0.14f_t\left(\frac{\varepsilon_c - \varepsilon_0}{0.0096 - \varepsilon_0}\right), \qquad for\ \varepsilon_0 < \varepsilon_c < 0.0096 \quad \textbf{(5.12)}$$

$$\sigma = 0.86f_t - 0.68f_t\left(\frac{\varepsilon_c - 0.0096}{\varepsilon_{tu} - 0.0096}\right), \qquad for\ \varepsilon_0 < \varepsilon_c < 0.0096 \tag{5.13}$$

where $f_{t.}$=peak tensile stress, $\varepsilon_0$= tensile strain at peak stress, $\varepsilon_c$= concrete strain at point in consideration, and $\varepsilon_{tu}$= 0.0217 the maximum tensile strain in the concrete determined by Hamoush et al. (2010).

(ii) For concrete in compression,

$$\sigma = 2f_c^{`}\left[\frac{\varepsilon_c/\varepsilon_0}{1 + \left[\varepsilon_c/\varepsilon_0\right]^2}\right], \qquad for\ 0 < \varepsilon_c < \varepsilon_0 \tag{5.14}$$

$$\sigma = f_c^{`} - 0.187f_c^{`}\left[\frac{\varepsilon_c - \varepsilon_0}{\varepsilon_{cu} - \varepsilon_0}\right], \qquad for\ \varepsilon_0 < \varepsilon_c < \varepsilon_{cu} \tag{5.15}$$

where $f`_c$=the concrete compressive strength, $\varepsilon_0$=compressive strain at peak stress, $\varepsilon_{cu}$=is the maximum compressive strain, and $\varepsilon_c$=is the compressive concrete strain at the point of interest.

For panels with GFRP laminates overlays, additional reinforcement layers were used to account for the GFRP laminates. The GFRP laminate was converted to an equivalent area of reinforcement and the known properties were used to calculate any stresses or forces. Once the strain in the laminates reached 0.015 in./in. then the laminate was assumed to debonded from the concrete and was ignored in any further steps. This is an assumption that was made based on the information that was determined during the testing of the small NWC beams with GFRP composite laminates; it was shown in this testing that the laminate at high strain rates could strain as much as 0.021 in./in.

5.3.3. Methodology. The moment curvature curve is developed using the following steps:

1. Slice the cross-section into layers and assume an initial value of the tensile strain in the concrete; model the reinforcement bars into slices as well.
2. Locate the center of the reinforcement slices with respect to their distance from the extreme compression fiber.
3. Find the area of each slice of concrete and reinforcement.
4. Determine the neutral axis location from the extreme compression fiber strain and determine the curvature of the panel. Equation (5.16) is used to determine the location of the neutral axis:

$$c = \frac{\varepsilon_c}{\varepsilon_c - \varepsilon_t} h \quad \textbf{(5.16)}$$

where, c=location of the neutral axis, $\varepsilon_c$=is the concrete compressive strain at the point of interest, $\varepsilon_c$=is the concrete tensile strain at the point of interest, and h=thickness of the panel. Equation (5.17) is used to determine the curvature:

$$\phi = \frac{0.003}{c} \quad \textbf{(5.17)}$$

where, φ=curvature, and 0.003=maximum compressive strain in the concrete.

5. Find the distance from the center of each slice of concrete or reinforcement to the neutral axis. Equation (5.18) is used to complete this step:

$$y_i = c - y_{top} \quad \textbf{(5.18)}$$

where, $y_i$=distance from the center of item in interest to the neutral axis, c=locations of the neutral axis, and $y_{top}$=distance from the center of the slice to the extreme compression fiber.

6. Find the tensile or compressive strain at the centroid of each slice of concrete or reinforcement. Equation (5.19) is used to determine the strain:

$$\varepsilon_c = (y_i)(\phi) \quad \textbf{(5.19)}$$

where, $y_i$=distance from the center of item in interest to the neutral axis, and φ=curvature.

7. Find the corresponding concrete stress or steel stress from the stress-strain relationship. Use the Todeschini's relationship for NWC and use the Hamoush's for the FRC. In some cases the stress in the reinforcement will be higher than the yield stress of the reinforcement material. If this is the case, cap the stress at the known yielding stress of the material. If the strain in the GFRP laminate is greater than 0.015 in./in. then the laminate has debonded from the concrete and should be ignored.
8. Find the tensile or compressive force in the concrete or reinforcement. Equation (5.20) is used to calculate the force:

$$P = A\sigma \quad \textbf{(5.20)}$$

where, P=force, A=area of concrete slice or reinforcement, and σ=stress in the slice or reinforcement.

9. The resultant axial force capacity of the panel is obtained by summing the force from each slice or reinforcement layer.
10. Find the bending moment for each slice of concrete and reinforcement. Equation (5.21) is used to compute the moment.

$$M = (Moment_{Arm})(P) \quad \textbf{(5.21)}$$

where, $Moment_{Arm}$=distance from the centroid of each slice or reinforcement to the center of the panel, and P=resultant compressive or tensile force.

11. The resultant moment capacity is obtained by summing the moment from each slice or reinforcement layer.
12. Determine the TRUE value of the tensile strain in the concrete. To do this solve for what the tensile strain in the concrete needs to be for the total axial load (from step 9) to be equal to zero. This zero point of total axial load is the point at which the tension and compression are equal.
13. Repeat steps 1 through 12 for different values of strain in the extreme compression fiber of the concrete.
14. Develop a moment-curvature curve for each panel by creating a plot of the moment for each concrete compression strain versus the corresponding

curvature. The maximum moment on the moment-curvature curve is the capacity of the panel.

15. Apply the DIF to the following properties to determine the dynamic effects: a DIF of 4 to the concrete strength, a DIF of 1.5 to the steel rebar strength if steel rebar was used, A DIF of 1.5 to the GFRP bars strength if GFRP bars were used, and 1.5 to the compression and tensile modulus of the GFRP laminate if used.

5.3.4. Computed moment capacities. The predicted static and dynamic moment capacity for each panel and the applied moment from the blast is shown in Table 5.4. Within the table is a column that calculates the ratio of the predicted capacity of the panel to the applied moment from the blast. This ratio is used to examine which panels performed better than others; the higher the ratio the better the panel performed. For example panel C4-14 has the highest ratio and from evidence gathered from the photos that panel performed the best; the ratio of panel A4-6 is the lowest ratio and that panel performed the worst.

## 5.4. Postblast Shear Capacity Model

5.4.1. Introduction. To predict the shear capacity, a modified strut-and-tie model was used. This provided a quick method to predict the shear capacity. The strut-and-tie model was calculated according to equations in Appendix A of The American Concrete Institute (ACI) Building Code Requirements for Structural Concrete and Commentary 318-08.

5.4.2. Assumptions. The strut-and-tie model is typically used for deep beams; because deep beams only have reinforcement in one direction, they are usually assumed to have only a two-dimensional failure plane. The panels in this research have reinforcement in

both directions in the tension zone of the concrete and therefore a modified two-dimensional failure plane must be considered, similar to a foundation footing.

The modified failure plane was used to account for the additional strength from the two-way dowel action in the panel. Development of the modified failure plane began by the fact that the deflection of the panel was greatest in the center. Because reinforcing bars are running in both directions, the bars that are parallel to the supports will not increase the shear capacity of the panel as much as reinforcing bars in the perpendicular direction of the supports. This was accounted for by only using a portion of the total area of bars for each direction in the model. If a reinforcing bar was directly underneath the loading plate in the perpendicular direction (with respect to the supports) the area of that bar was one; if the bar was not under the loading plate the area was one half. If the reinforcement bar was in the parallel direction to the supports then the area of the reinforcement directly underneath the loading plate was fully used; if the reinforcement bars were not under the loading plate then the area was not used, with an exception of the panels with a reinforcement spacing of 6 inches then the area of the two bars just outside the loading plate in the parallel direction was taken as half. An example for panel types with 12 in. reinforcement bar spacing and 6 in. reinforcement bar spacing are shown in Figures 5.9 and 5.10, respectively.

If the reinforcing bar was steel then it was assumed that the bar fully developed and the full strength was used. If a GFRP bar was used as reinforcement it was not assumed that the entire bar was fully developed; thus needing to calculate the strain in the bar that was caused by the postblast loading the strain rate was calculated using Eq. (5.22).

$$\varepsilon_s = \frac{\frac{M_f}{d_v} + V_f}{2E_r A_r} \quad \textbf{(5.22)}$$

where, $E_r$=elastic modulus of the reinforcement, $A_r$=area of the longitudinal reinforcement, $M_f$=moment at a distance *d* (*d*=effective depth of the tensile reinforcement) away from the maximum location, $V_f$=moment at a distance *d* away from the maximum location, and $d_v$=effective shear depth and flexural lever arm in panel; taken as 0.9 *d*. This equation was proposed by Hoult et al. (2008). Once the strain was determined the effective stress in the bar was then determined. Eq. (5.22) requires the moment and shear that is applied to the panel during the postblast testing; panel D4-10 was not computed in this model because it was not statically tested.

The panels with the GFRP composite laminate debonded on the tensile side as a result of the blast. The laminate was placed back on the tensile side of the panel; as the post-blast load was applied the laminate was clamped between the concrete panel and the support block, as shown in Figure 5.11. This was done only for panels E4-6 and E4-14; the laminate for E4-10 was lost in transportation. To account for the additional strength of the laminate the laminate was treated like another layer of steel reinforcement and assumed to only develop 30% of the strain capacity. To find the area of the laminate the clear distance of the panel was used time the thickness of the laminate in the direction of interest, either longitudinal or transverse direction.

5.4.3. Methodology. The shear model was developed in the following steps:

1. Define the known properties and loading conditions.
2. From the loading conditions assume a valid truss model; for this modified model a truss model must be assumed for both the perpendicular direction to the supports and the parallel direction, shown in Figures 5.12 and 5.13.

3. Check the width of the strut to make sure the width is within the dimensions of the panel. If the width of the strut is acceptable for the height of the panel move to the next step.
4. The strength of the steel in the perpendicular direction can be determined by: Determining the angle of the strut to the tie in each model, using Eq. (5.23).

$$\theta = \tan^{-1}\left(\frac{H}{L}\right) \quad \textbf{(5.23)}$$

where, θ= angle of the strut to the tie, H=height from bottom tie to bottom tie, and L=horizontal length from the start of the bottom tie to the start of the top tie. Variables are shown visually in Figures 5.12 and 5.13.

5. Calculate the effective area of reinforcement. This is done as described as above and in section 5.4.2, and using Eq. (5.24).

$$A_s = (n_{eff})(A_{bar}) \quad \textbf{(5.24)}$$

where, $A_s$=total area of reinforcing bar, $n_{eff}$=number of effective bars this is obtain using the method in section 5.4.2, and $A_{bar}$=area of each reinforcing bar.

To calculate the area of GFRP laminate if analyzing panel type E, use Eq. (5.25):

$$A_{GFRP} = (t)(l) \quad \textbf{(5.25)}$$

where, $A_{GFRP}$=Area of GFRP composite laminate, t=thickness of GFRP laminate (t=0.04 in.), and l=the clear length of the panel from the center of the support to the center of the other support (l=42 in.).

6. Calculate the strength of the reinforcement in the tie, using Eq. (5.26).

$$T = (A_s)(f_y) \tag{5.26}$$

where, T=strength of the tie, $A_s$=total area of reinforcing bar, and $f_y$=yielding strength of the reinforcement. If the reinforcement is GFRP bars then the strain in the GFRP bars must be calculated using Eq. (5.22); then the strength of the bar can be calculated, using Eq. (5.27).

$$f = \frac{\varepsilon_s}{\varepsilon_{max}} f_y \tag{5.27}$$

where, f=strength of the GFRP bar, $\varepsilon_s$=strain in the reinforcement bar calculated using Eqs (5.22), $\varepsilon_{max}$=0.0171 in./in. the maximum strain capacity of the GFRP bar, and $f_y$=104 ksi the yielding strength of the reinforcement.

7. Calculate the force in the strut from the force in the tie from step 6, using Eq. (5.28).

$$S = \frac{T}{\cos\theta} \tag{5.28}$$

where, S=force in the strut, T= strength of the tie from step 6, and θ= angle of the strut to the tie.

8. The shear capacity of the panel in the perpendicular direction can now be calculated by using Eq. (5.29).

$$P = 2(S)(\sin\theta) \quad \textbf{(5.29)}$$

where, P=shear capacity of the beam in the perpendicular direction, S=force in the strut, and θ= angle of the strut to the tie.

9. Repeat steps 4 through 8 for the parallel direction with the different effective areas of bars.
10. If the panel had GFRP composite laminates repeat steps 4 through 9 but instead of analyzing the steel analyze the GFRP composite with its corresponding properties. Add the capacity from the steel and the GFRP laminates.
11. The total shear capacity of the panel is the shear capacity of the panel in both the perpendicular and parallel direction.

5.4.4. Model Results. Table 5.5 summarizes the results of the shear model; the ratio of the predicted shear capacity of the panel to the applied force to the panel is computed. This ratio expresses how well the model can be used to predict the post-blast strength of a panel. During the process of developing the model a ratio greater than 0.70 was assumed to be a valid prediction and anything less than that was assume to not be a good prediction. In Table 5.5 there are a few panels where the ratio is less than the prescribed

0.70; this is because the panels fail in flexure and not in shear. The failure mode for each panel is listed in the second column in Table 5.5.

Table 5.6 lists the predicted capacity for each postblast panel based on their predicted mode of failure. This was done because Table 5.5 only listed the shear capacity of each panel, but some of the panels did not fail in shear they failed in flexure. The moment capacity was calculated using the same method as mentioned in Section 5.3, so the ratio therefore of the capacity over the applied load is greater than 1.0 now and this is because the method that was used in Section 5.3 did not account for the panels being previously damaged.

## 5.5. ASCE Performance

After a dynamic event such as an earthquake, certain structural performance levels and damage have been adopted by engineers. This is done to evaluate the damage that the earthquake has done to the structure. The criteria are outlined in a document by the American Society of Civil Engineers (ASCE) 41-06 (ASCE 2006) Seismic Rehabilitation of Existing Buildings. This document is used to rehabilitate buildings that are either vulnerable to damage or that were damaged during a seismic event; because both a seismic load and a blast load are considered a dynamic load this criteria from ASCE can be used to define the performance of the panels after the blast. The performance levels are controlled by measurable values of cracks in the concrete and drift in the member. The drift is defined as either the transient drift which is the drift that occurs during the dynamic event or the permanent drift which is the drift that is measured after the event is over. For this research the transient drift was not recorded; only the permanent drift was obtained from pictures and measurements.

ASCE 41-06 (ASCE 2006) lists the following structural performance levels for elements that are concrete frames:

- Collapse Prevention is defined as extensive cracking and hinge formation in the ductile elements of the structure and severe damage in any short columns. The drift is limited to 4% transient or permanent. Example of collapse prevention performance level is shown in Figure 5.14.
- Life Safety is defined as extensive damage to beams and in the ductile columns spalling of the concrete cover and shear cracking that is less than 0.125 inches. The drift is limited to less than 2% transient drift and 1% permanent drift. Example of life safety performance level is shown in Figure 5.15. The naming convention of "Life Safety" was considered by the author as vague and an open ended statement. The author decided to use the following from here on to describe this performance level "Incipient Structural Damage."
- Immediate Occupancy is defined as hairline cracking and limited yielding possible at a few locations. All concrete strains less than 0.003 and no crushing of concrete. The drift is limited to less than 1% transient drift and negligible permanent drift. An example of immediate occupancy performance level is shown in Figure 5.16.

These performance levels are applied to each panel that was tested with explosives. Table 5.7 summarizes the results of the performance levels.

Selection of the performance level for each panel was based on the following criteria. If the drift of the panel was less than 0.25% and the maximum crack width was less than 0.125 in. then the panel performance was Immediate Occupancy. If the drift was greater

than 1% but less than 4% and the crack width was less than 0.125 in. drift was less than 1.5% and the crack width was less than 0.5 in. the panel performance was Incipient Structural Damage. If the drift was greater than 4% then the panel performance was Collapse Prevention.

**Table 5.1 Possible failure modes**

| Specimen Thickness (in.) | Effective Depth (in.) | (a/d) | Possible Failure Mode |
|---|---|---|---|
| 6 | 4.625 | 4.5 | Flexure |
| 10 | 8.4 | 2.5 | Combination of Shear and Flexure |
| 14 | 12.375 | 1.7 | Shear |

**Table 5.2 Variation of the moment of inertia**

| Specimen | $I_{gt}$ ($in.^4$) | $I_{outer}$ ($in.^4$) Percent Used | $I_{outer}$ ($in.^4$) | $I_{inner}$ ($in.^4$) Percent Used | $I_{inner}$ ($in.^4$) |
|---|---|---|---|---|---|
| A4-6 | 906 | 20% | 181 | 5% | 45 |
| A4-10 | 4346 | 20% | 869 | 5% | 217 |
| A4-14 | 12251 | 20% | 2450 | 5% | 613 |
| C4-6 | 1039 | 100% | 1039 | 95% | 987 |
| C4-10 | 5446 | 100% | 5446 | 95% | 5173 |
| C4-14 | 16303 | 100% | 16303 | 95% | 15488 |
| D4-6 | 871 | 50% | 436 | 50% | 436 |
| D4-10 | 4033 | 20% | 807 | 15% | 605 |
| D4-14 | 11191 | 50% | 5596 | 30% | 3357 |
| E4-6 | 906 | 75% | 679 | 50% | 453 |
| E4-10 | 4346 | 75% | 3259 | 50% | 2173 |
| E4-14 | 12251 | 75% | 9188 | 50% | 6125 |

**Table 5.3 Results from deflection model**

| Specimen | Estimated Static Deflection (in.) | Estimated DIF Deflection (in.) | Alpha, α | Estimated Dynamic Deflection (in.) | Measured Deflection (in.) | Result Failed/Not |
|---|---|---|---|---|---|---|
| A4-6 | 2.060 | 1.177 | 1.57 | 3.24 | 3.500 | Failed |
| A4-10 | 0.769 | 0.446 | 1.58 | 1.21 | NA | Failed |
| A4-14 | 0.286 | 0.161 | 1.56 | 0.45 | NA | NA |
| C4-6 | 0.108 | 0.071 | 1.65 | 0.18 | 0.125 | Not |
| C4-10 | 0.037 | 0.024 | 1.65 | 0.06 | NA | Not |
| C4-14 | 0.007 | 0.005 | 1.66 | 0.01 | NA | Not |
| D4-6 | 0.228 | 0.129 | 1.57 | 0.36 | NA | Not |
| D4-10 | 0.296 | 0.168 | 1.57 | 0.46 | NA | Failed |
| D4-14 | 0.052 | 0.031 | 1.59 | 0.08 | NA | Not |
| E4-6 | 0.219 | 0.125 | 1.57 | 0.34 | NA | Not |
| E4-10 | 0.072 | 0.042 | 1.58 | 0.11 | NA | Not |
| E4-14 | 0.029 | 0.017 | 1.59 | 0.05 | NA | Not |

**Table 5.4 Results from moment capacity model**

| Specimen | Predicted Static Strength (kip-ft.) | Maximum Measured Crack Width (in.) | Predicted Dynamic Strength (kip-ft.) | Applied Blast Moment (kip-ft.) | Ratio Capacity/Applied |
|---|---|---|---|---|---|
| A4-6 | 20.1 | 0.625 | 30.3 | 207.6 | 0.146 |
| A4-10 | 67.1 | 0.5 | 101.4 | 370.6 | 0.273 |
| A4-14 | 151.2 | NA | 228.6 | Not Tested | NA |
| C4-6 | 66.7 | 0.0625 | 298.5 | 197.9 | 1.508 |
| C4-10 | 167.2 | 0.05 | 845.6 | 370.6 | 2.282 |
| C4-14 | 345.4 | 0 | 1688.2 | 370.6 | 4.555 |
| D4-6 | 66.0 | 0.0625 | 103.9 | 197.9 | 0.525 |
| D4-10 | 176.6 | 0.5 | 311.6 | 370.6 | 0.841 |
| D4-14 | 447.2 | 0.25 | 780.2 | 370.6 | 2.105 |
| E4-6 | 59.2 | 0.125 | 99.7 | 207.6 | 0.480 |
| E4-10 | 97.4 | 0.5 | 159.5 | 326.9 | 0.488 |
| E4-14 | 173.5 | 0.125 | 283.4 | 370.6 | 0.765 |

**Table 5.5 Results from postblast shear capacity model**

| Specimen | Failure Mode | Static Shear Capacity (kips) | Post-blast Applied Force (kips) | Ratio of Capacity/Applied |
|---|---|---|---|---|
| A4-6 | Flexure | 17.2 | NA | NA |
| A4-10 | Combination | 83.1 | NA | NA |
| A4-14 | Shear | 196.8 | 221.7 | 0.89 |
| C4-6 | Flexure | 29.5 | 67.9 | 0.43 |
| C4-10 | Combination | 142.6 | 181.1 | 0.79 |
| C4-14 | Shear | 337.9 | 399.0 | 0.85 |
| D4-6 | Flexure | 54.1 | 64.6 | 0.84 |
| D4-10 | Combination | NA | NA | NA |
| D4-14 | Shear | 134.5 | 141.9 | 0.95 |
| E4-6 | Flexure | 22.6 | 49.0 | 0.46 |
| E4-10 | Combination | 83.1 | 72.8 | 1.14 |
| E4-14 | Shear | 323.2 | 341.4 | 0.95 |

**Table 5.6 Panel capacity for postblast based on failure mode**

| Specimen | Failure Mode | Static Capacity Based on Failure Mode (kips) | Postblast Applied Force (kips) | Ratio of Capacity/Applied |
|---|---|---|---|---|
| A4-6 | Flexure | 22.9 | NA | NA |
| A4-10 | Combination | 83.1 | NA | NA |
| A4-14 | Shear | 196.8 | 221.7 | 0.89 |
| C4-6 | Flexure | 76.2 | 67.9 | 1.12 |
| C4-10 | Combination | 142.6 | 181.1 | 0.79 |
| C4-14 | Shear | 337.9 | 399.0 | 0.85 |
| D4-6 | Flexure | 75.4 | 64.6 | 1.17 |
| D4-10 | Combination | NA | NA | NA |
| D4-14 | Shear | 134.5 | 141.9 | 0.95 |
| E4-6 | Flexure | 73.7 | 49.0 | 1.50 |
| E4-10 | Combination | 83.1 | 72.8 | 1.14 |
| E4-14 | Shear | 323.2 | 341.4 | 0.95 |

**Table 5.7 Estimated performance levels**

| Specimen | Maximum Measured Crack Width (in.) | Estimated Deflection (in.) | Estimated Permanent Drift (%) | Estimated Performance Level |
|---|---|---|---|---|
| A4-6 | 0.625 | 3.24 | 13.50 | Collapse Prevention |
| A4-10 | 0.5 | 1.21 | 5.04 | Collapse Prevention |
| A4-14 | | 0.45 | 1.88 | Collapse Prevention |
| B4-6 | 0.4375 | NA | NA | Collapse Prevention |
| B4-10 | 0.0625 | NA | NA | Collapse Prevention |
| B4-14 | | NA | NA | Collapse Prevention |
| C4-6 | 0.0625 | 0.18 | 0.75 | Immediate Occupancy |
| C4-10 | 0.05 | 0.06 | 0.25 | Immediate Occupancy |
| C4-14 | 0 | 0.01 | 0.04 | Immediate Occupancy |
| D4-6 | 0.0625 | 1.42 | 5.92 | Collapse Prevention |
| D4-10 | 0.5 | 0.33 | 1.38 | Collapse Prevention |
| D4-14 | 0.25 | 0.08 | 0.33 | Incipient Structural Damage |
| E4-6 | 0.125 | 0.34 | 1.42 | Incipient Structural Damage |
| E4-10 | 0.5 | 0.11 | 0.46 | Incipient Structural Damage |
| E4-14 | 0.125 | 0.05 | 0.21 | Immediate Occupancy |

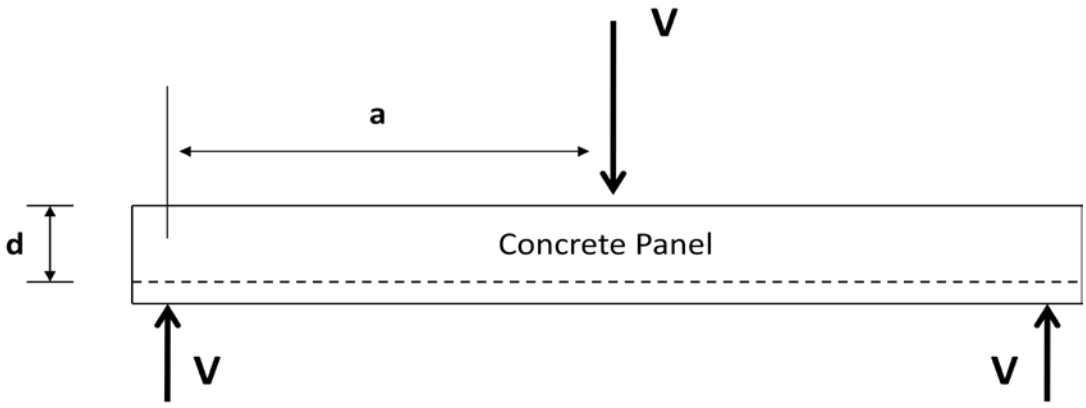


**Figure 5.1 Type of beam failure**

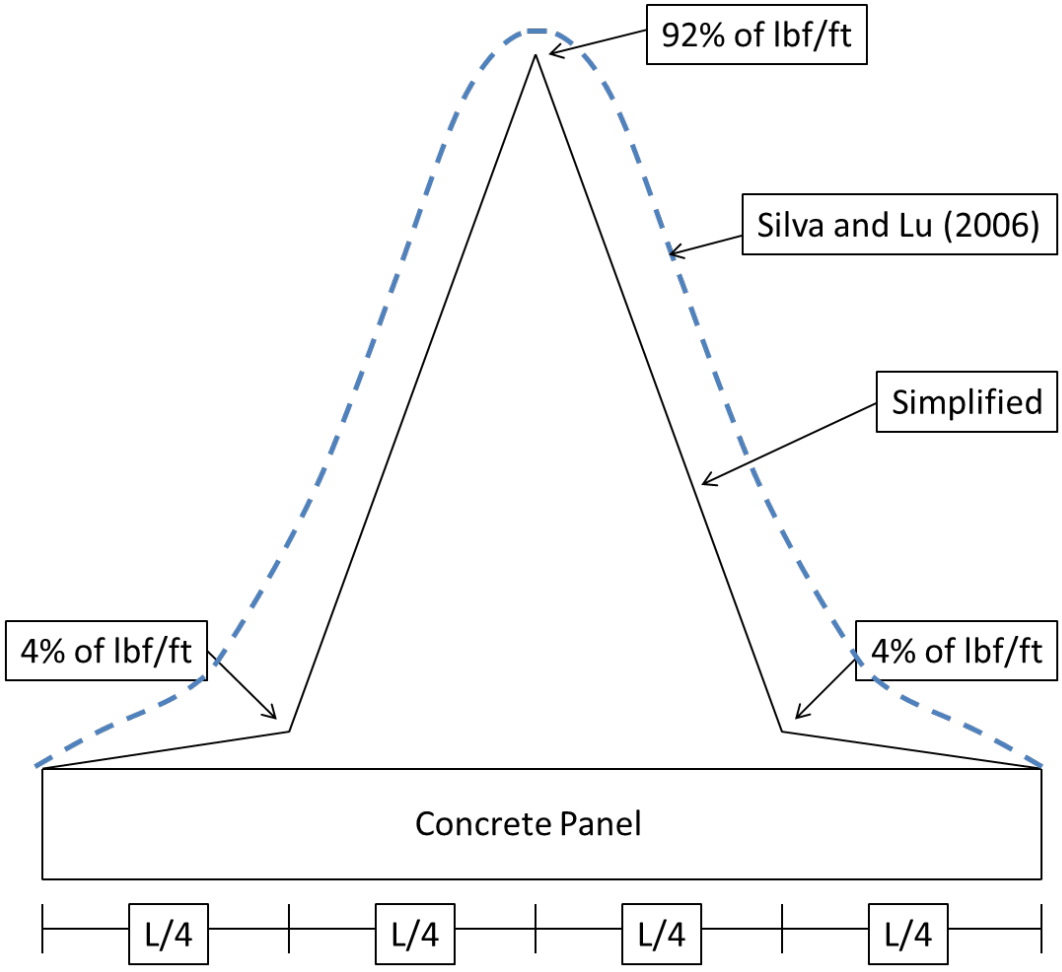


**Figure 5.2 Assumed loading**

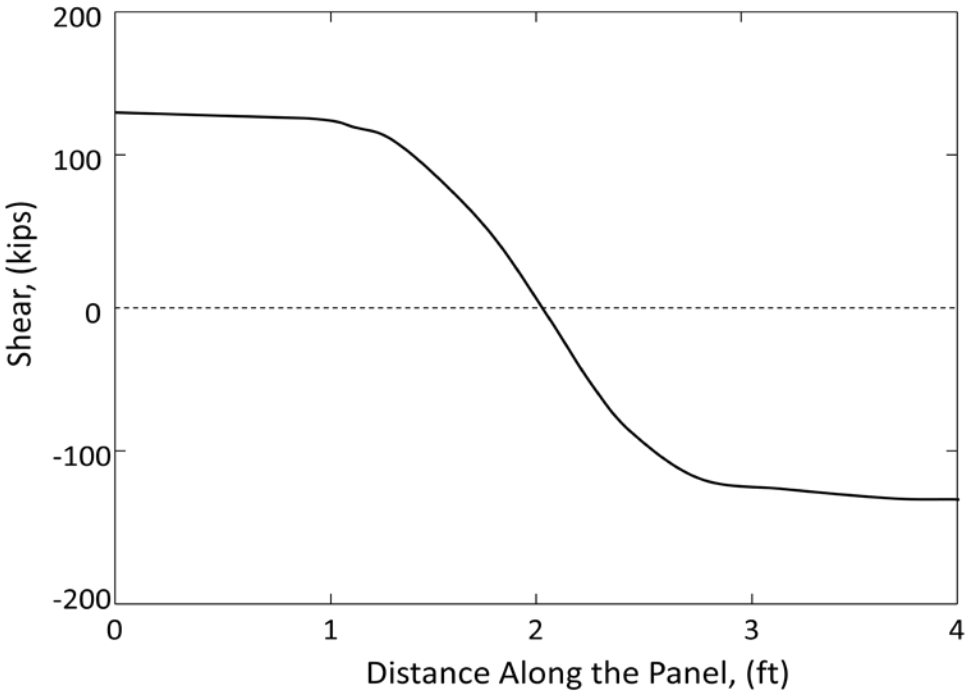


**Figure 5.3 Shear along beam A4-6**

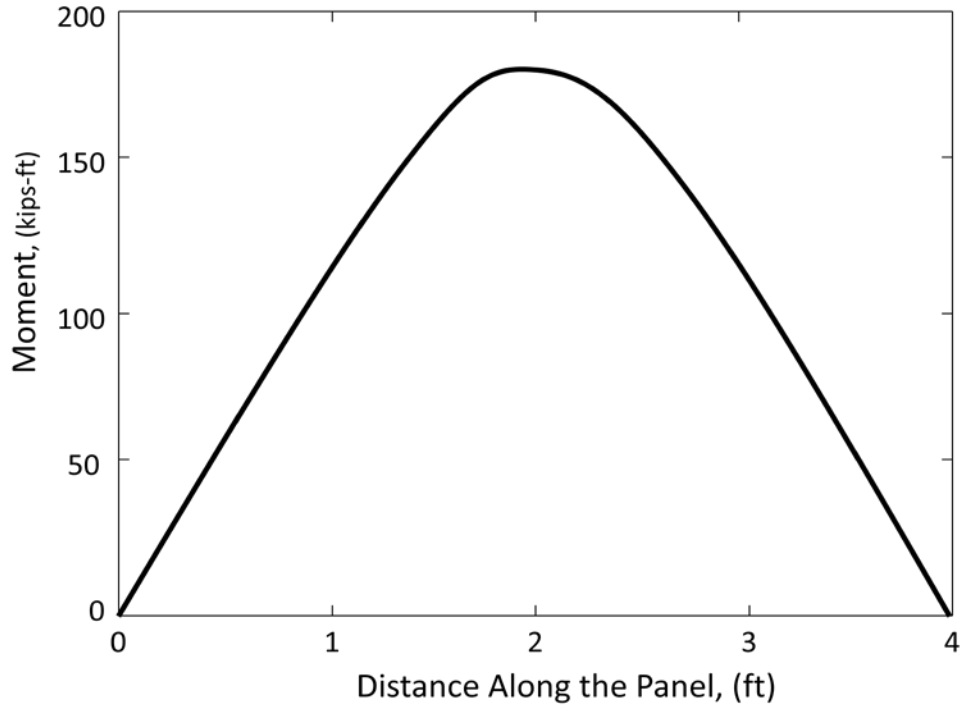


**Figure 5.4 Moment along beam A4-6**

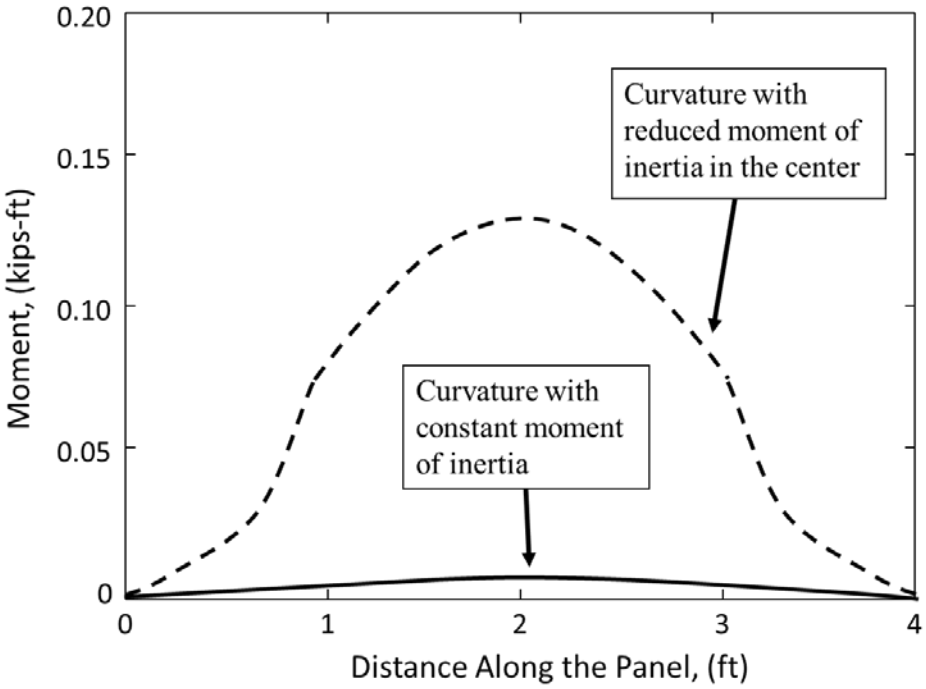


**Figure 5.5 Curvature along beam A4-6**

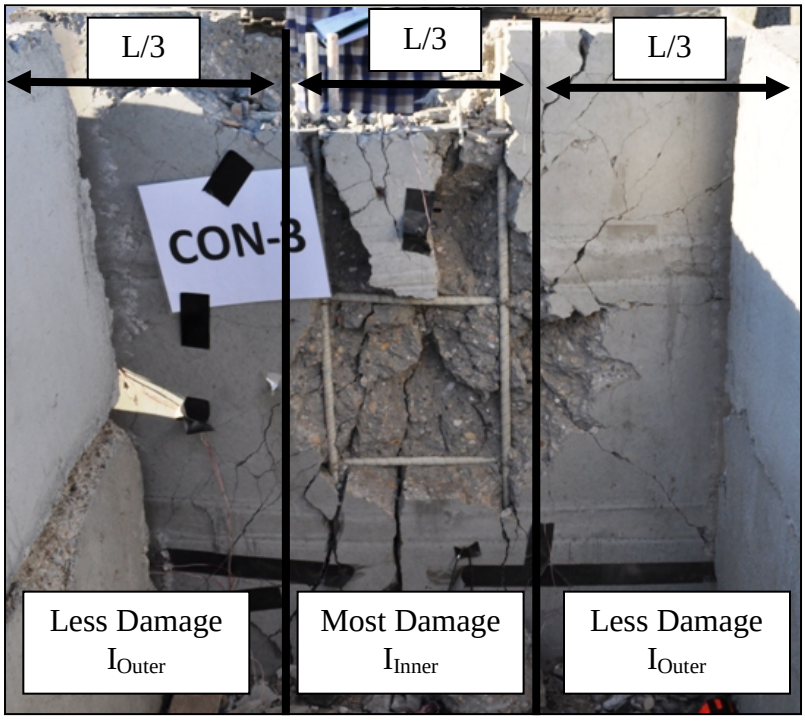


**Figure 5.6 Example of center damage**

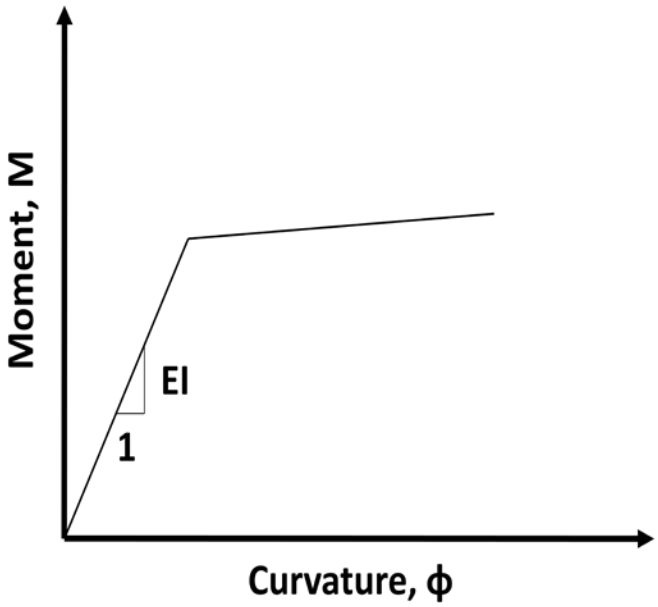


**Figure 5.7 Moment-Curvature curve**

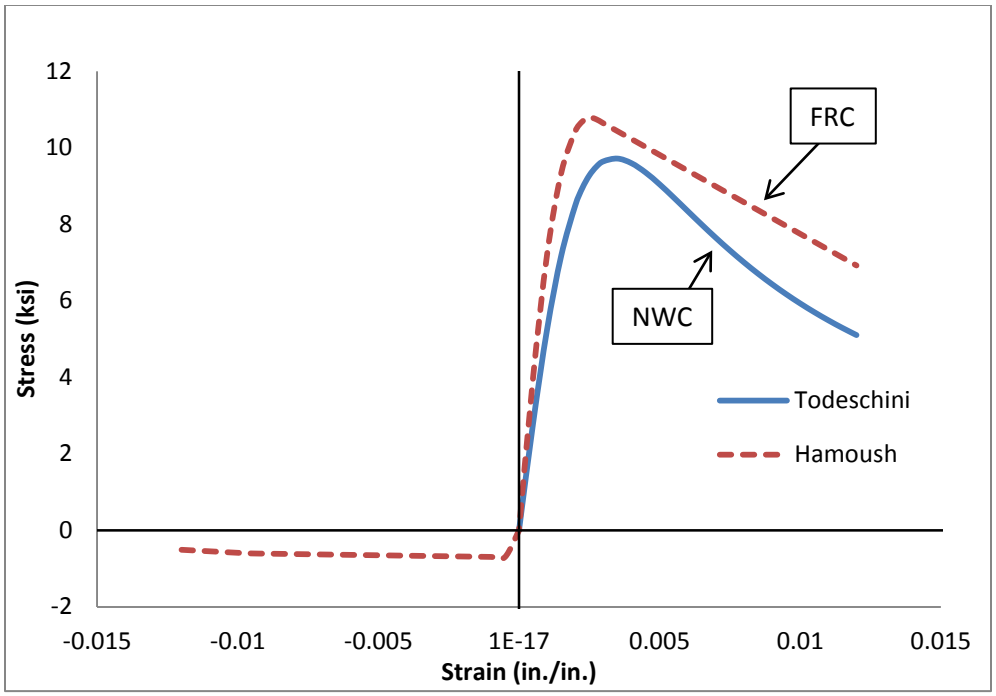


**Figure 5.8 Stress vs. strain relationships for NWC and FRC**

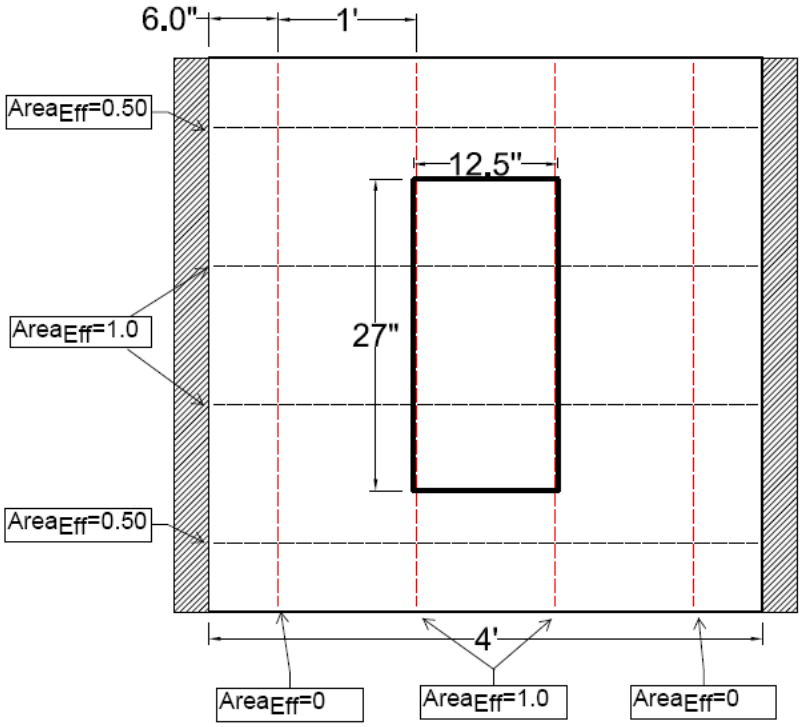


**Figure 5.9 Effective area of panels with 12 in. bar spacing**

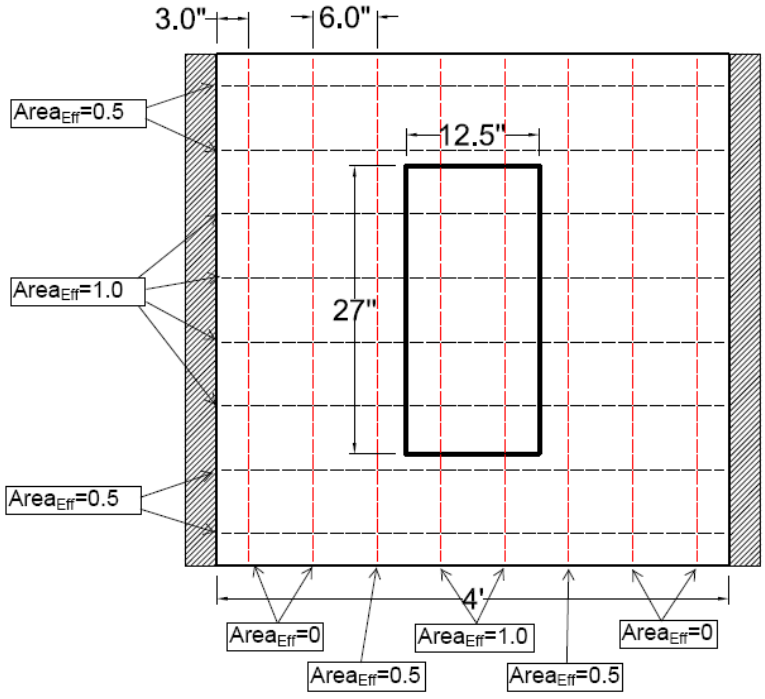


**Figure 5.10 Effective area of panels with 6 in. bar spacing**


**Figure 5.11 GFRP laminate clamped**

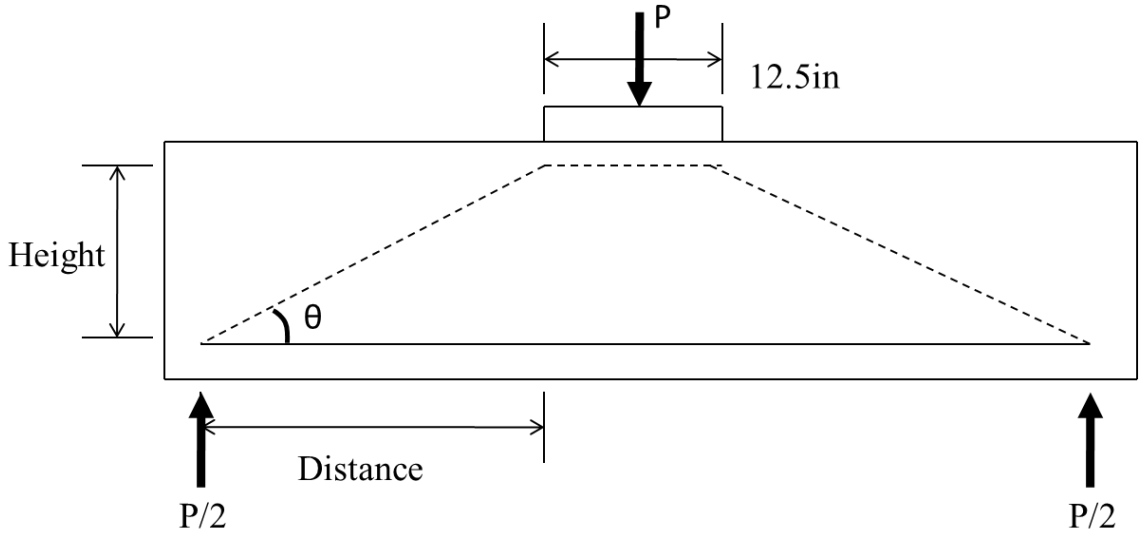


**Figure 5.12 Strut-and-tie model in the perpendicular direction**

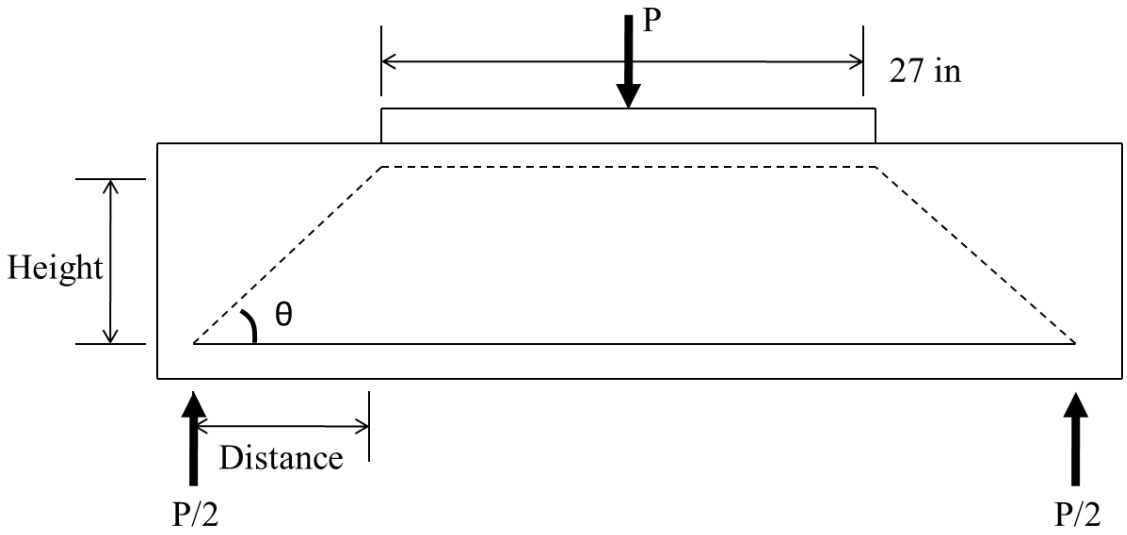


**Figure 5.13 Strut-and-tie model in the parallel direction**


**Figure 5.14 Collapse prevention performance level**

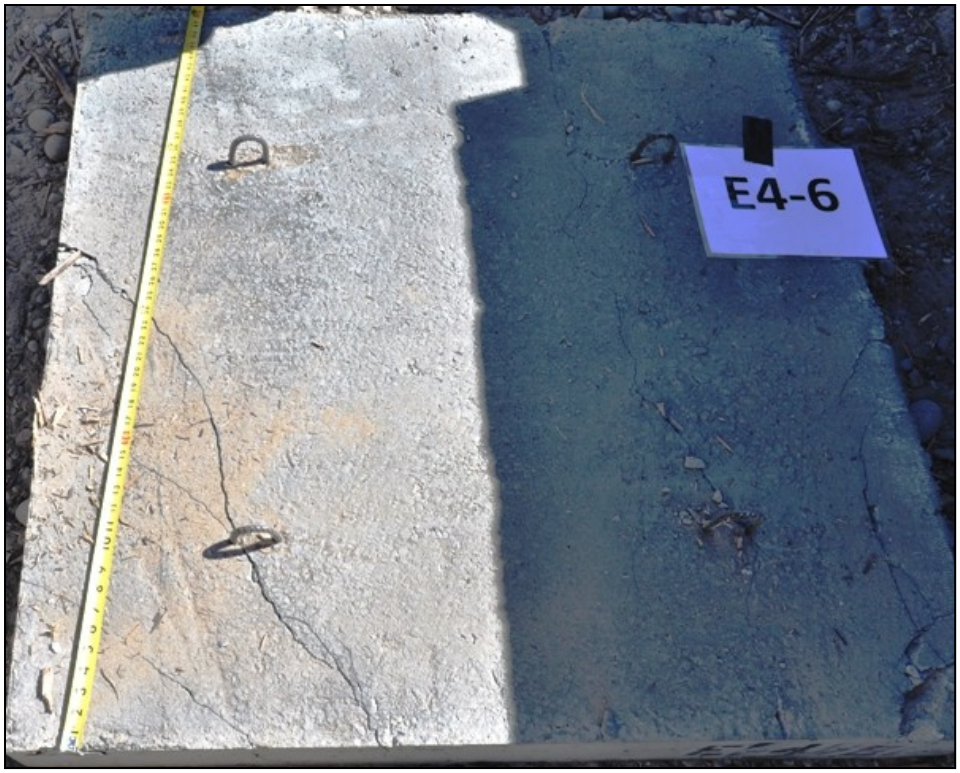


**Figure 5.15 Incipient structural damage performance level**

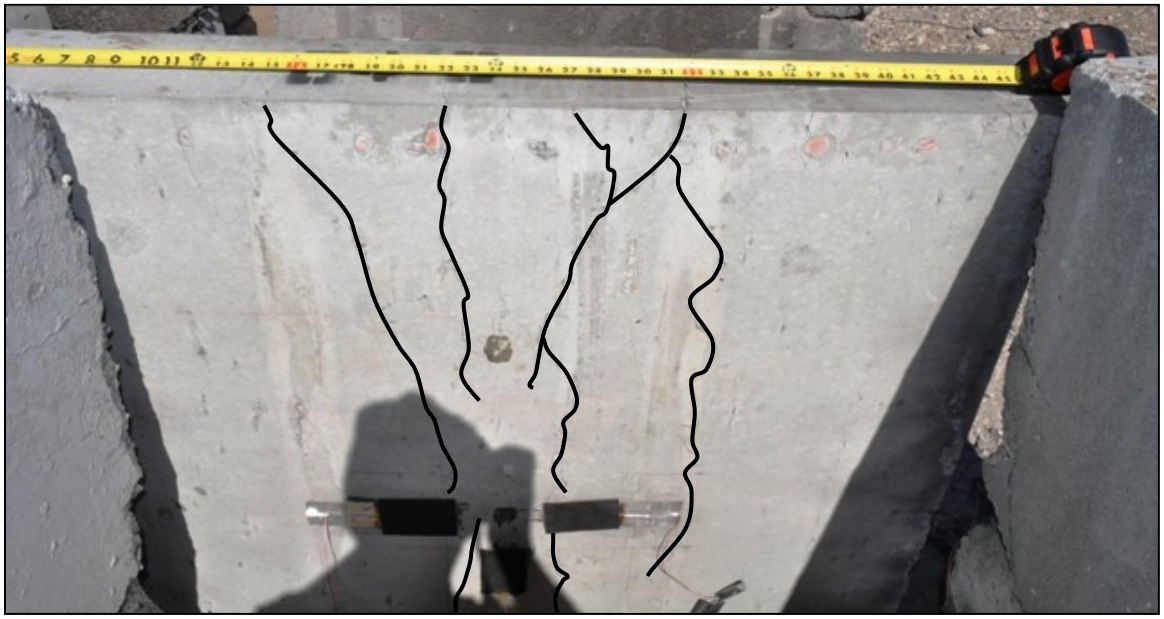

**Figure 5.16 Immediate occupancy performance level**

# 6. CONCLUSIONS AND RECOMMENDATIONS

## 6.1. Introduction

Different reinforcement types, concrete types, and panel thicknesses were studied to determine how the following combinations would perform to a blast load: NWC with steel rebar as internal reinforcement, designed to simulate how a wall already built could perform (panel type A); FRC with no additional reinforcement internally or externally, designed to evaluate FRC as the only reinforcement (panel type B); FRC with steel rebar as internal reinforcement, designed to simulate a newly constructed enhanced performance wall (panel type C); NWC with GFRP bars as internal reinforcement, designed to simulate a newly constructed wall (panel type D); NWC with steel rebar as internal reinforcement and GFRP composite laminates as an external reinforcement, designed to be a rehabilitation of an existing wall (panel type E).

## 6.2. Conclusions

This research was able to determine the following; the conclusions are organized to directly correlate to the project objective that was used to produce the result. These conclusions are only applicable to a 4 ft. X 4 ft. concrete panel.

1. The panels with the macrosynthetic fibers and the steel rebar sustained the least structural damage of all the panels tested, resulting in the best panel that is related to new construction. The panels with the GFRP laminates reduced

the amount of damage the panel sustained as a result of the blast when compared to the other panel types that did not have GFRP laminates, applicable to new construction or rehabilitation methods.

2. Results from the variables used in the panels:
    a. Increasing the thickness of the panel was found to be an effective method to reduce the damage. This increase is explained by a better formation of an adequate strut during the loading.
    b. FRC was determined to be the best type of concrete when proper global reinforcement was used. When proper reinforcement is not provided the FRC panels were broken into two pieces by the explosion; because the panels did break into two pieces this is the least recommended reinforcement option; a global reinforcement is a must.
    c. When reinforcement ratios are compared, the highest reinforcement ratio is not an indicator as to which panel will perform the best; an indicator to the best performance is the ductility and spacing of the reinforcement, and the type of concrete (NWC or FRC). The best reinforcement type is highly dependent upon the spacing of the reinforcement bars. If the bars are spaced closer together at 6 in. on center the GFRP and steel reinforcement bars performed similar to each other. When GFRP and steel reinforcement bars were placed at 12 in. on center the steel bars performed much better than GFRP bars. This is attributed to the ductile behavior of the steel bars which are able to absorb the energy of the blast by yielding, whereas GFRP bars

will reach their ultimate point and break therefore not absorbing any more energy.

d. It is also noticed that the panels experienced a progressive failure, meaning that the damage was cumulative. The panel will first crack at the top because of a lack of support and as the cracks progress they spread through the concrete and then the concrete spalls and fragments. It was observed that the boundary condition at the bottom of the panels restrained the panel causing less damage at the bottom, meaning that the cracking started at the top of the panel and progressed through the height of the panel to the bottom of the panel.

3. When compared across all the panel types and thicknesses panel type C during the static postblast testing was able to reach 27% greater peak load than the other panel types.
4. FRC was able to reach higher loads in splitting tension than the NWC concrete, but FRC was not able to reach higher load in the compressive strength when compared to the NWC. On average FRC was 10% stronger than NWC in splitting tension test.
5. A performance level was applied to each panel see Table 5.7 for the performance level for each panel according to the damage level caused by the blast.
6. The analytical models were able to replicate the level of damage that a panel experienced as a result of the blast.

## 6.3. Recommendations

A blast can be thought of as a catastrophic and disruptive event to engineers. When materials are subjected to a blast they no longer behave as they do when loaded in a static manner. To fully understand how a blast will affect concrete and especially fiber reinforced concrete, more knowledge is needed. The author feels that the items listed below need more research and understands that there are many more things that need to be studied relating to reinforced concrete and blast, but these are more direct recommendations for future research:

- FRC to evaluate the effect of different types of fibers and various volumes of fibers that are mixed into the concrete.
- Different sizes and shapes of panel need to be studied to determine if there are any size or shape factors that affect the performance of the concrete.
- Further research is needed to determine the best type of external reinforcement, because in this research only one type of external reinforcement was tested, GFRP. The GFRP performed well, but not enough data are available to make the claim that it is the best type of external reinforcement. Because the composite laminates debonded further research needs to consider anchoring the laminate to the concrete. Anchorage was not considered for this research because it was assumed that the anchors would not be placed any closer than 4 ft., the size of the concrete panels, in practical applications, but from this research it is now known that further research needs to be conducted with using anchors spaced less than 4 ft.

- The effects of negative pressures (suction phase) on the concrete panels and especially how the GFRP composite laminate bond is affected by the negative pressure.
- The interaction of the panel and the ground and how this affects the assumption of a one-way simply supported system.

# REFERENCES


ACI Committee 318. (2008). *Building Code Requirements for Structural Concrete (ACI 318-08) and Commentary.* Farmington Hills: American Concrete Institute.

ACI Committee 363. (1997). *State-of-the-Art Report on High-Strength Concrete Reported by ACI Committee 363.* Farmington Hills: American Concrete Institute.

ACI Committee 440.1 R-06. (2006). *Guide for the Design and Construction of Structural Concrete Reinforces with FRP Bars.* Farmington Hills: American Concrete Institute.

ACI Committee 440.2 R-08. (2008). *Guide for the Design and Construction of Externally Bonded FRP Systems for Strengthening Concrete Structures.* Farmington Hills: American Concrete Institute.

Altoubat, S. Y.-A. (2007). *Effect of Synthetic Macro-Fibers on Shear Behavior of Concrete Beams.* Farmington Hills: American Concrete Institute.

American Society for Testing Materials. (2004). *ASTM C496 / C496M - 04e1 Standard Test Method for Splitting Tensile Strength of Cylindrical Concrete Specimens.* West Conshohocken: ASTM International.

American Society for Testing Materials. (2007). *ASTM C31 / C31M - 10 Standard Practice for Making and Curing Concrete Test Specimens in the Field.* West Conshohocken: ASTM International.

American Society for Testing Materials. (2010). *ASTM C39 / C39M - 10 Standard Test Method for Compressive Strength of Cylindrical Concrete Specimens.* West Conshohocken: ASTM International.

American Society for Testing Materials. (2010). *C1609/C1609M -10 Standard Test Method for Flexural Performance of Fiber-Reinforced Concrete (Using Beam With Third-Point Loading).* West Conshohocken: ASTM International.

Behnood, A. G. (2009). Comparision of compressive and splitting tensile strength of high-strength concrete with and without polypropylene fibers headed to high temperatures. *Fire Safety Journal*, 1015-1022.

Brara, A. C. (2001). Experimental and numerical study of concrete at high strain rates in tension. *Mechanics of Materials*, 33-45.

Cooper, P. W. (1996). *Introduction to the Technology of Explosives.* Hoboken: Wiley-VCH.

Coughlin, A. M. (2010). Behavior of portable fiber reinforced concrete vehicle barriers subjected to blast from contact charges. *International Journal of Impact Engineering*, 521-529.

Haifeng, L. J. (2009). Mechanical behavior of reinforced concrete subjected to impact loading. *Mechanics of Materials*, 1298-1308.

Hamoush, S. A.-L. (2010). Deflection Behavior of Concrete Beams Reinforced wih PVA Micro-Fibers. *Construction and Building Materials*, 2285-2293.

Hosur, M. A. (2001). High strain rate compression response of carbon/epoxy laminate composites. *Composite Structures*, 405-417.

Hoult, N. A. (2008). Does the Use of FRP Reinforcement Change the One-Way Shear Behavior of Reinforced Concrete Slabs. *Journal of Composites for Construction*, 125-133.

Lan, S. L.-S. (2005). Composite structural panels subjected to explosive loading. *Construction and Building Materials*, 387-395.

Lawver, D. D. (2003). Composite Retrofits of Reinforced Concrete Slabs to Resist Blast Loading. *74th Shock and Vibrations Symposium*, (p. 11). San Diego.

MacGregor, J. G. (2005). *Reinforced Concrete Mechanics and Designs* . Upper Saddle River: Pearson Education Inc.

Maji, A. K. (2008). Full-Scale Testing and Analysis for Blast-Resistant Design. *Journal of Aerospace Engineering*, 217-225.

Malvar, L. J. (1998). Review of Strain Rate Effects for Concrete in Tension. *ACI Materials Journal*, 735-739.

McMullin, P. P. (2003). CFRP Composite Connector for Concrete Members. *Journal of Composites for Construction*, 73-82.

Mosalam, K. M. (2001). Nonlinear transient analysis of reinforced concrete slabs subjected to blast loading and retrofitted with CFRP composites. *Composites Part B: Engineering*, 623-636.

Muszynski, L. C. (2003). Composite Reinforcement to Strengthen Exisiting Concrete Structures against Air Blast. *Journal of Composite for Construction*, 93-97.

Naaman, A. E.-M. (2007). Punching Shear Response of High-Performace Fiber-Reinforce Cementitious Composite Slabs. *ACI Structural Journal*, 170-179.

Razaqpur, A. G. (2007). Blast loading response of reinforced concrete panels reinforforced with externally bonded GFRP laminates. *Composites Part B: Engineering*, 535-546.

Ross, C. A. (1995). Effects of Strain Rate on Concrete Strength. *ACI Materials Journal*, 37-45.

Silva, P. F. (2006). Improving the blast resistance capacity of RC slabs with innovative composite materials. *Composites Part B: Engineering*, 523-534.

Tedesco, J. W. (1999). *Structural Dynamics: Theory and Applications.* Boston: Addison Wesley Longman.

Todeschini, C. E. (1964). Behavior of Concrete Columns Reinforced with High Strength Steels. *Journal of the American Concrete Institute*, 701-716.

Weerheijm, J. V. (2006). Tensile failure of concrete at high loading rates: New test data on strength and fracture energy from insturment spalling tests. *International Journal of Impact Engineering*, 609-626.

Wu, C. O. (2009). Blast testing of ultra-high performance fibre and FRP-retrofitted concrete slabs. *Engineering Structures*, 2060-2069.

Zhang, X. X. (2009). Fracture behaviour of high-strength concrete at a wide range loading rates. *International Journal of Impact Engineering*, 1204-1209.